Coexistence of Superconductivity and Excitonic Ferromagnetism

Philip M. R. Brydon

THE AUSTRALIAN
NATIONAL UNIVERSITY

A thesis submitted for the degree of
Honours in Theoretical Physics at
The Department of Physics and Theoretical Physics
The Faculty of Science
The Australian National University

Honours Thesis submitted November, 2002

Declaration

This thesis is an account of research undertaken in 2002 at the Department of Theoretical Physics, the Research School of Physical Sciences and Engineering, the Australian National University, Canberra, Australia.

Except where acknowledged in the customary manner, the material presented in this thesis is, to the best of my knowledge, original and has not been submitted in whole or part for a degree in any university.

Philip M. R. Brydon
November, 2002

Acknowledgements

This past year has been an exhilarating intellectual experience. I can look back at my achievements over the last twelve months with justifiable pride. Not only have I learnt the rudiments of the quantum field theory of the many-body problem, I have also learnt how to apply this knowledge in order to extract useful information from several complicated systems.

I have also discovered much about the way that science is conducted. In general, I have been dismayed at the stark differences between my naive ideals and the brutal reality. Nevertheless, I remain firmly convinced that mine is a life for theoretical physics. It is therefore with great eagerness that I look forward to pursuing postgraduate studies.

In the final analysis, however, the most important thing this year has not been my study. Nor has it been any growth in self-knowledge, or even my shallow musings upon the nature of science. Rather, it has been about the people who believed in me and whose support has made all this possible. I am grateful to you all for making this such a memorable year.

To my supervisor Dr Miklós Gulácsi I give my heartfelt thanks. Your selfless care and guidance, your limitless patience, your uproarious sense of humour - it is these qualities that make not only the ideal supervisor, but also the good friend. For introducing me to the beautiful world of quantum field theory you have my unending gratitude.

To my fellow honours students I must have seemed invisible this year. Not only did I avoid most of the course-work, but I was hardly ever in the physics department. Nevertheless, you were often in my thoughts, and I feel privileged to have studied physics with you all. I must also thank my colleagues at the Research School. Morning and afternoon tea never failed to "disconnect" me from my study - to begin and to end the day laughing is something of great value.

To my friends I extend a warm and heartfelt thank you. I have often found myself overwhelmed and humbled by your unfeigned interest in my work, your unwavering affection, and the certainty of your presence when I needed it. It is hard to believe that I have been anything but the undeserving recipient of your love, being too absorbed in my study to properly return it.

Finally, I would like to thank my family. Without your unconditional love and support grandma, grandpa, mum and Naomi, none of this would have been worth the effort. I must single out my sister for special mention: despite study and work of her own, she was always available for a heart-to-heart at the ridiculous hours when I came home from the office. It was wonderful to have you at B&G this year Naomi.

I end with some more formal recognitions. My study this year was supported monetarily by the ANU Honours scholarship and a "top-up" from the Research School of Physical Sciences and Engineering. In the final production of this thesis, I must acknowledge the invaluable proof-reading efforts of Eloise Clare and Bianca Haberl. Their comments and suggestions were truly appreciated. I would also like to thank Dr Tim Thompson for his help with the binding.

Abstract

A rich variety of phenomena is displayed by solid state systems undergoing correlation-induced metal-insulator transitions. In a large class of these materials, the instability of the normal metallic state is ascribed to a peculiar topology of its Fermi surface. Such systems can support charge- or spin-density waves.

An important theoretical model of these systems is provided by the excitonic insulator. One of the most interesting predictions of this model is the appearance of ferromagnetic order in the system due to the interference of charge- and spin-density waves. This state is the so-called excitonic ferromagnet.

The coexistence of superconductivity with charge- and spin-density waves has been observed in a diverse range of materials. In many of these compounds, the superconductivity has an unusually high critical temperature. Theoretical studies of the coexistence of these two phenomena have worked within the simple framework of the excitonic insulator model.

In contrast to the coexistence with density waves, the simultaneous appearance of superconductivity and ferromagnetic order is both rare and poorly understood. The study and characterization of systems in which the two phenomena coexist is an important and challenging problem.

In this thesis, we present the results of an investigation into the appearance of superconductivity in the excitonic ferromagnet. We find that such a coexistence is possible at zero temperature within the self-consistent Hartree-Fock approximation.

Contents

Introduction

1.1 Overview

It was not long after the development of quantum mechanics that theorists first became interested in applying the "new physics" to solid state systems. The success of the pioneering efforts of Bloch and Wilson is most eloquently testified to by the continuing practical importance of their quantum band theory of solids [1].

In spite of the enormous success of the Bloch-Wilson theory, it was not until the late 1950s and early 1960s that the quantum theory of solids actually came of age. In this period, the newly-developed techniques of quantum field theory allowed spectacular progress to be made upon the outstanding problems of the 1930s and 1940s. Two defects of the traditional band theory were of greatest interest: the lack of an explanation for the phenomenon of superconductivity; and the inability to accurately predict the conducting and insulating states of certain oxides. The first problem was remedied in 1957 with the publication of the Bardeen-Cooper-Schrieffer (BCS) theory of superconductivity [2–4]; Mott's concept of the correlation-induced metal-insulator transition provided a solution to the second [5, 6].

The BCS theory of superconductivity was soon recognized as a particularly special achievement: it was the first soluble non-perturbative theory of a many-body system. The BCS solution was quickly found to be of a very general character, and its basic form has been applied in a wide variety of contexts [7]. One such application has been to the excitonic instability in semimetals, where the spontaneous formation of excitons (electron-hole pairs) causes a metal-insulator transition to occur [8]. This new state is the so-called excitonic insulator. Due to the rich variety of phenomena that it is predicted to display, the excitonic insulator has proved to be of importance in the description of many condensed-matter systems. Of particular note is the appearance of electron-density waves, and the possibility of a ferromagnetic ordering of the band electrons (the excitonic ferromagnet).

The excitonic insulator played a conspicuous role in early efforts to raise the critical temperature of superconductors [9]. This was in part motivated by the observation that the highest temperature superconductors known prior to 1986, the A15 and C15 compounds (Laves phases), exhibited a density-wave phenomenon [10]. Indeed, the most successful theoretical models of these materials have utilized an approach based upon the realization of a state closely related to the excitonic insulator [11]. There are several features of the excitonic insulator state itself that suggest the possibility of a critical temperature enhancement; such an effect has been verified theoretically [12, 13]. Modifications of the excitonic insulator scenario have been proposed in order to study more realistic systems; the results have given good agreement with experiment.

Contemporaneous with the development of the BCS theory of superconductivity was the recognition that the absence of ferromagnetic superconductors was an experimental fact of some significance [14, 15]. It soon became apparent that the phenomena of ferromagnetism and superconductivity were fundamentally antagonistic. In order to better understand both, much effort was directed at finding examples of their coexistence, which was rewarded in the mid-1960s with the discovery of the first ferromagnetic superconductors [16]. In the majority of these materials, however, the ferromagnetism and superconductivity appear in non-overlapping regions of mesoscopic dimensions; in the rare cases where both phases are uniformly realized throughout the material,

one (or both) of the coexisting phases often cannot be characterized by traditional theories. The study of these systems is therefore the subject of great interest [17–19].

1.2 Aim and Motivation

In this thesis, we aim to investigate a system simultaneously displaying spatially uniform ferromagnetism and superconductivity. We believe that an ideal candidate for such a study is provided by the excitonic ferromagnet. The reason for this is two-fold: the basic mechanism responsible for excitonic ferromagnetism is known not to be inconsistent with BCS superconductivity; and the peculiar characteristics of the excitonic ferromagnet make it less likely to hinder superconductivity than other possible mechanisms for ferromagnetism.

Some motivation is also provided by the recent discovery of weak ferromagnetism in the impurity- and vacancy-doped alkaline earth hexaborides CaB_6, SrB_6 and BaB_6 [20, 21]. Attempts were made to explain the observed ferromagnetic behaviour of these materials in terms of the excitonic ferromagnet, sparking renewed interest in this state [22, 23]. Although further experimental and theoretical work have cast doubt upon the validity of the excitonic scenario, it remains the most convincing interpretation [24]. In spite of some suggestive hints, superconductivity has not been observed in these systems. We do not aim, therefore, to explicitly apply our results to the hexaborides, but rather to broaden the current understanding of the excitonic ferromagnet.

1.3 Thesis Plan

We commence in chapter 2 with an introduction to the quantum field theory of many-body systems. In this chapter, we summarize the most important features of the Green's function approach to the study of the many-body problem. We include discussions of the approximations used in the rest of the work, and the theory of phase transitions in Fermi systems.

In chapter 3 we apply these methods for the first time to the simplest system considered here: the BCS superconductor. Simple variations on the analysis developed here will be used repeatedly in the rest of the work. We shall follow this chapter with a review of important concepts in magnetism in general and ferromagnetism in particular (chapter 4).

The excitonic insulator and ferromagnet will be considered in detail in chapter 5. We combine the results of this chapter and chapter 3 in the following study of superconductivity in an excitonic insulator (chapter 6). These three chapters provide the essential background for chapter 7, where we present a detailed original analysis of the superconducting excitonic ferromagnet state. Due to the relative obscurity of their topics, chapters 5, 6 and 7 all include a review of experimental evidence for the states they are each concerned with.

We conclude with an appraisal of our work and a discussion of possible directions for future efforts in chapter 8. We attach a detailed mathematical appendix.

1.4 Note on Notation

The reader will probably note the absence of $\hbar$ in the following work; we adopt the standard notation and set $\hbar = 1$ throughout [25]. This is done in the interests of clarity, so as not to clutter the formulas. We also note the standard dual usage of β: as a subscript, it is a spin-index; appearing elsewhere in formulas it is the inverse temperature $\beta = (k_B T)^{-1}$.

Quantum Field Theory of Many-Body Systems

The study of the physics of many-body systems was revolutionized in the mid-1950s by the application of the techniques of quantum field theory. Originally developed for the study of elementary particles, the remarkable success of these methods has made them indispensable to the theoretical study of condensed-matter physics [25–30]. Central to the unified and elegant quantum field theoretic approach is the Green's function.

All the most important physical properties of a many-body system can be determined from its Green's functions. Although a bewildering variety of these functions have been developed for the study of the many-body problem, we shall work almost exclusively with the single-particle Green's function. It may be interpreted as a generalized scattering amplitude, detailing the 'propagation' of a particle through the system. Not only is this Green's function particularly simple to work with, it also gives the physics of greatest interest, such as the electronic excitation spectrum, the macroscopic thermodynamics and the ensemble average of any single-particle operator.

In this chapter we present the basic theory of the single-particle Green's function in the Matsubara finite temperature formalism. We commence in section 2.1 with a review of the grand canonical ensemble and the rudiments of the Matsubara formalism. We proceed in section 2.2 to a definition of the single-particle temperature Green's function and an examination of its properties. In particular, we shall consider its equation of motion (subsection 2.2.2) and its relation to observables (subsection 2.2.3). We also introduce the many-particle Green's function (subsection 2.2.1). This is followed by a discussion of Wick's theorem (section 2.3) and the approximations that we have used in our work (section 2.4). We conclude with a brief outline of important concepts in the theory of phase transitions in Fermi system (section 2.5).

2.1 The Grand Canonical Ensemble

The grand canonical ensemble provides the most versatile statistical-mechanical description of equilibrium many-body systems. It is used to study situations where only the volume V, temperature T and chemical potential μ are known, and therefore allows for the possibility of small fluctuations in the total energy of the system, and the number of particles in it.

The grand canonical ensemble of a many-body system is the set of the system's microscopic states consistent with the given V, T and μ. Each of the states in the ensemble is assigned a statistical weight corresponding to the probability of its occurrence: if $|\psi\rangle$ is a possible state of the system, its statistical weight is proportional to $\langle\psi|e^{-\beta(\hat{H}-\mu\hat{N})}|\psi\rangle$ where $\hat{N}$ is the number operator, $\hat{H}$ is the system's Hamiltonian and $\beta = (k_B T)^{-1}$.

We define the grand canonical partition function Z_G as the sum of these statistical weights:

$$Z_G = \mathrm{Tr}\left\{e^{-\beta(\hat{H}-\mu\hat{N})}\right\} \tag{2.1}$$

The trace in 2.1 is taken over the states in the ensemble. Z_G is related to the thermodynamic potential Ω by the relation

$$\Omega = -k_B T \ln(Z_G) \tag{2.2}$$

and so we may, in principle, determine the macroscopic equilibrium thermodynamic behaviour of the system from the grand canonical partition function. Equations 2.1 and 2.2 enable us to define the grand canonical statistical operator

$$\hat{\rho}_G = {Z_G}^{-1} e^{-\beta(\hat{H}-\mu\hat{N})} = e^{\beta(\Omega-\hat{H}+\mu\hat{N})} \tag{2.3}$$

The inner product $\langle\psi|\hat{\rho}_G|\psi\rangle$ gives the probability that the system will be found in the state $|\psi\rangle$.

We consider an observable O of the system. O is associated with the operator $\hat{\mathcal{O}}$. We imagine making a large number of independent measurements of this quantity O, thus obtaining an average value $\bar{O}$. If the system can be studied in terms of a grand canonical ensemble, this value $\bar{O}$ may be determined by averaging the value of O across all the states in the ensemble in such a way that each value is weighted according to the probability that the corresponding state is realized. The weighted average of these different values of O is the so-called ensemble average $\langle\hat{\mathcal{O}}\rangle$ of the operator $\hat{\mathcal{O}}$. It is defined

$$\langle\hat{\mathcal{O}}\rangle = \mathrm{Tr}\left\{\hat{\rho}_G\hat{\mathcal{O}}\right\} = \bar{O} \tag{2.4}$$

where the trace is again over all the states in the ensemble.

2.1.1 The Matsubara Formalism

The grand canonical Hamiltonian $\hat{K}$ for a system with Hamiltonian $\hat{H}$ is defined by

$$\hat{K} = \hat{H} - \mu\hat{N} \tag{2.5}$$

The grand canonical Hamiltonian allows us to significantly simplify the expressions for the partition function (equation 2.1) and the statistical operator (equation 2.3):

$$Z_G = \mathrm{Tr}\left\{e^{-\beta\hat{K}}\right\} \qquad \hat{\rho}_G = {Z_G}^{-1} e^{-\beta\hat{K}} = e^{\beta(\Omega-\hat{K})} \tag{2.6}$$

In the Matsubara formalism, $\hat{K}$ is also used to define the 'modified' Heisenberg picture: for any Schrödinger operator $\hat{\mathcal{O}}_S(\mathbf{r})$ we define the 'modified' Heisenberg operator

$$\hat{\mathcal{O}}_K(\mathbf{r},\tau) = e^{\hat{K}\tau}\hat{\mathcal{O}}_S(\mathbf{r})e^{-\hat{K}\tau} \tag{2.7}$$

where τ is considered to be real. The operator $\hat{\mathcal{O}}_K(\mathbf{r},\tau)$ obeys the equation of motion

$$\frac{\partial\hat{\mathcal{O}}_K(\mathbf{r},\tau)}{\partial\tau} = \left[\hat{K},\hat{\mathcal{O}}_K(\mathbf{r},\tau)\right]_- \tag{2.8}$$

It is readily apparent that the equations 2.7 and 2.8 follow from the corresponding relations for the original Heisenberg picture, with the replacements $\hat{H}\to\hat{K}, it\to\tau$. We note that τ is real, however, and so the identity $it=\tau$ implies that the time t is an imaginary quantity. Thus, the Matsubara finite temperature formalism is often referred to as the 'imaginary-time' approach.

We almost exclusively utilize the 'modified' Heisenberg picture in what follows. Thus, for simplicity, we henceforth suppress the subscript K. We assume, unless stated to the contrary, that the presence of a τ-argument indicates that the operators are in the 'modified' Heisenberg picture; the absence of a τ-argument indicates that the operators are in the Schrödinger representation. When we speak of operators in the Heisenberg picture, we shall always refer to operators in the 'modified' Heisenberg picture introduced above.

We limit ourselves to the study of systems which may be described by a grand canonical Hamiltonian consisting of the sum of single-particle ($\hat{K}_0$) and two-particle interaction ($\hat{K}_1$) terms.

Explicitly, we have

$$\begin{aligned}\hat{K} &= \hat{K}_0 + \hat{K}_1 \qquad (2.9)\\ &= \sum_{\mathbf{k}',\nu} (\epsilon_{\mathbf{k}'} - \mu)\hat{a}^\dagger_{\mathbf{k}'\nu}\hat{a}_{\mathbf{k}'\nu} \\ &\quad + \frac{1}{2V}\sum_{\mathbf{k}_1,\mathbf{k}_1',\mathbf{k}_2,\mathbf{k}_2'}\sum_{\nu,\nu',\eta,\eta'} U_{\nu\eta\eta'\nu'}(\mathbf{k}_1,\mathbf{k}_2;\mathbf{k}_2',\mathbf{k}_1')\hat{a}^\dagger_{\mathbf{k}_1\nu}\hat{a}^\dagger_{\mathbf{k}_2\eta}\hat{a}_{\mathbf{k}_2'\eta'}\hat{a}_{\mathbf{k}_1'\nu'} \qquad (2.10)\end{aligned}$$

where V is the volume of the system. The function $U_{\nu\eta\eta'\nu'}(\mathbf{k}_1,\mathbf{k}_2;\mathbf{k}_2',\mathbf{k}_1')$ in the second term in equation 2.10 is the two-body interaction potential. Note that the the operators appearing in the expression for the grand canonical Hamiltonian are in the Schrödinger representation: referring to equation 2.8, we immediately see that $\hat{K}$ is τ-independent.

2.2 Green's Functions

The single-particle temperature Green's function is defined as

$$\begin{aligned}\mathcal{G}_{\alpha\beta}(\mathbf{k}_1,\tau_1;\mathbf{k}_2,\tau_2) &= -\mathrm{Tr}\left\{\hat{\rho}_G T_\tau\left[\hat{a}_{\mathbf{k}_1\alpha}(\tau_1)\hat{a}^\dagger_{\mathbf{k}_2\beta}(\tau_2)\right]\right\} \\ &= -\left\langle T_\tau\left[\hat{a}_{\mathbf{k}_1\alpha}(\tau_1)\hat{a}^\dagger_{\mathbf{k}_2\beta}(\tau_2)\right]\right\rangle \qquad (2.11)\end{aligned}$$

where the trace is over the same states as in equation 2.1 and the $\hat{a}_{\mathbf{k}\alpha}(\tau)$, $\hat{a}^\dagger_{\mathbf{k}\alpha}(\tau)$ are the Heisenberg field operators for a fermion with momentum $\mathbf{k}$ and spin α. The super-operator T_τ is the imaginary-time Wick's chronological ordering operator. The 'τ-product' $T_\tau[A(\tau_1)B(\tau_2)\ldots C(\tau_3)]$ of the Fermi operators $A(\tau_1), B(\tau_2), \ldots, C(\tau_3)$ is the product of these operators such that those with greater values of τ are written to the left of those with smaller values (so-called 'chronological order'), multiplied by the factor $(-1)^p$ where p is the number of transpositions of the Fermi operators required to transform the original product $A(\tau_1)B(\tau_2)\ldots C(\tau_3)$ into chronological order. Thus for the τ-product in 2.11 we have

$$T_\tau[\hat{a}_{\mathbf{k}_1\alpha}(\tau_1)\hat{a}^\dagger_{\mathbf{k}_2\beta}(\tau_2)] = \begin{cases}\hat{a}_{\mathbf{k}_1\alpha}(\tau_1)\hat{a}^\dagger_{\mathbf{k}_2\beta}(\tau_2) & \tau_1 > \tau_2 \\ -\hat{a}^\dagger_{\mathbf{k}_2\beta}(\tau_2)\hat{a}_{\mathbf{k}_1\alpha}(\tau_1) & \tau_2 > \tau_1\end{cases} \qquad (2.12)$$

and so we may re-write equation 2.11 as

$$\mathcal{G}_{\alpha\beta}(\mathbf{k}_1,\tau_1;\mathbf{k}_2,\tau_2) = -\theta(\tau_1-\tau_2)\left\langle\hat{a}_{\mathbf{k}_1\alpha}(\tau_1)\hat{a}^\dagger_{\mathbf{k}_2\beta}(\tau_2)\right\rangle + \theta(\tau_2-\tau_1)\left\langle\hat{a}^\dagger_{\mathbf{k}_2\beta}(\tau_2)\hat{a}_{\mathbf{k}_1\alpha}(\tau_1)\right\rangle \qquad (2.13)$$

$\mathcal{G}_{\alpha\beta}(\mathbf{k}_1,\tau_1;\mathbf{k}_2,\tau_2)$ is undefined when $\tau_1 = \tau_2$. We may regard equation 2.11 as defining the elements of a 2×2 matrix in the spin-indices: the so-called matrix Green's function is defined as

$$\mathbf{G}(\mathbf{k}_1,\tau_1;\mathbf{k}_2,\tau_2) = \begin{bmatrix}\mathcal{G}_{\uparrow\uparrow}(\mathbf{k}_1,\tau_1;\mathbf{k}_2,\tau_2) & \mathcal{G}_{\uparrow\downarrow}(\mathbf{k}_1,\tau_1;\mathbf{k}_2,\tau_2) \\ \mathcal{G}_{\downarrow\uparrow}(\mathbf{k}_1,\tau_1;\mathbf{k}_2,\tau_2) & \mathcal{G}_{\downarrow\downarrow}(\mathbf{k}_1,\tau_1;\mathbf{k}_2,\tau_2)\end{bmatrix} \qquad (2.14)$$

It is frequently convenient to assume (if only for computational tractability) that the system is spatially infinite and homogeneous. Since the real system may be considered to be enclosed within a macroscopic volume V where $V^{1/3}$ is much larger than the characteristic length scale of the system, taking the limit $V\to\infty$ is reasonable. We note that this limit is usually taken at the end of the analysis (see section A.1 of the mathematical appendix). The latter assumption, however, is substantially more radical. It ignores the periodic potential produced by the crystalline lattice in a solid, essentially treating the system as an interacting Fermi gas in free space. As such, the assumption of homogeneity can only give a qualitative description of the behaviour of a real solid state system. Nevertheless, this assumption is commonly utilized and gives remarkable agreement with experiment for the systems considered here. We shall therefore adopt both of these assumptions. All succeeding results are for spatially infinite and homogeneous systems,

unless explicitly stated otherwise.

We have assumed that the systems that we shall study are invariant under spatial translation. Hence, by Noether's theorem, the total momentum operator

$$\hat{\mathcal{P}} = \sum_{\mathbf{k},\alpha} \mathbf{k} \hat{a}^{\dagger}_{\mathbf{k}\alpha} \hat{a}_{\mathbf{k}\alpha} \tag{2.15}$$

commutes with the grand canonical Hamiltonian $\hat{K}$. It is therefore possible to choose the trace in equation 2.11 to be over the simultaneous eigenstates of $\hat{\mathcal{P}}$ and $\hat{K}$. Since the action of the operator $\hat{a}_{\mathbf{k}\alpha}(\tau)$ ($\hat{a}^{\dagger}_{\mathbf{k}\alpha}(\tau)$) is to lower (raise) the total momentum of the system by $\mathbf{k}$ for all 'times' τ, it follows that the trace in equation 2.11 will vanish unless $\mathbf{k}_1 = \mathbf{k}_2 = \mathbf{k}$ [28]. Furthermore, for the τ-independent systems considered here, only the τ-difference $\tau = \tau_1 - \tau_2$ has an unambiguous interpretation. Thus, the single-particle temperature Green's function may be re-written as

$$\mathcal{G}_{\alpha\beta}(\mathbf{k},\tau) = -\left\langle T_{\tau}\left[\hat{a}_{\mathbf{k}\alpha}(\tau)\hat{a}^{\dagger}_{\mathbf{k}\beta}(0)\right]\right\rangle \tag{2.16}$$

It is customary to assume that $\mathcal{G}_{\alpha\beta}(\mathbf{k},\tau)$ is diagonal in its spin indices.

It is convenient to regard the Green's function 2.16 as an antiperiodic function in τ with periodicity β. That is, for any integer n

$$\mathcal{G}_{\alpha\beta}(\mathbf{k},\tau+n\beta) = (-1)^n \mathcal{G}_{\alpha\beta}(\mathbf{k},\tau) \tag{2.17}$$

This allows the expansion of $\mathcal{G}_{\alpha\beta}(\mathbf{k},\tau)$ in a Fourier series

$$\mathcal{G}_{\alpha\beta}(\mathbf{k},\tau) = \frac{1}{\beta}\sum_{n=-\infty}^{\infty} e^{-i\omega_n\tau}\mathcal{G}_{\alpha\beta}(\mathbf{k},\omega_n) \tag{2.18}$$

where $\omega_n = \frac{n\pi}{\beta}$ and the Fourier coefficients $\mathcal{G}_{\alpha\beta}(\mathbf{k},\omega_n)$ are given by

$$\mathcal{G}_{\alpha\beta}(\mathbf{k},\omega_n) = \frac{1}{2}\int_{-\beta}^{\beta} d\tau e^{i\omega_n\tau}\mathcal{G}_{\alpha\beta}(\mathbf{k},\tau) \tag{2.19}$$

These Fourier coefficients may themselves be interpreted as Green's functions in the conjugate ω-space. It may be shown that $\mathcal{G}_{\alpha\beta}(\mathbf{k},\omega_n)$ vanishes whenever n is odd (see [26]), and so the Fourier representation of $\mathcal{G}_{\alpha\beta}(\mathbf{k},\tau)$ may be re-written

$$\mathcal{G}_{\alpha\beta}(\mathbf{k},\tau) = \frac{1}{\beta}\sum_{n \text{ odd}} e^{-i\omega_n\tau}\mathcal{G}_{\alpha\beta}(\mathbf{k},\omega_n) \tag{2.20}$$

The Fourier coefficients of the Green's functions are of particular importance as their poles give the single-particle excitation spectrum of the system. That is, if the conjugate matrix Green's function $\mathbf{G}(\mathbf{k},\omega)$ is of the form

$$\mathbf{G}(\mathbf{k},\omega) = \sum_{m=1}^{M} \frac{\mathbf{\Phi}_m(\mathbf{k},\omega)}{i\omega - \epsilon_m(\mathbf{k})} \tag{2.21}$$

where the $\mathbf{\Phi}_m(\mathbf{k},\omega)$ are holomorphic matrix functions of ω, then the dispersion relations for the electronic excitation spectrum are given by the $\epsilon_m(\mathbf{k})$. A demonstration of this important property is beyond the scope of this brief discussion: the reader is referred to [26, 27].

2.2.1 Many-Particle Green's Functions

It is possible to generalize the concept of the Green's function to more than one particle. The many-particle Green's function 'propagates' several particles through the system, taking into account the correlations between them. This allows the study of collective effects in a many-body system.

For time-independent, homogeneous and spatially infinite systems, the n-particle Green's function $\mathcal{G}^{(n)}$ is defined as

$$\begin{aligned}\mathcal{G}^{(n)}_{\alpha\ldots\beta\alpha'\gamma'\ldots\beta'}(\mathbf{k}_1\tau_1,\ldots,\mathbf{k}_n\tau_n;\mathbf{k}_2{}'\tau_2{}',\ldots,\mathbf{k}_n{}'\tau_n{}') \\ = (-1)^n\left\langle T_\tau\left[\hat{a}_{\mathbf{k}_1\alpha}(\tau_1)\ldots\hat{a}_{\mathbf{k}_n\beta}(\tau_n)\hat{a}^\dagger_{\mathbf{k}_n{}'\beta'}(\tau_n{}')\ldots\hat{a}^\dagger_{\mathbf{k}_2{}'\gamma'}(\tau_2{}')\hat{a}^\dagger_{\mathbf{k}\alpha'}(0)\right]\right\rangle \end{aligned} \tag{2.22}$$

where $\mathbf{k}=\mathbf{k}_1+\mathbf{k}_2\ldots+\mathbf{k}_n-\mathbf{k}_2{}'-\mathbf{k}_3{}'\ldots-\mathbf{k}_n{}'$. A Fourier representation in each of the τ-variables of the many-particle Green's function may also be developed, and a conjugate many-particle Green's function thereby defined.

2.2.2 The Equation of Motion

The single-particle Green's function obeys an 'equation of motion' in its τ-variable. More precisely, it is the first in an infinite hierarchy of coupled differential equations for the n-particle Green's functions. Although these equations of motion cannot therefore be used to exactly solve for the Green's functions, the hierarchy may be truncated to admit their approximate calculation. Such a method is particularly easy to employ when calculating the Green's function in the self-consistent Hartree-Fock approximation and is further discussed in section 2.4.

From equation 2.16, we have for the single-particle Green's function

$$\mathcal{G}_{\alpha\beta}(\mathbf{k},\tau) = -\theta(\tau)\left\langle\hat{a}_{\mathbf{k}\alpha}(\tau)\hat{a}^\dagger_{\mathbf{k}\beta}(0)\right\rangle+\theta(-\tau)\left\langle\hat{a}^\dagger_{\mathbf{k}\beta}(0)\hat{a}_{\mathbf{k}\alpha}(\tau)\right\rangle \tag{2.23}$$

Taking the derivative of $\mathcal{G}_{\alpha\beta}(\mathbf{k},\tau)$ with respect to τ, we obtain

$$\begin{aligned}\frac{\partial}{\partial\tau}\mathcal{G}_{\alpha\beta}(\mathbf{k},\tau) = &-\theta(\tau)\left\langle\frac{\partial\hat{a}_{\mathbf{k}\alpha}(\tau)}{\partial\tau}\hat{a}^\dagger_{\mathbf{k}\beta}(0)\right\rangle+\theta(-\tau)\left\langle\hat{a}^\dagger_{\mathbf{k}\beta}(0)\frac{\partial\hat{a}_{\mathbf{k}\alpha}(\tau)}{\partial\tau}\right\rangle \\ &-\delta(\tau)\left\langle\left[\hat{a}_{\mathbf{k}\alpha}(\tau),\hat{a}^\dagger_{\mathbf{k}\beta}(0)\right]_+\right\rangle\end{aligned} \tag{2.24}$$

Note that the 'derivative' of the Heaviside step function $\theta(\tau)$ is $\delta(\tau)$. We consider the last term on the RHS of equation 2.24. Since this term vanishes except when $\tau=0$, it is necessary only to calculate the trace for this case. The anticommutator evaluates

$$\left[\hat{a}_{\mathbf{k}\alpha}(0),\hat{a}^\dagger_{\mathbf{k}\beta}(0)\right]_+ = \left[\hat{a}_{\mathbf{k}\alpha},\hat{a}^\dagger_{\mathbf{k}\beta}\right]_+ = \delta_{\alpha\beta} \tag{2.25}$$

Since $\langle\delta_{\alpha\beta}\rangle=\delta_{\alpha\beta}$, we may therefore re-write equation 2.24 as

$$-\frac{\partial}{\partial\tau}\mathcal{G}_{\alpha\beta}(\mathbf{k},\tau) = \delta(\tau)\delta_{\alpha\beta}+\left\langle T_\tau\left[\frac{\partial\hat{a}_{\mathbf{k}\alpha}(\tau)}{\partial\tau}\hat{a}^\dagger_{\mathbf{k}\beta}(0)\right]\right\rangle \tag{2.26}$$

After a simple but tedious calculation yields the equation of motion for the annihilation operator $\hat{a}_{\mathbf{k}\alpha}(\tau)$, we obtain for equation 2.26

$$\begin{aligned}-\frac{\partial}{\partial\tau}\mathcal{G}_{\alpha\beta}(\mathbf{k},\tau) = &\ \delta(\tau)\delta_{\alpha\beta}+(\epsilon_{\mathbf{k}}-\mu)\mathcal{G}_{\alpha\beta}(\mathbf{k},\tau) \\ &+\frac{1}{2V}\sum_{\mathbf{k}_1',\mathbf{k}_2,\mathbf{k}_2'}\sum_{\nu',\eta,\eta'}\left[U_{\eta\alpha\eta'\nu'}(\mathbf{k}_2,\mathbf{k};\mathbf{k}_2',\mathbf{k}_1')-U_{\alpha\eta\eta'\nu'}(\mathbf{k},\mathbf{k}_2;\mathbf{k}_2',\mathbf{k}_1')\right] \\ &\times\left\langle T_\tau\left[\hat{a}^\dagger_{\mathbf{k}_2\eta}(\tau)\hat{a}_{\mathbf{k}_2'\eta'}(\tau)\hat{a}_{\mathbf{k}_1'\nu'}(\tau)\hat{a}^\dagger_{\mathbf{k}\beta}(0)\right]\right\rangle\end{aligned} \tag{2.27}$$

Note that we have interchanged the order of the sum and the trace on the RHS of 2.27: this is possible as the trace and sum are both convergent.

We consider the τ-product on the RHS of equation 2.27. We see that the τ-product of $\hat{a}^\dagger_{\mathbf{k}_2\eta}(\tau)\hat{a}_{\mathbf{k}_2'\eta'}(\tau)\hat{a}_{\mathbf{k}_1'\nu'}(\tau)\hat{a}^\dagger_{\mathbf{k}\beta}(0)$ will be equal to the τ-product of $\hat{a}_{\mathbf{k}_2'\eta'}(\tau)\hat{a}_{\mathbf{k}_1'\nu'}(\tau)\hat{a}^\dagger_{\mathbf{k}_2\eta}(\tau)\hat{a}^\dagger_{\mathbf{k}\beta}(0)$, as

the two products differ by an even number of transpositions of Fermi operators. Thus, we see that

$$\begin{aligned}\left\langle T_\tau\left[\hat{a}^\dagger_{\mathbf{k}_2\eta}(\tau)\hat{a}_{\mathbf{k}'_2\eta'}(\tau)\hat{a}_{\mathbf{k}'_1\nu'}(\tau)\hat{a}^\dagger_{\mathbf{k}\beta}(0)\right]\right\rangle &= \left\langle T_\tau\left[\hat{a}_{\mathbf{k}'_2\eta'}(\tau)\hat{a}_{\mathbf{k}'_1\nu'}(\tau)\hat{a}^\dagger_{\mathbf{k}_2\eta}(\tau)\hat{a}^\dagger_{\mathbf{k}\beta}(0)\right]\right\rangle \\ &= \delta_{\mathbf{k}\,\mathbf{k}'_1+\mathbf{k}'_2-\mathbf{k}_2}\mathcal{G}^{(2)}_{\eta'\nu'\beta\eta}(\mathbf{k}'_2\tau,\mathbf{k}'_1\tau^-_{(1)};\mathbf{k}_2\tau^-_{(2)}) \quad (2.28)\end{aligned}$$

where $\tau^-_{(1)}$ and $\tau^-_{(2)}$ are interpreted respectively as $\lim_{\delta_1\to 0^-}(\tau+\delta_1)$ and $\lim_{\delta_2\to 0^-}(\tau+\delta_2)$ where $\delta_1 > \delta_2$. This notation reminds us that we must always write the product

$$\hat{a}_{\mathbf{k}'_2\eta'}(\tau)\hat{a}_{\mathbf{k}'_1\nu'}(\tau)\hat{a}^\dagger_{\mathbf{k}_2\eta}(\tau)$$

in this order. Substituting equation 2.28 into equation 2.27 and rearranging, we obtain the equation of motion for $\mathcal{G}_{\alpha\beta}(\mathbf{k},\tau)$:

$$\begin{aligned}-\frac{\partial}{\partial\tau}\mathcal{G}_{\alpha\beta}(\mathbf{k},\tau) &= \delta(\tau)\delta_{\alpha\beta} + (\epsilon_{\mathbf{k}}-\mu)\mathcal{G}_{\alpha\beta}(\mathbf{k},\tau) \\ &+\frac{1}{2V}\sum_{\mathbf{k}'_1,\mathbf{k}'_2}\sum_{\nu',\eta,\eta'}\left[U_{\eta\alpha\eta'\nu'}(\mathbf{k}'_1+\mathbf{k}'_2-\mathbf{k},\mathbf{k};\mathbf{k}'_2,\mathbf{k}'_1) - U_{\alpha\eta\eta'\nu'}(\mathbf{k},\mathbf{k}'_1+\mathbf{k}'_2-\mathbf{k};\mathbf{k}'_2,\mathbf{k}'_1)\right] \\ &\times\mathcal{G}^{(2)}_{\eta'\nu'\beta\eta}(\mathbf{k}'_2\tau,\mathbf{k}'_1\tau^-_{(1)};\mathbf{k}'_1+\mathbf{k}'_2-\mathbf{k}\tau^-_{(2)}) \quad (2.29)\end{aligned}$$

where we have used the Kronecker-delta in equation 2.28 to eliminate the summation over $\mathbf{k}_2$.

In order to solve equation 2.29 for $\mathcal{G}_{\alpha\beta}(\mathbf{k},\tau)$ we must have the two-particle Green's function. An expression for the two-particle Green's function may be obtained by solving its equation of motion, which may be derived by following a procedure essentially identical to that outlined above. In general, however, this will involve both single- and three-particle Green's functions. We therefore require the three-particle Green's function: its equation of motion, however, involves the four-particle Green's function. Continuing this argument, we obtain an infinite hierarchy of coupled differential equations for the Green's functions, with the differential equation for the n-particle Green's function coupled to those of the $(n-1)$- and $(n+1)$-particle Green's functions. It is, however, possible to truncate the series in a controlled and well-defined manner at, say, the m-particle Green's function $\mathcal{G}^{(m)}$. This yields a finite set of coupled differential equations for the one-, two-, three-,...m-particle Green's functions [30].

2.2.3 Relation to Observables

For a homogeneous, spatially infinite and time-independent system, an arbitrary single-particle operator $\hat{J}$ may be written in the Schrödinger picture as

$$\hat{J} = \sum_{\mathbf{k},\alpha,\beta} J_{\beta\alpha}(\mathbf{k})\hat{a}^\dagger_{\mathbf{k}\beta}\hat{a}_{\mathbf{k}\alpha} = \sum_{\mathbf{k},\alpha,\beta} J_{\beta\alpha}(\mathbf{k})\hat{a}^\dagger_{\mathbf{k}\beta}(0)\hat{a}_{\mathbf{k}\alpha}(0) \quad (2.30)$$

where $J_{\beta,\alpha}(\mathbf{k})$ is the operator in first-quantization representation. The ensemble average of $\hat{J}$ is given by equation 2.4:

$$\langle\hat{J}\rangle = \sum_{\mathbf{k},\alpha,\beta} J_{\beta\alpha}(\mathbf{k})\left\langle\hat{a}^\dagger_{\mathbf{k}\beta}(0)\hat{a}_{\mathbf{k}\alpha}(0)\right\rangle \quad (2.31)$$

From equation 2.16 it is easy to see that

$$\mathcal{G}_{\alpha\beta}(\mathbf{k},0^-) = \lim_{\tau\to 0^-}\mathcal{G}_{\alpha\beta}(\mathbf{k},\tau) = \left\langle\hat{a}^\dagger_{\mathbf{k}\beta}(0)\hat{a}_{\mathbf{k}\alpha}(0)\right\rangle \quad (2.32)$$

Substituting equation 2.32 into equation 2.31, the ensemble average $\langle\hat{J}\rangle$ is rewritten as

$$\langle\hat{J}\rangle = \sum_{\mathbf{k},\alpha,\beta} J_{\beta\alpha}(\mathbf{k})\mathcal{G}_{\alpha\beta}(\mathbf{k},0^-) = \sum_{\mathbf{k}}\mathrm{Tr}\left\{\mathbf{J}(\mathbf{k})\mathbf{G}(\mathbf{k},0^-)\right\} \quad (2.33)$$

where $\mathbf{G}(\mathbf{k},\tau)$ is the single-particle matrix Green's function of the system and $\mathbf{J}(\mathbf{k})$ is the first quantization operator as a matrix in its spin-indices.

The ensemble average of any n-particle operator may be calculated from the n-particle Green's function via a natural extension of the method outlined above for the single-particle case.

2.3 Wick's Theorem

For operators with τ-dependence as given by the Heisenberg picture (equation 2.7), Wick's theorem holds only for non-interacting systems (i.e. $\hat{K}_1 = 0$). In the following, the subscript '0' will denote that the expression refers to the non-interacting system. The theorem concerns the evaluation of expressions of the form

$$\mathrm{Tr}\left\{\hat{\rho}_{G0}T_\tau\left[\hat{A}(\tau_A)\hat{B}(\tau_B)\hat{C}(\tau_C)\ldots\hat{F}(\tau_F)\right]\right\} \tag{2.34}$$

where $\hat{\rho}_{G0} = \exp(\beta[\Omega_0 - \hat{K}_0])$ and the $\hat{A},\hat{B},\hat{C},\ldots,\hat{F}$ are a set of an even number of creation and annihilation operators, each with its own τ-variable. The contraction of two such operators is defined by

$$\hat{A}^{\cdot}\hat{B}^{\cdot} \;=\; \mathrm{Tr}\left\{\hat{\rho}_{G0}T_\tau\left[\hat{A}\hat{B}\right]\right\} \tag{2.35}$$

Of particular note are the results

$$\begin{aligned} \hat{a}_{\mathbf{k}\alpha}(\tau)^{\cdot}\hat{a}_{\mathbf{k}'\beta}(\tau')^{\cdot} &= \hat{a}^\dagger_{\mathbf{k}\alpha}(\tau)^{\cdot}\hat{a}^\dagger_{\mathbf{k}'\beta}(\tau')^{\cdot} = 0 \\ -\hat{a}_{\mathbf{k}\alpha}(\tau)^{\cdot}\hat{a}^\dagger_{\mathbf{k}'\beta}(\tau')^{\cdot} &= \hat{a}^\dagger_{\mathbf{k}'\beta}(\tau')^{\cdot}\hat{a}_{\mathbf{k}\alpha}(\tau)^{\cdot} = \delta_{\mathbf{k}\mathbf{k}'}\mathcal{G}^0_{\alpha\beta}(\mathbf{k},\tau-\tau') \end{aligned} \tag{2.36}$$

where $\mathcal{G}^0_{\alpha\beta}$ is the single-particle Green's function of the non-interacting system.

The generalized Wick's theorem states that equation 2.34 is equal to the sum of all possible contractions of the operators $\hat{A},\hat{B},\hat{C},\ldots,\hat{F}$, i.e.

$$\begin{aligned} &\mathrm{Tr}\left\{\hat{\rho}_{G0}T_\tau\left[\hat{A}(\tau_A)\hat{B}(\tau_B)\hat{C}(\tau_C)\ldots\hat{F}(\tau_F)\right]\right\} \\ &\quad= \hat{A}^{\cdot}\hat{B}^{\cdot}\hat{C}^{\cdot\cdot}\hat{D}^{\cdot\cdot}\ldots\hat{F}^{\cdot\cdot} + \hat{A}^{\cdot}\hat{B}^{\cdot\cdot}\hat{C}^{\cdot}\hat{D}^{\cdot\cdot}\ldots\hat{F}^{\cdot\cdot} + \hat{A}^{\cdot}\hat{B}^{\cdot\cdot}\hat{C}^{\cdot\cdot}\hat{D}^{\cdot}\ldots\hat{F}^{\cdot\cdot} + \ldots \end{aligned} \tag{2.37}$$

where the terms of the form $\hat{A}^{\cdot}\hat{B}^{\cdot\cdot}\hat{C}^{\cdot}\ldots\hat{E}^{\cdot\cdot}\ldots\hat{F}^{\cdot\cdot}$ are to be interpreted as $(-1)^p\hat{A}^{\cdot}\hat{C}^{\cdot}\hat{B}^{\cdot\cdot}\hat{E}^{\cdot\cdot}\ldots\hat{F}^{\cdot\cdot}$ where p is the number of transpositions of the operators required to transform the ordering $\hat{A}\hat{B}\hat{C}\ldots\hat{E}\ldots\hat{F}$ into $\hat{A}\hat{C}\hat{B}\hat{E}\ldots\hat{F}$.

2.4 The Self-Consistent Hartree-Fock Approximation

Although much important information about a many-body system may be extracted from its single-particle Green's functions, the exact calculation of these functions for even the simplest interacting systems is very difficult. It is therefore common to make some simplifying assumptions regarding the interactions between the particles. The most basic of these is the self-consistent Hartree-Fock (SCHF) or 'mean field' approximation.

In a non-interacting system, each particle occupies a definite single-particle state. In an interacting system, however, the notion of each particle having an individual state is no longer strictly tenable: the interactions may correlate the behaviour of groups of particles, causing them to act collectively. Despite this, the single-particle picture provides a remarkably good description of many condensed-matter systems. Such systems are typically well characterized by the SCHF approximation, which neglects all dynamical correlations between individual particles [25, 26]. The SCHF approximation retains the single-particle picture by treating the inter-particle interactions as producing an effective single-particle potential in which the individual particles move. This potential (the so-called 'mean field') constitutes the average interaction experienced between a particle and the rest of the system.

In the SCHF approximation, a particle propagates through the system essentially independently of the other particles. We may therefore expect to be able to express the two-particle Green's function in terms of the single-particle Green's functions. We do this by assuming that we may apply Wick's theorem to the interacting system; that is, we may replace $\hat{\rho}_{G0}$ in the formulas 2.34, 2.36 and 2.37 by the interacting system's statistical operator $\hat{\rho}_G$. Therefore, by the definition of the two-particle Green's function, we have

$$\begin{aligned}
\mathcal{G}^{(2)}_{\alpha\beta\gamma\delta}(\mathbf{k}_1\tau_1,\mathbf{k}_2\tau_2;\mathbf{k}_2'\tau_2') &= \mathrm{Tr}\left\{\hat{\rho}_G T_\tau\left[\hat{a}_{\mathbf{k}_1\alpha}(\tau_1)\hat{a}_{\mathbf{k}_2\beta}(\tau_2)\hat{a}^\dagger_{\mathbf{k}_2'\delta}(\tau_2')\hat{a}^\dagger_{\mathbf{k}_1+\mathbf{k}_2-\mathbf{k}_2'\gamma}(0)\right]\right\} \\
&\approx \hat{a}_{\mathbf{k}_1\alpha}(\tau_1)\dot{}\,\hat{a}_{\mathbf{k}_2\beta}(\tau_2)\dot{}\,\hat{a}^\dagger_{\mathbf{k}_2'\delta}(\tau_2')\ddot{}\,\hat{a}^\dagger_{\mathbf{k}_1+\mathbf{k}_2-\mathbf{k}_2'\gamma}(0)\ddot{} \\
&\quad -\hat{a}_{\mathbf{k}_1\alpha}(\tau_1)\dot{}\,\hat{a}^\dagger_{\mathbf{k}_2'\delta}(\tau_2')\dot{}\,\hat{a}_{\mathbf{k}_2\beta}(\tau_2)\ddot{}\,\hat{a}^\dagger_{\mathbf{k}_1+\mathbf{k}_2-\mathbf{k}_2'\gamma}(0)\ddot{} \\
&\quad +\hat{a}_{\mathbf{k}_1\alpha}(\tau_1)\dot{}\,\hat{a}^\dagger_{\mathbf{k}_1+\mathbf{k}_2-\mathbf{k}_2'\gamma}(0)\dot{}\,\hat{a}_{\mathbf{k}_2\beta}(\tau_2)\ddot{}\,\hat{a}^\dagger_{\mathbf{k}_2'\delta}(\tau_2')\ddot{} \qquad (2.38) \\
&\approx \delta_{\mathbf{k}_2\mathbf{k}_2'}\mathcal{G}_{\alpha\gamma}(\mathbf{k}_1,\tau_1)\mathcal{G}_{\beta\delta}(\mathbf{k}_2,\tau_2-\tau_2') \\
&\quad -\delta_{\mathbf{k}_1\mathbf{k}_2'}\mathcal{G}_{\alpha\delta}(\mathbf{k}_1,\tau_1-\tau_2')\mathcal{G}_{\beta\gamma}(\mathbf{k}_2,\tau_2) \qquad (2.39)
\end{aligned}$$

where we have used the results 2.36 in going from 2.38 to 2.39. The importance of the relation 2.39 lies in its use to decouple the equation of motion for $\mathcal{G}_{\alpha\beta}(\mathbf{k},\tau)$ from the hierarchy: substituting equation 2.39 into equation 2.29 we obtain a linear differential equation in τ for the single-particle Green's function.

2.4.1 The High-Density Approximation

The density of a system is characterized by the dimensionless parameter r_s, defined by

$$V = \frac{4}{3}\pi(r_s a_0)^3 N \qquad (2.40)$$

where a_0 is the Bohr radius and N is the number of particles in the volume V. It is clear from 2.40 that the distance $r_s a_0$ may be interpreted as the interparticle spacing. The SCHF approximation yields asymptotically correct results in the high density limit $r_s \to 0$. Although correlation effects might be expected to be of great importance in this limit, screening by the other particles reduces the range of the two-body interactions to $\sim r_s a_0$ [31]. As particles separated by more than the average interparticle distance interact only very weakly, the correlations in their motion should be correspondingly small. This may be illustrated by the homogeneous electron gas: assuming only Coulomb interactions between the electrons, the interaction energy in the SCHF approximation goes as r_s^{-1}, whereas the corrections introduced by considering interparticle correlations are of order $\ln(r_s)$ [26, 28]. We therefore see that correlation effects are still significant at high density, but their contribution to the total energy of the system is dominated by the SCHF contribution. The SCHF approximation must accordingly be expected to give good results in the limit of very high densities only.

The high density limit may also be interpreted as equivalent to the limit of very short-range two-body interactions. As mentioned above, screening effects limit the range of the interparticle potentials to approximately the interparticle spacing. The limiting case of infinite density therefore corresponds to δ-function interaction potentials in coordinate-space. This greatly reduces the complexity of the interaction Hamiltonian $\hat{K}_1$, as the two-body interaction potential $U_{\nu\eta\eta'\nu'}(\mathbf{k}_1,\mathbf{k}_2;\mathbf{k}_2',\mathbf{k}_1')$ is constant in its momentum-arguments. Treating the two-body interactions as having zero range constitutes the so-called high-density approximation. Unfortunately, the value of r_s typically ranges between 2 and 6 in metals, and so the limit $r_s \to 0$ gives a poor description of the band-electron density in realistic systems [1]. In spite of this objection, the results of calculations in the high density approximation give remarkably good agreement with experiment for the systems here considered. In what follows, we shall therefore always work in the high-density SCHF approximation.

2.5 Phase Transitions in Fermi Systems

The work that follows will be exclusively concerned with systems that differ radically from the free electron gas (the so-called normal phase). Such systems arise from the normal phase due to the presence of interactions which cause the normal phase to become unstable. As a result of this instability, there is a phase transition to a new stable phase. The new phase is fundamentally different to the original: it cannot be obtained from the normal phase by any order of perturbation theory [30]. Rather, the system is said to be 'rebuilt' by the phase transition [27]. The nature of this 'rebuilding' gives rise to the important differences between the two phases.

The study of phase transitions in many-body systems has a long and distinguished history, touching every aspect of condensed-matter physics. A summary of the major results of this field is therefore beyond the scope of this work. We instead introduce the reader to three concepts of importance to the following analysis: the order parameter; the determination of the energetically stable phase in a system; and the $T = 0$ limit.

2.5.1 The Order Parameter

The transition from the normal phase to each of the phases studied below are all examples of second-order phase transitions. It was first realized by Landau that such phase transitions are characterized by the breaking of some symmetry of the system [32]. This is best illustrated by the paramagnet-ferromagnet transition, the classic example of a second-order transition (see also chapter 4). In the paramagnetic (normal) phase, the microscopic spins in the system are randomly oriented; the appearance of ferromagnetism may be characterized at the microscopic level by the alignment of these spins in one direction, breaking the translational symmetry of the system. We note that the symmetry broken by the phase transition can be much more abstract, such as time-reversal or gauge-invariance.

The symmetry exhibited by a system is a purely qualitative feature: it cannot be broken gradually, but only abruptly at some fixed values of the relevant thermodynamic variables. Landau's achievement was to demonstrate that second-order transitions could also be characterized by the so-called order parameter. This parameter is only non-zero in the symmetry breaking phase, vanishing continuously as the boundary with the normal phase is approached in the phase diagram. It may be a microscopic or macroscopic property of the system, and is not limited to directly observable quantities. For example, in the macroscopic description of the paramagnet-ferromagnet transition, the order parameter is the magnetization; for the BCS superconductor, it is a feature of the 'rebuilt' electronic excitation spectrum (see chapter 3). The order parameter concept may also be generalized to a set of different quantities, each of which must be non-zero for the new phase to be realized.

2.5.2 Energetic Stability

In order to determine whether a particular phase is realized or not, it is necessary to assess its stability relative to all other possible phases. As the system always attempts to adopt the state which minimizes its free energy F, the new phase will be realized as an energetically stable state if its free energy is less than that of any other possible phase.

We modify the definition 2.9 of the grand canonical Hamiltonian by introducing a variable coupling constant $0 \leq \lambda \leq 1$ which controls the strength of the two-body interaction:

$$\hat{K}(\lambda) \;=\; \hat{K}_0 + \lambda \hat{K}_1 \tag{2.41}$$

When $\lambda = 0$ in equation 2.41 we have the simple non-interacting case; when $\lambda = 1$ we recover the grand canonical Hamiltonian for the fully-interacting system. Thus, increasing λ from zero to one gradually "turns on" the interaction. By the finite-temperature Feynman-Pauli theorem [26, 28] we have

$$\frac{\partial F_\lambda}{\partial \lambda} \;=\; \frac{1}{V} \frac{\langle \lambda \hat{K}_1 \rangle_\lambda}{\lambda} \tag{2.42}$$

where $\langle \ldots \rangle_\lambda$ is the ensemble average and F_λ the free energy per unit volume for the system described by $\hat{K}(\lambda)$. Integrating equation 2.42 with respect to λ, we obtain

$$\delta F = \frac{1}{V} \int_0^1 \frac{d\lambda}{\lambda} \langle \lambda \hat{K}_1 \rangle_\lambda \tag{2.43}$$

where $\delta F = F_1 - F_0$ is the free energy change per unit volume of the system produced by "turning on" the interaction term $\hat{K}_1$. The new phase will be stable relative to the old if $\delta F < 0$.

2.5.3 The Zero Temperature Limit

In the preceding discussion we have developed the Matsubara finite-temperature formalism for the quantum field theory of the many-body problem. A distinct zero temperature formalism may also be developed, but for obvious reasons it is much less versatile than the finite temperature equivalent [26]. Although we shall utilize the (simpler) finite temperature formalism in the following work, we shall restrict our analysis to the limit of zero temperature ($\beta = (k_B T)^{-1} \to \infty$).

This dichotomous approach is motivated by the nature of the 'rebuilt' phases considered, and also economy in calculation. In all cases, the 'rebuilt' phases are due to purely quantum effects, which are disrupted by thermal fluctuations at finite temperature. Above a certain critical temperature, these thermal fluctuations dominate, and the systems undergoes a phase transition into the normal phase. In order to study the 'rebuilt' phase at its most stable, therefore, it is necessary to study it at zero temperature: if it is not realized in this limit, it is highly unlikely to be realized at all. Because of the absence of thermal fluctuations, the physics of the 'rebuilt' systems is most transparently revealed in the zero temperature limit. Hence, the motivation for working in the (unphysical) zero temperature regime. The motivation for using the finite-temperature formalism in our calculations is due to considerations of economy: not only can we easily recover the zero temperature behaviour by simply taking the $\beta \to \infty$ limit, we may also later return to our calculations in order to study the finite temperature behaviour of the system, instead of having to recalculate from first principles.

Superconductivity

Since its discovery by Kamerlingh Onnes in 1911, superconductivity has provided a constant challenge to theories of the solid state. A successful microscopic explanation for the remarkable properties of the superconductor was only arrived at in 1957 with the publication of the Bardeen-Cooper-Schrieffer (BCS) theory. The behaviour of most low-temperature superconductors is excellently accounted for by the BCS scheme. We will only be concerned with such 'traditional' superconducting systems in this work. The mechanism responsible for the amazing properties of the high-temperature superconductors and the so-called heavy-fermion systems is still yet to be found: what is certain is that the BCS theory in its original form cannot provide it [29].

Below a certain critical temperature $T_{\rm S} \sim 1$K, the behaviour of a superconductor exhibits many remarkable features which distinguish them from normal conductors. The most striking of these are

- superconductivity: a superconductor can carry DC currents less than some critical current $\mathbf{j}_{\rm S}$ without electrical resistance.
- perfect diamagnetism: in the presence of a magnetic field of strength less than some critical value $H_{\rm S}$, a superconductor carries a surface current that precisely cancels the field in the bulk. Above the critical field, superconductivity disappears.
- energy gap: there is a 'gap' in the spectrum of allowed one-electron levels centred about the Fermi energy ϵ_F. It is evidence that superconductivity arises only from electrons within a thin shell about the Fermi surface, the "superconducting shell" [30].

In the ensuing discussion, we will only address the third point; the other (more familiar) two require a prohibitively sophisticated treatment. The implications of the second point, however, will be considered in chapter 4. In this chapter, we provide an elementary review of the BCS theory (section 3.1) before considering the quantum field theoretic treatment of the model BCS superconductor (sections 3.2, 3.3 and 3.4).

3.1 Elementary BCS Theory

The basic mechanism responsible for traditional superconductivity is the attractive interaction between the band electrons and the positive ions in the crystal lattice. As an electron moves through the solid, it attracts the nearest ions towards it, creating a region of enhanced ion charge density. This polarization of the lattice tends to attract other electrons, producing an indirect attractive electron-electron interaction. This interaction may be modelled as the exchange of a "virtual" phonon between the two electrons, a process described by the well-known Frölich Hamiltonian [26]. For our purposes, the most important feature of the Frölich Hamiltonian is that the exchange of a "virtual" phonon yields an attractive interaction between two electrons with kinetic energies differing by less than $\sim \omega_D$ (the characteristic phonon or Debye energy). Of course, the net interaction between two electrons includes repulsive terms, such as the screened Coulomb interaction. In non-superconducting substances, these dominate. For superconductors, however, the inter-electron interaction due to "virtual" phonon exchange is unusually strong. In

particular, for the very small energy differences between electrons within the "superconducting shell", the net interaction is attractive [31].

The presence of attractive interactions between electrons sufficiently near the Fermi surface suggests the possibility of forming bound electron pairs. In his famous 1956 paper, Cooper demonstrated that this was indeed true for two interacting electrons just above the Fermi surface [2]. By the Pauli exclusion principle, the two interacting electrons cannot scatter into states below the Fermi energy, limiting them to energy states $> \epsilon_F$. For arbitrarily weak attractive interactions, however, the binding energy of the two electrons is lower than the Fermi energy, and so the bound state is realized. This bound pair is most stable when the constituent electrons have opposite momenta and spins. Such a "quasimolecule" is known as the Cooper pair.

The connection between Cooper's two-body problem and superconductivity was made by Bardeen, Cooper and Schrieffer in the following year [3, 4]. The authors extended Cooper's idea to the entire "superconducting shell", constructing a new ground state of the system on the assumption that all these electrons formed Cooper pairs in the superconducting phase. By a simple variational calculation, it was determined that this new ground state had a lower energy than the original. The BCS ground state is characterized by the macroscopic occupation of a single Cooper pair energy state, in analogy to Bose-Einstein condensation. This Cooper pair 'condensate' carries the supercurrent, and it is ultimately responsible for the many remarkable properties of superconductors.

In the detailed quantum field theoretic description of the BCS system that follows, we will not utilize the approach adopted in the original BCS papers. The authors' use of a canonical transformation to construct the BCS ground state is cumbersome and difficult to generalize to more complicated systems. Rather, we employ the elegant approach due to Gor'kov, which is based upon the methods outlined in chapter 2 [33].

3.2 The Model System

Although the exact form of the effective interaction for electrons near the Fermi surface is unknown, it may be well approximated by a negative constant, $\lambda < 0$ say. We therefore may describe the system by the model Hamiltonian [29]:

$$\hat{K} = \sum_{\mathbf{k}',\nu} \xi_{\mathbf{k}'} \hat{a}^\dagger_{\mathbf{k}'\nu} \hat{a}_{\mathbf{k}'\nu} + \frac{\lambda}{2V} \sum_{\mathbf{k}',\mathbf{k}''} \sum_{\nu,\nu'} \hat{a}^\dagger_{\mathbf{k}'\nu} \hat{a}^\dagger_{-\mathbf{k}'\nu'} \hat{a}_{\mathbf{k}''\nu'} \hat{a}_{-\mathbf{k}''\nu} \tag{3.1}$$

where $\xi_{\mathbf{k}}$ are the single-particle (kinetic) energies in the normal phase. It is convenient to define the Fermi energy by $\xi_{\mathbf{k}} = 0$. As electrons with energies lying outside the narrow "superconducting shell" do not participate in the Cooper-pairing, we regard λ as vanishing for processes where $|\xi_{\mathbf{k}}|$, $|\xi_{\mathbf{k}'}| > \varpi$, some "cut-off" on the order of ω_D.

It is quite obvious that Cooper-pairing must cause the motion of the electrons involved to become highly correlated. As such, it would seem that the SCHF approximation is fundamentally unsuitable for a description of a superconductor. This difficulty may be overcome, however, by dividing the system into two components: the Cooper pair condensate, for which correlation effects are of essential importance; and the 'uncondensed' part, consisting of the unbound electrons, to which the SCHF approximation may be applied. In modelling the behaviour of the uncondensed part, we consider the Cooper pair condensate as acting like a reservoir into and from which two electrons with opposite momenta and spins are scattered upon the formation or destruction of a Cooper pair respectively. To account for this, the so-called Gor'kov Green's functions [27, 33] are introduced in addition to the standard one-particle Green's functions:

$$\mathcal{F}_{\alpha\beta}(\mathbf{k},\tau) = \langle T_\tau \left[\hat{a}_{\mathbf{k}\alpha}(\tau)\hat{a}_{-\mathbf{k}\beta}(0)\right]\rangle \tag{3.2}$$

$$\mathcal{F}^\dagger_{\alpha\beta}(\mathbf{k},\tau) = \left\langle T_\tau \left[\hat{a}^\dagger_{-\mathbf{k}\alpha}(\tau)\hat{a}^\dagger_{\mathbf{k}\beta}(0)\right]\right\rangle \tag{3.3}$$

$\mathcal{F}_{\alpha\beta}(\mathbf{k},\tau)$ and $\mathcal{F}^\dagger_{\alpha\beta}(\mathbf{k},\tau)$ describe the scattering of an electron pair into and out of the reservoir

respectively. They are therefore off-diagonal in their spin-indices. In the normal phase, these functions are vanishing as there is no Cooper pair reservoir.

3.3 The Equations of Motion

After a straightforward calculation, the equation of motion of the Green's function $\mathcal{G}_{\uparrow\uparrow}(\mathbf{k},\tau)$ for the model system 3.1 is obtained:

$$\begin{aligned} -\frac{\partial}{\partial\tau}\mathcal{G}_{\uparrow\uparrow}(\mathbf{k},\tau) &= \delta(\tau)+\xi_{\mathbf{k}}\mathcal{G}_{\uparrow\uparrow}(\mathbf{k},\tau) \\ &\quad +\frac{\lambda}{2V}\sum_{\mathbf{k}'',\nu}\left[\mathcal{G}^{(2)}_{\uparrow\nu\uparrow\nu}(\mathbf{k}''\tau,-\mathbf{k}''\tau^-_{(1)};-\mathbf{k}\tau^-_{(2)})-\mathcal{G}^{(2)}_{\nu\uparrow\uparrow\nu}(\mathbf{k}''\tau,-\mathbf{k}''\tau^-_{(1)};-\mathbf{k}\tau^-_{(2)})\right] \end{aligned} \tag{3.4}$$

We consider the decomposition of the two-particle Green's functions in equation 3.4. The standard SCHF decomposition, however, does not account for the presence of the Gor'kov Green's functions. In order to do so, we retain the extra term in the decomposition 2.38:

$$\begin{aligned} \mathcal{G}^{(2)}_{\alpha\beta\gamma\delta}(\mathbf{k}_1\tau_1,\mathbf{k}_2\tau_2;\mathbf{k}'_2\tau'_2) \approx\ & \delta_{\mathbf{k}_1+\mathbf{k}_20}\mathcal{F}_{\alpha\beta}(\mathbf{k}_1,\tau_1-\tau_2)\mathcal{F}^\dagger_{\delta\gamma}(-\mathbf{k}'_2,\tau'_2) \\ &+\delta_{\mathbf{k}_2\mathbf{k}'_2}\mathcal{G}_{\beta\delta}(\mathbf{k}_2,\tau_2-\tau'_2)\mathcal{G}_{\alpha\gamma}(\mathbf{k}_1,\tau_1) \\ &-\delta_{\mathbf{k}_1\mathbf{k}'_2}\mathcal{G}_{\alpha\delta}(\mathbf{k}_1,\tau_1-\tau'_2)\mathcal{G}_{\beta\gamma}(\mathbf{k}_2,\tau_2) \end{aligned} \tag{3.5}$$

The extra term describes the coupling of the normal part to the Cooper pair condensate: it is only present when the system is in the superconducting phase. Following convention [27, 29, 33], we keep only this term in the expansion of the two-particle Green's functions in 3.4. Including the other terms leads to a renormalization of the single-particle excitation spectrum. This contributes very little to the physical description of the superconductor, whilst significantly complicating the equations, obscuring the important differences between the superconducting and the normal phases. We therefore have

$$-\frac{\partial}{\partial\tau}\mathcal{G}_{\uparrow\uparrow}(\mathbf{k},\tau) = \delta(\tau)+\xi_{\mathbf{k}}\mathcal{G}_{\uparrow\uparrow}(\mathbf{k},\tau)+\frac{\lambda}{2V}\sum_{\mathbf{k}''}\left[\mathcal{F}_{\uparrow\downarrow}(\mathbf{k}'',0^+)-\mathcal{F}_{\downarrow\uparrow}(\mathbf{k}'',0^+)\right]\mathcal{F}^\dagger_{\downarrow\uparrow}(\mathbf{k},\tau) \tag{3.6}$$

We define the BCS gap Σ as

$$\Sigma = -\frac{\lambda}{2V}\sum_{\mathbf{k}'}\left[\mathcal{F}_{\uparrow\downarrow}(\mathbf{k}',0^+)-\mathcal{F}_{\downarrow\uparrow}(\mathbf{k}',0^+)\right] \tag{3.7}$$

As is standard for this simple analysis, we assume that Σ is real [26]. The gap Σ is the order parameter for the superconducting state. We therefore have for the equation of motion of $\mathcal{G}_{\uparrow\uparrow}(\mathbf{k},\tau)$

$$\left(-\frac{\partial}{\partial\tau}-\xi_{\mathbf{k}}\right)\mathcal{G}_{\uparrow\uparrow}(\mathbf{k},\tau)+\Sigma\mathcal{F}^\dagger_{\downarrow\uparrow}(\mathbf{k},\tau) = \delta(\tau) \tag{3.8}$$

In order to solve 3.8, we must obtain the equation of motion for $\mathcal{F}^\dagger_{\downarrow\uparrow}(\mathbf{k},\tau)$. This is carried out in precise analogy to that for the standard Green's function in subsection 2.2.2:

$$-\frac{\partial}{\partial\tau}\mathcal{F}^\dagger_{\downarrow\uparrow}(\mathbf{k},\tau) = -\delta(\tau)\left\langle\left[\hat{a}^\dagger_{-\mathbf{k}\downarrow}(\tau),\hat{a}^\dagger_{\mathbf{k}\uparrow}(0)\right]_+\right\rangle-\left\langle T_\tau\left[\frac{\partial\hat{a}^\dagger_{-\mathbf{k}\downarrow}(\tau)}{\partial\tau}\hat{a}^\dagger_{\mathbf{k}\uparrow}(0)\right]\right\rangle \tag{3.9}$$

The anticommutator of course evaluates to zero; we therefore have

$$-\frac{\partial}{\partial\tau}\mathcal{F}^\dagger_{\downarrow\uparrow}(\mathbf{k},\tau) = -\xi_{\mathbf{k}}\mathcal{F}^\dagger_{\downarrow\uparrow}(\mathbf{k},\tau)-\frac{\lambda}{2V}\sum_{\mathbf{k}',\nu}\left\{\left\langle T_\tau\left[\hat{a}^\dagger_{\mathbf{k}'\downarrow}(\tau)\hat{a}^\dagger_{-\mathbf{k}'\nu}(\tau^-_{(1)})\hat{a}_{\mathbf{k}\nu}(\tau^-_{(2)})\hat{a}^\dagger_{\mathbf{k}\uparrow}(0)\right]\right\rangle\right.$$

$$-\left\langle T_\tau\left[\hat{a}^\dagger_{\mathbf{k}'\nu}(\tau)\hat{a}^\dagger_{-\mathbf{k}'\downarrow}(\tau^-_{(1)})\hat{a}_{\mathbf{k}\nu}(\tau^-_{(2)})\hat{a}^\dagger_{\mathbf{k}\uparrow}(0)\right]\right\rangle\Big\} \tag{3.10}$$

We use Wick's theorem to decompose the τ-products into products of the single particle and Gor'kov Green's functions:

$$\begin{aligned}\left\langle T_\tau\left[\hat{a}^\dagger_{\mathbf{k}'\downarrow}(\tau)\hat{a}^\dagger_{-\mathbf{k}'\nu}(\tau^-_{(1)})\hat{a}_{\mathbf{k}\nu}(\tau^-_{(2)})\hat{a}^\dagger_{\mathbf{k}\uparrow}(0)\right]\right\rangle &\approx -\mathcal{F}^\dagger_{\downarrow\nu}(-\mathbf{k}',0^+)\mathcal{G}_{\nu\uparrow}(\mathbf{k},\tau)+\ldots\\ \left\langle T_\tau\left[\hat{a}^\dagger_{\mathbf{k}'\nu}(\tau)\hat{a}^\dagger_{-\mathbf{k}'\downarrow}(\tau^-_{(1)})\hat{a}_{\mathbf{k}\nu}(\tau^-_{(2)})\hat{a}^\dagger_{\mathbf{k}\uparrow}(0)\right]\right\rangle &\approx -\mathcal{F}^\dagger_{\nu\downarrow}(-\mathbf{k}',0^+)\mathcal{G}_{\nu\uparrow}(\mathbf{k},\tau)+\ldots\end{aligned}$$

As before, we keep only the term which describes the coupling to the Cooper pair condensate. Substituting these decompositions into the equation of motion 3.10 and using the identities

$$\begin{aligned}\mathcal{F}^\dagger_{\alpha\beta}(-\mathbf{k},0^+) &= \left\langle\hat{a}^\dagger_{\mathbf{k}\alpha}\hat{a}^\dagger_{-\mathbf{k}\beta}\right\rangle = -\left\langle\hat{a}^\dagger_{-\mathbf{k}\beta}\hat{a}^\dagger_{\mathbf{k}\alpha}\right\rangle = -\mathcal{F}^\dagger_{\beta\alpha}(\mathbf{k},0^+)\\ \mathcal{F}^\dagger_{\alpha\beta}(\mathbf{k},0^+) &= \left\langle\hat{a}^\dagger_{-\mathbf{k}\alpha}\hat{a}^\dagger_{\mathbf{k}\beta}\right\rangle = \langle\hat{a}_{\mathbf{k}\beta}\hat{a}_{-\mathbf{k}\alpha}\rangle^* = (\mathcal{F}_{\beta\alpha}(\mathbf{k},0^+))^*\end{aligned} \tag{3.11}$$

we obtain

$$-\frac{\partial}{\partial\tau}\mathcal{F}^\dagger_{\downarrow\uparrow}(\mathbf{k},\tau) = -\xi_{\mathbf{k}}\mathcal{F}^\dagger_{\downarrow\uparrow}(\mathbf{k},\tau)+\frac{\lambda}{2V}\sum_{\mathbf{k}'}\left[\left(\mathcal{F}_{\uparrow\downarrow}(\mathbf{k}',0^+)\right)^*-\left(\mathcal{F}_{\downarrow\uparrow}(\mathbf{k}',0^+)\right)^*\right]\mathcal{G}_{\uparrow\uparrow}(\mathbf{k},\tau) \tag{3.12}$$

We recognize the coefficient of $\mathcal{G}_{\uparrow\uparrow}(\mathbf{k},\tau)$ in equation 3.12 as the negative complex conjugate of the BCS gap. But Σ is assumed real, and so $\Sigma^* = \Sigma$. We hence have for the equation of motion of $\mathcal{F}^\dagger_{\downarrow\uparrow}(\mathbf{k},\tau)$ in more compact form

$$\left(-\frac{\partial}{\partial\tau}+\xi_{\mathbf{k}}\right)\mathcal{F}^\dagger_{\downarrow\uparrow}(\mathbf{k},\tau)+\Sigma\mathcal{G}_{\uparrow\uparrow}(\mathbf{k},\tau) = 0 \tag{3.13}$$

We therefore have a set of coupled differential equations for $\mathcal{G}_{\uparrow\uparrow}(\mathbf{k},\tau)$ and $\mathcal{F}^\dagger_{\downarrow\uparrow}(\mathbf{k},\tau)$ (equations 3.8 and 3.13). Coupled differential equations may also be obtained for $\mathcal{G}_{\downarrow\downarrow}(\mathbf{k},\tau)$ and $\mathcal{F}^\dagger_{\uparrow\downarrow}(\mathbf{k},\tau)$ which, up to sign of Σ, are identical in form to the above equations.

The coupled differential equations 3.8 and 3.13 are solved by taking the Fourier transform to the conjugate ω-space in order to obtain the algebraic system

$$\begin{aligned}(i\omega_n-\xi_{\mathbf{k}})\,\mathcal{G}_{\uparrow\uparrow}(\mathbf{k},\omega_n)+\Sigma\mathcal{F}^\dagger_{\downarrow\uparrow}(\mathbf{k},\omega_n) &= 1\\ (i\omega_n+\xi_{\mathbf{k}})\,\mathcal{F}^\dagger_{\downarrow\uparrow}(\mathbf{k},\omega_n)+\Sigma\mathcal{G}_{\uparrow\uparrow}(\mathbf{k},\omega_n) &= 0\end{aligned} \tag{3.14}$$

These, and the equivalent expressions for $\mathcal{G}_{\downarrow\downarrow}(\mathbf{k},\omega_n)$ and $\mathcal{F}^\dagger_{\uparrow\downarrow}(\mathbf{k},\omega_n)$, may easily be solved to obtain the Green's functions for the BCS system:

$$\mathcal{G}_{\alpha\beta}(\mathbf{k},\omega_n) = \delta_{\alpha\beta}\frac{i\omega_n+\xi_{\mathbf{k}}}{(i\omega_n)^2-{\xi_{\mathbf{k}}}^2-\Sigma^2} \tag{3.15}$$

$$\mathcal{F}^\dagger_{\alpha\beta}(\mathbf{k},\omega_n) = i\sigma^y_{\alpha\beta}\frac{\Sigma}{(i\omega_n)^2-{\xi_{\mathbf{k}}}^2-\Sigma^2} \tag{3.16}$$

where $\sigma^y_{\alpha\beta}$ is the (α,β) element of the Pauli y spin matrix.

3.4 The 'Rebuilt' System

The Green's functions 3.15 and 3.16 have simple poles at

$$i\omega_n = \pm\sqrt{{\xi_{\mathbf{k}}}^2+\Sigma^2} = \pm E_{\mathbf{k}} \tag{3.17}$$

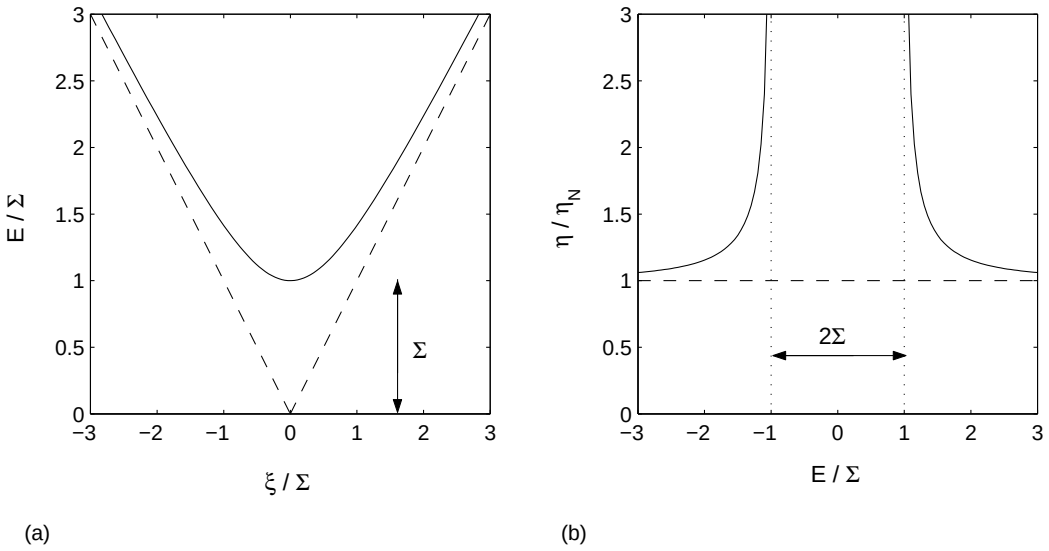

Figure 3.1: The electron and hole excitation spectrum of the 'rebuilt' system (solid line) compared to the original system (dashed line). The hole excitation spectrum is given for $\xi < 0$, the electron excitation spectrum for $\xi > 0$. Note the appearance of the gap of width 2Σ separating the lowest-energy electron and hole states in the superconducting phase. (b) The DOS η_S in the superconductor (solid line) compared to the DOS in the normal phase (dashed line). For the superconductor, the DOS is zero between $\epsilon_F - \Sigma$ and $\epsilon_F + \Sigma$.

These poles define the 'rebuilt' electron ($\xi_{\mathbf{k}} > 0$) and hole ($\xi_{\mathbf{k}} < 0$) excitation spectra of the uncondensed part. The most notable feature of the 'rebuilt' spectrum is the disappearance of the Fermi surface with the opening of a gap of width 2Σ about the Fermi energy (see figure 3.1). This is the energy gap mentioned earlier. Another interesting feature of the rebuilt system concerns the behaviour of the density of states (DOS) η near the Fermi energy. The DOS in the superconductor η_S is related to the DOS of the normal phase η_N by

$$\eta_S = \eta_N \frac{d\xi}{dE} = \eta_N \frac{E}{\sqrt{E^2 - \Sigma^2}} \tag{3.18}$$

The square-root divergence at $E = \pm\Sigma$ is an important characteristic of the BCS state. We illustrate it in figure 3.1(b). We note that this DOS-enhancement is responsible for the well-known Josephson effect [29].

The BCS gap Σ may be linked to the interaction strength λ. From the expression for the Gor'kov Green's functions (3.16), the definition of Σ (3.7) and the identity 3.11, we have

$$\begin{aligned} \Sigma &= -\frac{\lambda}{2\beta V} \sum_{\mathbf{k},n} \left[\mathcal{F}^\dagger_{\downarrow\uparrow}(\mathbf{k},\omega_n) - \mathcal{F}^\dagger_{\uparrow\downarrow}(\mathbf{k},\omega_n) \right] e^{-i\omega_n 0^+} \\ &= \frac{\lambda}{2\beta V} \sum_{\mathbf{k},n} \frac{\Sigma}{E_{\mathbf{k}}} \left[\frac{1}{i\omega_n - E_{\mathbf{k}}} - \frac{1}{i\omega_n + E_{\mathbf{k}}} \right] e^{-i\omega_n 0^+} \end{aligned} \tag{3.19}$$

We ignore the trivial solution $\Sigma = 0$ to equation 3.19. Thus, after cancelling Σ from both sides and performing the Matsubara sums (see section A.2 of the Mathematical Appendix), we have

$$\begin{aligned} 1 &= \frac{\lambda}{4V} \sum_{\mathbf{k}} \frac{1}{E_{\mathbf{k}}} \left[1 - \tanh\left(\frac{\beta E_{\mathbf{k}}}{2}\right) - 1 + \tanh\left(\frac{-\beta E_{\mathbf{k}}}{2}\right) \right] \\ &= -\frac{\lambda}{2V} \sum_{\mathbf{k}} \frac{1}{E_{\mathbf{k}}} \tanh\left(\frac{\beta E_{\mathbf{k}}}{2}\right) \rightarrow -\lambda\eta_N(0) \int_0^\varpi \frac{d\xi}{E} \tanh\left(\frac{\beta E}{2}\right) \end{aligned} \tag{3.20}$$

where we have converted the sum over $\mathbf{k}$ to an integral over the energies of the normal phase ξ (see section A.1 of the Mathematical Appendix). Taking the limit of zero temperature ($\beta \to \infty$) in 3.20, we obtain the so-called self-consistency equation

$$-\frac{1}{\lambda \eta_{\mathrm{N}}(0)} \;=\; \int_0^{\varpi} \frac{d\xi}{\sqrt{\epsilon^2 + \Sigma^2}} \;\approx\; \ln\left(\frac{2\varpi}{\Sigma}\right) \tag{3.21}$$

where we make the standard assumption that $\varpi \gg \Sigma > 0$ in evaluating the integral in 3.21 [26]. Solving for Σ, we obtain the well-known result

$$\Sigma \;=\; 2\varpi \exp\left(\frac{1}{\lambda \eta_{\mathrm{N}}(0)}\right) \tag{3.22}$$

We note that Σ increases with increasing values of $|\lambda|$, as we expect. We also note that $\Sigma \neq 0$ for all $\lambda \neq 0$: this shows that the BCS state forms no matter how weak the interactions are.

We conclude this section by considering the energetic stability of the BCS state relative to the normal phase. At zero temperature, we have by the Feynman-Pauli theorem

$$\delta F \;=\; \frac{1}{2V^2} \int_0^{\lambda} d\lambda' \sum_{\mathbf{k}',\mathbf{k}''} \sum_{\nu,\nu'} \left\langle \hat{a}^{\dagger}_{\mathbf{k}'\nu} \hat{a}^{\dagger}_{-\mathbf{k}'\nu'} \hat{a}_{\mathbf{k}''\nu'} \hat{a}_{-\mathbf{k}''\nu} \right\rangle_{\lambda'} \tag{3.23}$$

Following the analysis of Fetter and Walecka [26], we consider the ensemble average to be the $\tau \to 0^+$ limit of a τ-product; this may be decomposed using Wick's theorem as follows:

$$\begin{aligned} \left\langle \hat{a}^{\dagger}_{\mathbf{k}'\nu} \hat{a}^{\dagger}_{-\mathbf{k}'\nu'} \hat{a}_{\mathbf{k}''\nu'} \hat{a}_{-\mathbf{k}''\nu} \right\rangle_{\lambda'} \;&=\; \lim_{\tau \to 0+} \left\langle T_\tau \left[\hat{a}^{\dagger}_{\mathbf{k}'\nu}(\tau) \hat{a}^{\dagger}_{-\mathbf{k}'\nu'}(\tau^-_{(1)}) \hat{a}_{\mathbf{k}''\nu'}(\tau^-_{(2)}) \hat{a}_{-\mathbf{k}''\nu}(0) \right] \right\rangle_{\lambda'} \\ &\approx\; \mathcal{F}^{\dagger\,\lambda'}_{\nu\nu'}(-\mathbf{k}', 0^+) \mathcal{F}^{\lambda'}_{\nu'\nu}(\mathbf{k}'', 0^+) + \ldots \end{aligned} \tag{3.24}$$

$\mathcal{F}^{\dagger\,\lambda'}_{\alpha\beta}$ and $\mathcal{F}^{\lambda'}_{\alpha\beta}$ are the Gor'kov Green's functions for the system with interaction constant λ'. We neglect the other terms in the expansion 3.24 for the same reasons as in the decoupling of the equations of motion. Therefore,

$$\delta F \;\approx\; \frac{1}{2V^2} \int_0^{\lambda} d\lambda' \sum_{\mathbf{k}',\mathbf{k}''} \sum_{\nu,\nu'} \mathcal{F}^{\dagger\,\lambda'}_{\nu\nu'}(-\mathbf{k}', 0^+) \mathcal{F}^{\lambda'}_{\nu'\nu}(\mathbf{k}'', 0^+) \tag{3.25}$$

Using the identities 3.11 and the result $\mathcal{F}^{\dagger}_{\uparrow\downarrow} = -\mathcal{F}^{\dagger}_{\downarrow\uparrow}$ (equation 3.16), the expression 3.7 may be re-written

$$\Sigma \;=\; -\frac{\lambda}{V} \sum_{\mathbf{k}} \mathcal{F}^{\dagger}_{\downarrow\uparrow}(\mathbf{k}, 0^+) \;=\; \frac{\lambda}{V} \sum_{\mathbf{k}} \mathcal{F}_{\downarrow\uparrow}(\mathbf{k}, 0^+)$$

Letting Σ' be the gap for the system with interaction constant λ', we have for δF, after accounting for the sum over spin indices,

$$\delta F \;=\; \int_0^{\lambda} \frac{\Sigma'^2}{\lambda'^2} d\lambda' \;=\; -\frac{1}{2} \eta_{\mathrm{N}}(0) \Sigma^2 \tag{3.26}$$

where the integral was evaluated using the expression 3.22. We see that $\delta F < 0$: we conclude that the superconducting state is stable towards the normal phase.

Ferromagnetism

The study of magnetic solid state systems is a subject of vast scope and dazzling complexity. The range and diversity of magnetic materials is matched only by the models developed to explain their often remarkable properties. In this chapter, we can offer only the briefest of introductions to the field. In section 4.1, an overview of the theory of magnetism is presented with a discussion of important phenomenological and theoretical concepts in ferromagnetism; in section 4.2, the traditional Stoner ferromagnet is studied; this aids in an understanding of the generally antagonistic relationship between ferromagnetism and superconductivity (section 4.3).

4.1 Basic Concepts

In this section, the fundamentals of the theory of magnetism are summarized. We introduce the major classes of magnetic behaviour via the concept of long-range magnetic order (subsection 4.1.1), with a special focus upon the phenomenology and theory of ferromagnetic materials (subsections 4.1.2 and 4.1.3 respectively).

4.1.1 Magnetic Order

In a solid, the band electrons, and sometimes also the atoms in the crystalline lattice, carry a microscopic magnetic moment. In the case of electrons, this is due to the spin angular momentum; atomic moments stem from the orbital motion of the shell electrons, or incompletely filled inner shells. It is important to note a significant difference in character between these moment-carriers. The atoms, and therefore also their moments, are localized at the crystal lattice points. The band electrons, however, propagate through the crystal as Bloch waves, and are regarded as delocalized. Consequently, it is necessary to consider a density of their spins, which is a continuously varying function of position.

In a non-magnetic material there is no long-range ordering of the microscopic magnetic moments: over sufficiently large distances, the orientation of the localized moments on the atoms varies randomly, and the departures from the band-electron's average spin density of zero are uncorrelated. Thus, in both cases, the magnetization $\mathbf{M}$ (the average moment per unit volume) is zero. The application of an external magnetic field $\mathbf{H}$ has two effects: to align the microscopic magnetic moments in the direction of the field; and to induce anti-aligned moments due to the orbital response of the electrons. When the former process is dominant, the material is paramagnetic; dominance by the latter leads to diamagnetism. In both cases, the external field induces a magnetization, assumed proportional to $\mathbf{H}$:

$$\mathbf{M} = \chi \mathbf{H} \tag{4.1}$$

χ is the magnetic susceptibility of the material and is positive for paramagnets, negative for diamagnets. For both materials, the magnetization vanishes when the external field is removed, the system returning to its original disordered state.

In a magnetic material there exists a spontaneous long-range ordering of the microscopic moments. This is due to so-called exchange interactions between the moment-carriers. There are

two major classes of magnetic materials exhibiting spontaneous order: ferromagnets and antiferromagnets. In ferromagnetic materials, the exchange interactions tend to align the moments in one direction, giving the material a non-zero magnetization. The favoured direction of alignment (the so-called easy axis) is determined by secondary coupling to the crystal field (e.g. spin-orbit effects) [34]. In contrast to ferromagnets, the exchange interactions in antiferromagnetic materials tend to periodically order the moments in such a way that there is no overall magnetization of the system. In both ferromagnets and antiferromagnets the tendency of the exchange interactions to order the moments is counteracted by thermal fluctuations; in the limit of zero temperature, the thermal agitations which destroy the ordering vanish, and the degree of order is limited only by quantum effects.

4.1.2 Ferromagnetism: Phenomenology

The characteristic property of a ferromagnet is the spontaneous magnetization produced by the exchange interactions. This magnetization is not necessarily uniform across the specimen: a ferromagnet may be divided into macroscopic volumes called domains, each possessing a randomly orientated magnetic moment. The application of an external magnetic field results in an expansion of the domains with moments aligned with the field at the expense of those with anti-aligned moments. This process is irreversible and so leads to a permanent increase in the magnetization of the sample (hysteresis effect). The magnitude of the spontaneous magnetization of a domain obtains a maximum in the limit of zero temperature. This maximum magnetization is referred to as the saturation magnetization of the material.

Due to the dominance of thermal fluctuations, the spontaneous magnetization of a ferromagnet disappears above a certain critical temperature, the Curie point T_F. Generally, a ferromagnetic material becomes paramagnetic above its Curie point, but certain rare-earth elements exhibit antiferromagnetic ordering at temperatures higher than T_F [34]. The phase transition from the ferromagnetic to the paramagnetic phase (the 'normal' phase) is the classic example of a second-order phase transition [7].

4.1.3 Ferromagnetism: Theory

Theoretical attempts at a microscopic theory of ferromagnetism generally regard either the magnetic ordering of the lattice atoms or the band electrons as of primary importance. Such models are classified as 'localized' and 'itinerant' respectively. Although in any real system, both localized and itinerant effects are likely to be present to differing degrees, it is usually possible to expect one to dominate the other. For example, the rare-earth ferromagnets and their ionic compounds (such as EuO and $GdCl_2$) are regarded as good examples of localized systems, whereas the ferromagnetism of the $3d$ transition metals (iron, nickel and cobalt) and a number of alloys of non-magnetic elements (e.g. $ZrZn_2$ and Sc_3In) is best explained by the itinerant scheme [34,35].

Theoretical study of itinerant electron models began in 1929 with the pioneering efforts of Bloch. His work indicated that ferromagnetism was only likely to appear in the homogeneous electron gas at very low densities, $r_s \sim 6$; more sophisticated studies have proved that the homogeneous electron gas is not ferromagnetic at typical metallic densities [35]. This has been confirmed by computational studies which predict the onset of ferromagnetic ordering only at extremely low densities $r_s \sim 50$. There is, however, much disagreement about the precise density range, and the physicality of these low density regimes should be regarded with caution [36,37].

More sophisticated models of itinerant electron systems have met with considerably better success than the naive homogeneous electron gas approximation. These models have demonstrated the crucially important role played by the band structure in determining whether or not itinerant electron ferromagnetism will appear in a material. Of particular note is the so-called Stoner model, which gives a criterion for the appearance of ferromagnetism in terms of the DOS at the Fermi energy. The Stoner model gives a very basic phenomenological description of an itinerant system, and considerable improvement has been made upon it [7,38]. Nevertheless, it has provided a useful starting point for the study of itinerant electron ferromagnetism.

4.2 The Stoner Ferromagnet

The molecular field concept was first developed in 1907 by Weiss to explain the ferromagnetic ordering of localized spins [1]. It was generalized in the 1930s by Slater and Stoner to accommodate the itinerant description [39,40]. The resulting Stoner model is extremely crude, but it nevertheless captures the essential physics of the traditional itinerant ferromagnet.

4.2.1 The Molecular Field

The exchange interactions between the moment-carriers in a ferromagnet are in general very complicated, and several distinct exchange interactions may be present in the material to differing degrees of importance. We therefore ignore the details of these interactions and instead consider the overall effect of their presence in the system. We assume that the exchange interactions between the microscopic magnetic moments causes them to behave as if they had been placed in an intense magnetic field. This imaginary field is referred to as the molecular field.

The molecular field $\mathbf{H}_M$ experienced by each moment-carrier in the system is assumed to be the same, and it is considered to be proportional to the overall magnetization of the system $\mathbf{M}$. We therefore write

$$\mathbf{H}_M \;=\; q\mathbf{M} \tag{4.2}$$

where q is referred to as the molecular field constant. The assumed homogeneity of $\mathbf{H}_M$ implies that the short-range ordering of the moment-carriers, apart from that which follows from the long-range ordering, is neglected. Hence, any local deviation of the spin-density from its mean value is ignored. Molecular field theory cannot therefore be supposed to give a rigorous treatment of the system: it should be regarded as at best a semi-quantitative phenomenological analysis.

4.2.2 The Stoner Model

We consider a metallic system in the absence of the exchange interactions between the band electrons. In such a material, the one-electron energy states are degenerate in the electron spin, as dictated by the Pauli exclusion principle. The DOS of each spin species therefore coincides; the DOS of electrons with spin σ, $\eta_\sigma(\epsilon)$, is related to the total DOS $\eta(\epsilon)$ by

$$\eta_\sigma(\epsilon) \;=\; \frac{1}{2}\eta(\epsilon) \tag{4.3}$$

We treat the exchange interactions between the electrons as a perturbation on this system. These interactions are modelled by a molecular field $\mathbf{H}_M$. In addition to the molecular field, we assume that there is also an external magnetic field present, so that the electrons move in an effective internal magnetic field

$$\mathbf{H}_i \;=\; \mathbf{H} + q\mathbf{M} \tag{4.4}$$

Neglecting the orbital response of the electrons to this internal field (i.e. assuming the electron to have spin magnetic moment but no charge), and taking the electron's gyromagnetic ratio $g = 2$, the interaction with the internal magnetic field lowers (raises) the energy of an electron with spin-orientation parallel (anti-parallel) to the field by $\mu_B H_i$, where μ_B is the Bohr magneton. We shall henceforth refer to the parallel spin orientation as 'spin-up' and the anti-parallel spin orientation as 'spin-down'.

All spin-up and spin-down electrons experience the same shift in energy. The effect of $\mathbf{H}_i$ is therefore to lift the degeneracy of the one-electron states, by uniformly lowering (raising) the energy of the spin-up (spin-down) states by $\mu_B H_i$ (see figure 4.1). The DOS of the spin-up (+) and spin-down (−) electrons is therefore given in terms of η by

$$\eta_\pm(\epsilon) \;=\; \frac{1}{2}\eta(\epsilon \pm \mu_B H_i) \tag{4.5}$$

To first approximation the chemical potential μ does not change upon shifting of the sub-bands; the shifting may therefore lead to a net increase (decrease) in the number of one-electron spin-up (spin-

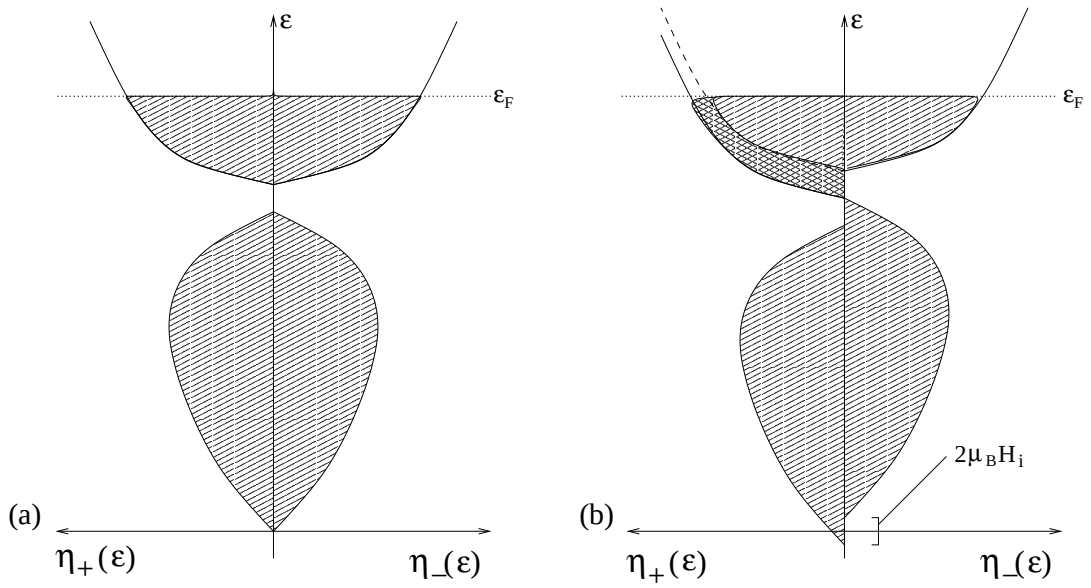

Figure 4.1: The band structure of a Stoner ferromagnet in its non-magnetic (a) and magnetic (b) phases. Note the excess spin-up electron population in figure (b), illustrated by the dark shading.

down) states below the chemical potential. This may create an imbalance in the spin-populations, giving the system a net magnetic moment. Such a situation is illustrated in figure 4.1(b).

The magnetization of the system is given by the relation

$$M = \mu_B \int_0^\infty \{\eta_+(\epsilon) - \eta_-(\epsilon)\} f(\epsilon, T) d\epsilon \tag{4.6}$$

where $f(\epsilon, T)$ is the Fermi-Dirac distribution at temperature T. In the limit where the magnitude of the internal field approaches zero, we may expand $\eta_+(\epsilon)$ and $\eta_-(\epsilon)$ in a Taylor series:

$$2\eta_\pm(\epsilon) = \eta(\epsilon \pm \mu_B H_i) = \eta(\epsilon) \pm \mu_B H_i \frac{\partial \eta(\epsilon)}{\partial \epsilon} + \ldots \tag{4.7}$$

We substitute the Taylor expansion 4.7 into 4.6 and solve for the susceptibility χ, obtaining

$$\chi = \frac{M}{H} = \frac{\mu_B^2 I(T)}{1 - q\mu_B^2 I(T)}, \qquad I(T) = \int_0^\infty \eta(\epsilon) \left[-\frac{\partial f(\epsilon, T)}{\partial \epsilon} \right] d\epsilon \tag{4.8}$$

We observe that the susceptibility diverges when $q\mu_B^2 I = 1$. This defines the onset of ferromagnetic order. For $q\mu_B^2 I(T) > 1$, the susceptibility is negative; this indicates that the system is in the ferromagnetic phase.

The expression for the susceptibility provides a simple condition for the appearance of ferromagnetic order in the system. For the system to be ferromagnetic at finite temperatures, we require that its Curie point be greater than 0K, i.e. $q\mu_B^2 I(0) > 1$. At zero temperature, the Fermi-Dirac distribution in the integral I is a step function with discontinuity at ϵ_F. Thus, the derivative of $f(\epsilon, 0)$ with respect to ϵ is given by a δ-function at ϵ_F. The condition for the appearance of ferromagnetism at finite temperature may therefore be written in the more succinct form

$$q\mu_B^2 \eta(\epsilon_F) > 1 \tag{4.9}$$

This is the famous Stoner condition for itinerant ferromagnetism.

Although the Stoner condition appears to give a practical test of the possibility of any material to show itinerant ferromagnetic order, the presence of the molecular field constant q in 4.9 severely

limits its utility, as q is difficult to accurately determine. Detailed comparison of the Stoner model with experiment is also made problematic by the critical dependence upon the density of states, which is generally an extremely complex function of the energy. Computational studies of realistic band-structures using approximate values of q, however, have revealed good agreement with the Stoner model in the iron-group $3d$ transition metals and a number of their alloys [38].

4.3 Ferromagnetism and Superconductivity

The coexistence of ferromagnetism and superconductivity is a challenging problem for experimental and theoretical condensed-matter physicists alike. Of the many thousands of materials known to superconduct or possess magnetic order, only a very small fraction fall into both categories. This may be strikingly illustrated by the following statistic: by 1976, 36 elements were known to superconduct, and 17 elements had been found to display ferromagnetism; only one of these elements, cerium, exhibited both phenomena, and only under very special conditions [1]. This picture remains basically the same today: the recent discovery of superconductivity in iron under intense pressure reinforces the conclusion that superconductivity and magnetism are fundamentally incompatible phenomena [41]. The basic mechanism behind this antagonism is two-fold: the electromagnetic behaviour of the superconductor, and the effect of exchange correlations in hindering Cooper-pairing. We briefly describe both mechanisms below.

In the presence of sufficiently weak magnetic fields, superconductors exhibit perfect diamagnetism: there is zero magnetic flux through the bulk of the superconductor. This is due to the appearance of currents on the surface of the superconductor which completely cancel the magnetic field in the interior. As the magnetic field is increased, the surface currents required for the screening of the interior also increase. Above a critical magnetic field, H_s, the surface currents exceed the critical current at zero temperature; superconductivity is completely suppressed. This is the well-known Meissner-Oschenfeld effect. Its importance in preventing the coexistence of ferromagnetism and superconductivity has long been understood [14]: for most ferromagnets, the surface currents required to screen the bulk from the spontaneous magnetization well exceed the critical currents; the possibility of coexistence with superconductivity is therefore limited to very weak ferromagnets.

In itinerant-electron systems, the spin-splitting of the electronic spectrum due to the presence of exchange interactions between the band-electrons also has a deleterious effect upon superconductivity [15, 42]. This may be understood with reference to the Stoner model. In the Stoner ferromagnet, the interaction of the electrons with the internal field $\mathbf{H}_i$ lowers (raises) the energy of the spin-up (spin-down) electrons by $\mu_B H_i$; thus, the spin-up electrons at the Fermi surface have kinetic energy $\epsilon_F + \mu_B H_i$ whilst the spin-down electrons have kinetic energy $\epsilon_F - \mu_B H_i$. In order to Cooper-pair, two electrons must have kinetic energy within $\sim \omega_D$ of ϵ_F. Although assumed to be small, the "exchange-potential" $\mu_B H_i$ is typically much larger than the Debye energy; this essentially forbids the Cooper-pairing of electrons in the standard spin-singlet configuration. In localized systems, the (non-magnetic) conduction electrons may also couple to the exchange field, leading to a similar effect.

In spite of these objections, the coexistence of ferromagnetism and superconductivity has been observed since the late 1960s. In the majority of these systems, however, the ferromagnetism is localized in nature, or the system is divided into non-overlapping ferromagnetic and superconducting regions of mesoscopic dimensions [16, 43]. Examples of the coexistence between spatially uniform superconductivity and itinerant-electron ferromagnetism are particularly rare. The recent discovery of two such systems, UGe_2 and $ZrZn_2$, has therefore been the cause for great excitement in the solid state physics community [17, 18]. The mechanism responsible for superconductivity in these systems is generally regarded as exotic: the possibility of spin-triplet Cooper-pairing has been raised to describe the apparently cooperative coexistence between superconductivity and ferromagnetism in the weak Stoner ferromagnet $ZrZn_2$ [44]; the behaviour of UGe_2 has been studied from a much more radical perspective [19].

Excitons in Semimetals

The study of correlation-induced metal-insulator transitions has long been of intense interest to solid state physicists. The staggering wealth of possible mechanisms, and the practical applications to semiconductor technology, has made this a major field of endeavour [6]. In this chapter, we describe an exciton-mediated metal-insulator transition that is predicted to occur in semimetals with a peculiar topology of the Fermi surface (sections 5.1 and 5.2). A quantum-field theoretic description of this state is then developed (sections 5.3 and 5.4). The possibility of ferromagnetic ordering of the band-electron spins as a result of this transition is discussed in detail (section 5.5). We conclude with a survey of experimental evidence for the existence of this state (section 5.6).

5.1 The Nested Semimetal

The concept of a semimetal is best introduced via the more familiar notion of a semiconductor. In a semiconductor, the (filled) valence band and the (empty) conduction band are separated by a band gap $E_G > 0$; the Fermi energy (which defines our energy zero as in chapter 3) lies within the range of forbidden energies. The width of the energy gap is typically $\sim$ 1eV. At finite temperatures, electrons may be excited from the valence band into the conduction band, leaving a hole behind them in the valence band. In the limit of zero temperature, however, the thermal energy of the electrons in the valence band is not sufficient to induce a transition to the conduction band and so the system behaves like an insulator: at 0K there are no excited electrons in the conduction band, and no holes in the valence band.

A semimetal may be profitably regarded as a semiconductor with a negative band gap, i.e. the valence and conduction bands overlap by an amount E_G. The Fermi energy lies within the range of energy overlap, and so there is a Fermi surface. The Fermi surface in the conduction band is referred to as the electron Fermi surface; in the valence band we have the hole Fermi surface. The occupied states at the bottom of the conduction band behave like excited electrons in a semiconductor; the empty states at the top of the valence band like holes. As such, there is always a population of electrons and holes in a semimetal, even at absolute zero.

We confine our attention to semimetals where the energy spectra of the conduction and the valence bands, $\varepsilon_C(\mathbf{k})$ and $\varepsilon_V(\mathbf{k})$ respectively, satisfy the condition

$$\varepsilon_C(\mathbf{k}) \;=\; -\varepsilon_V(\mathbf{k}-\mathbf{Q}) \tag{5.1}$$

for some set of energies about the Fermi surface. When 5.1 is satisfied, the conduction and valence bands are said to be 'nested', i.e. some portion of the electron and hole Fermi surfaces are identical and separated by the constant nesting vector $\mathbf{Q}$ in the reciprocal lattice.

We consider the simple case where the conduction band minima and valence band maxima are isotropic (i.e. dependent upon $|\mathbf{k}|$ only) and parabolic. We further assume the effective masses of the valence band holes and the conduction band electrons to be equal. The nesting condition 5.1 thus requires that

$$\varepsilon_C(\mathbf{k}) \;=\; -\varepsilon_V(\mathbf{k}-\mathbf{Q}) \;=\; \xi_{\mathbf{k}} \;=\; k^2 - \frac{1}{2}E_G \tag{5.2}$$

This model spectrum is plotted in figure 5.1. For the Fermi energy at $\varepsilon_C = \varepsilon_V = 0$, this situation is

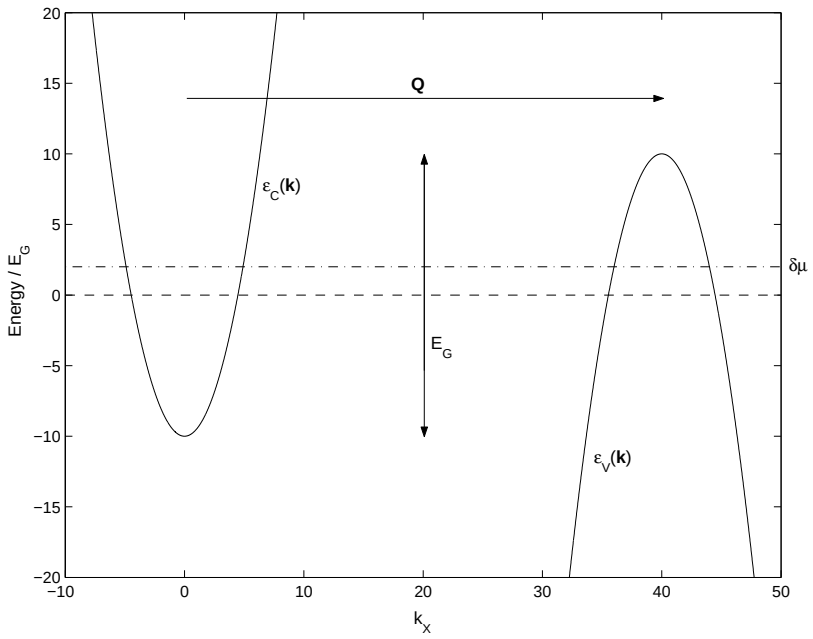

Figure 5.1: The model system of the nested semimetal. The conduction and valence bands overlap by an amount E_G; their respective minima and maxima are separated by a vector $\mathbf{Q}$ in the reciprocal space. At perfect nesting, the Fermi energy corresponds to the dashed line; adding electrons to the system raises the Fermi energy to $\delta\mu$ (dot-dashed line)

referred to as "perfect" nesting. Although useful as a limiting case, "perfect" nesting of parabolic bands is too simplistic a scenario to be realized in any real system - there will always be departures from the condition 5.2 due to band anisotropy, differing electron and hole effective masses, etc. Taking these effects into account does not lead to significant qualitative revisions of the predictions based upon the model band structure 5.2 [45,46].

The simplest case of 'imperfect' nesting corresponds to the addition of excess particles (electrons or holes) to the system, so that the Fermi energy no longer corresponds to $\xi_{\mathbf{k}} = 0$. We may characterize this change in the Fermi energy by the parameter $\delta\mu$ (see figure 5.1). It is convenient to consider these excess particles as being introduced by impurity doping (n-type for excess electrons, p-type for excess holes). As the concentration of impurities in the system is constant, $\delta\mu$ is determined by the condition that the number of electrons in the system is conserved. The value of $\delta\mu$ is therefore determined by the form of the electronic excitation spectrum and the electron-hole concentration difference δn. Since doping with electrons must raise the Fermi level whilst hole-doping lowers it, $\delta\mu$ must be an odd function of δn and *vice versa*. We shall only consider electron-doping below.

5.2 The Exciton Instability in the Nested Semimetal

Due to the attractive Coulomb interaction between the electrons and the holes, it is possible for stable bound states of the two particles to be formed. The bound electron-hole pair is a well-known example of a "quasimolecule", the exciton. Excitons bear a superficial resemblance to the Cooper pairs of the BCS superconductor. They can freely propagate through the system, playing an important role in energy transport. The Coulomb attraction between the electron and hole in an exciton makes these "quasimolecules" much more robust than the tenuously-bound Cooper pairs. Again in contrast to Cooper pairs, the constituent electron and hole of the exciton may bind in both the spin-singlet and spin-triplet configurations.

The formation of excitons is central to the description of the optical behaviour of semiconduc-

tors; they also occupy a position of importance in the physics of the metal-insulator transition, first discussed by Mott in 1961 [5]. In this pioneering work, the possibility of a transition to an insulating state due to exciton-mediated hybridization of the conduction and valence bands in a semimetal was first raised. Using the simple model adopted here, the instability of the semimetallic state was rigorously demonstrated by several authors in the mid-1960s. Although not appreciated until later, the nesting of the electron and hole Fermi surfaces is essential for the appearance of this instability [8, 47–49].

In the scenario outlined in these papers, the presence of arbitrarily small attractive interactions between the conduction band electrons and valence band holes in the semimetal results in the spontaneous formation of a macroscopic number of excitons, 'rebuilding' the system. The new phase is called the excitonic insulator (EI). As we shall see below, the term 'insulator' is actually a misnomer, as electrons may be doped into the 'rebuilt' conduction band, causing the EI phase to exhibit metallic behaviour. In complete analogy to the BCS system, the characteristic properties of the EI phase are due to the excitons condensating into a single exciton energy state. In the ensuing work, we follow the approach of Keldysh and Kopaev to the study of the EI phase [8]. Generalizing the Gor'kov analysis of the BCS state, they divided the system into the exciton condensate and the uncondensed part, consisting of the unbound electrons and holes. The exciton condensate acts as a reservoir into and from which particles in the uncondensed part of the system may be scattered. This allows a simple application of the techniques introduced in chapter 3.

5.3 The Green's Functions

The form of the Hamiltonian used to describe the excitonic insulator is given by

$$\begin{aligned}\hat{K} &= \sum_{\mathbf{k}',\nu}\left[(\xi_{\mathbf{k}'}-\delta\mu)\hat{a}^{\dagger}_{1\mathbf{k}'\nu}\hat{a}_{1\mathbf{k}'\nu}+(-\xi_{\mathbf{k}'}-\delta\mu)\hat{a}^{\dagger}_{2\mathbf{k}'\nu}\hat{a}_{2\mathbf{k}'\nu}\right] \\ &\quad+\frac{1}{2V}\sum_{\mathbf{k}',\mathbf{k}''}\sum_{\nu,\nu',\zeta,\zeta'}\left(g_s\delta_{\nu\nu'}\delta_{\zeta\zeta'}+g_t\sigma^z_{\nu\nu'}\sigma^z_{\zeta\zeta'}\right)\hat{a}^{\dagger}_{1\mathbf{k}'\nu}\hat{a}_{2\mathbf{k}'\nu'}\hat{a}^{\dagger}_{2\mathbf{k}''\zeta}\hat{a}_{1\mathbf{k}''\zeta'} \qquad (5.3)\end{aligned}$$

The subscripts 1 and 2 refer to the different bands: the operators $\hat{a}^{\dagger}_{1\mathbf{k}\alpha}$ and $\hat{a}^{\dagger}_{2\mathbf{k}\alpha}$ create electrons in the conduction and valence bands respectively. These band indices are to be treated as a new quantum number of the system. The annihilation and creation operators are assumed to anticommute in their band indices, i.e.

$$\left[\hat{a}_{i\mathbf{k}\alpha},\hat{a}^{\dagger}_{j\mathbf{k}'\beta}\right]_{+} = \delta_{ij}\delta_{\mathbf{k}\mathbf{k}'}\delta_{\alpha\beta}$$

For the sake of clarity, we adopt the simplifying notation of measuring the momentum in the valence band from the valence band maxima at $\mathbf{Q}$. Thus, $\hat{a}^{\dagger}_{2\mathbf{k}\alpha}$ should be interpreted as creating an electron in the valence band with spin α and momentum $\mathbf{k}+\mathbf{Q}$. Obviously, this does not affect the form of the anticommutator above.

Creating an electron in the valence band is equivalent to destroying a hole; we may therefore interpret $\hat{a}^{\dagger}_{2\mathbf{k}\alpha}$ as annihilating a hole with momentum $-\mathbf{k}-\mathbf{Q}$ and spin $-\alpha$ in the valence band. The second term in equation 5.3 therefore represents the interaction between a conduction-band electron and a valence-band hole; the coupling constants $g_s,\ g_t<0$ describe the strength of the interactions that lead to singlet and triplet electron-hole pairing respectively. The term $\sigma^z_{\alpha\beta}$ in the expression for the spin-structure of the triplet-pairing interaction refers to the (α,β) element of the Pauli z spin matrix.

There are four Green's functions to consider in the excitonic-insulator phase: the two intraband Green's functions

$$\mathcal{G}^{11}_{\alpha\beta}(\mathbf{k},\tau) = -\delta_{\alpha\beta}\left\langle T_\tau\left[\hat{a}_{1\mathbf{k}\alpha}(\tau)\hat{a}^{\dagger}_{1\mathbf{k}\beta}(0)\right]\right\rangle \qquad (5.4)$$

$$\mathcal{G}^{22}_{\alpha\beta}(\mathbf{k},\tau) = -\delta_{\alpha\beta}\left\langle T_\tau\left[\hat{a}_{2\mathbf{k}\alpha}(\tau)\hat{a}^{\dagger}_{2\mathbf{k}\beta}(0)\right]\right\rangle \qquad (5.5)$$

which are present also in the normal phase; and the interband Green's functions

$$\mathcal{G}^{21}_{\alpha\beta}(\mathbf{k},\tau) = -\delta_{\alpha\beta}\left\langle T_\tau\left[\hat{a}_{2\mathbf{k}\alpha}(\tau)\hat{a}^\dagger_{1\mathbf{k}\beta}(0)\right]\right\rangle \tag{5.6}$$

$$\mathcal{G}^{12}_{\alpha\beta}(\mathbf{k},\tau) = -\delta_{\alpha\beta}\left\langle T_\tau\left[\hat{a}_{1\mathbf{k}\alpha}(\tau)\hat{a}^\dagger_{2\mathbf{k}\beta}(0)\right]\right\rangle \tag{5.7}$$

which are only present in the 'rebuilt' state. As $\hat{a}_{2\mathbf{k}\alpha}(\tau)$ annihilates a hole in the valence band at 'time' τ, we see that the interband Green's functions $\mathcal{G}^{12}_{\alpha\beta}$ and $\mathcal{G}^{21}_{\alpha\beta}$ are essentially analogous to the Gor'kov Green's functions in the description of a traditional BCS superconductor, scattering an electron-hole pair into and out of the exciton reservoir respectively.

As in the analysis for the BCS superconductor, a gap is opened in the excitation spectrum by the presence of the exciton condensate. This gap fulfils the role of order parameter(s) for the 'rebuilt' state. The presence of singlet excitons is indicated by the gap Δ_s; triplet excitons by Δ_t. These gaps may be defined in terms of the interband Green's functions:

$$\Delta_s = \frac{g_s}{2V}\sum_{\mathbf{k}}\left\{\mathcal{G}^{12}_{\uparrow\uparrow}(\mathbf{k},0^+) + \mathcal{G}^{12}_{\downarrow\downarrow}(\mathbf{k},0^+)\right\} \tag{5.8}$$

$$\Delta_t = \frac{g_t}{2V}\sum_{\mathbf{k}}\left\{\mathcal{G}^{12}_{\uparrow\uparrow}(\mathbf{k},0^+) - \mathcal{G}^{12}_{\downarrow\downarrow}(\mathbf{k},0^+)\right\} \tag{5.9}$$

Both the singlet and the triplet order parameters are assumed to be either purely real or purely imaginary [49, 50]. We shall only consider the case of real order parameters: the physical systems corresponding to imaginary order parameters have apparently not yet been observed [44].

We obtain the equation of motion of the intraband Green's function $\mathcal{G}^{11}_{\uparrow\uparrow}(\mathbf{k},\tau)$ after a simple but tedious calculation:

$$\begin{aligned}-\frac{\partial}{\partial\tau}\mathcal{G}^{11}_{\uparrow\uparrow}(\mathbf{k},\tau) &= \delta(\tau) + (\xi_{\mathbf{k}} - \delta\mu)\mathcal{G}^{11}_{\uparrow\uparrow}(\mathbf{k},\tau) \\ &\quad -\frac{1}{2V}\sum_{\mathbf{k}''}\sum_{\nu',\zeta,\zeta'}\left(g_s\delta_{\uparrow\nu'}\delta_{\zeta\zeta'} + g_t\sigma^z_{\uparrow\nu'}\sigma^z_{\zeta\zeta'}\right)\left\langle T_\tau\left[\hat{a}_{2\mathbf{k}\nu'}(\tau)\hat{a}^\dagger_{2\mathbf{k}''\zeta}(\tau)\hat{a}_{1\mathbf{k}''\zeta'}(\tau)\hat{a}^\dagger_{1\mathbf{k}\uparrow}(0)\right]\right\rangle\end{aligned} \tag{5.10}$$

In line with the SCHF approximation adopted, we decompose the τ-product in equation 5.10 keeping only the terms describing the coupling to the exciton reservoir:

$$\left\langle T_\tau\left[\hat{a}_{2\mathbf{k}\nu'}(\tau)\hat{a}^\dagger_{2\mathbf{k}''\zeta}(\tau)\hat{a}_{1\mathbf{k}''\zeta'}(\tau)\hat{a}^\dagger_{1\mathbf{k}\uparrow}(0)\right]\right\rangle = -\mathcal{G}^{12}_{\zeta'\zeta}(\mathbf{k}'',0^+)\mathcal{G}^{21}_{\nu'\beta}(\mathbf{k},\tau) + \ldots \tag{5.11}$$

Replacing the τ-product in equation 5.10 by its expansion 5.11, we obtain

$$\begin{aligned}-\frac{\partial}{\partial\tau}\mathcal{G}^{11}_{\uparrow\uparrow}(\mathbf{k},\tau) &= \delta(\tau) + (\xi_{\mathbf{k}} - \delta\mu)\mathcal{G}^{11}_{\uparrow\uparrow}(\mathbf{k},\tau) \\ &\quad + \frac{1}{2V}\sum_{\mathbf{k}'}\sum_{\nu',\zeta,\zeta'}\left(g_s\delta_{\uparrow\nu'}\delta_{\zeta\zeta'} + g_t\sigma^z_{\uparrow\nu'}\sigma^z_{\zeta\zeta'}\right)\mathcal{G}^{12}_{\zeta'\zeta}(\mathbf{k}',0^+)\mathcal{G}^{21}_{\nu'\uparrow}(\mathbf{k},\tau)\end{aligned} \tag{5.12}$$

Using the definition of the order parameters, equations 5.8 and 5.9, we rewrite equation 5.12 as

$$\left(-\frac{\partial}{\partial\tau} - \xi_{\mathbf{k}} + \delta\mu\right)\mathcal{G}^{11}_{\uparrow\uparrow}(\mathbf{k},\tau) = \delta(\tau) + \sum_{\nu'}\left(\Delta_s\delta_{\uparrow\nu'} + \Delta_t\sigma^z_{\uparrow\nu'}\right)\mathcal{G}^{21}_{\nu'\uparrow}(\mathbf{k},\tau) \tag{5.13}$$

We may regard the coefficient of $\mathcal{G}^{21}_{\nu'\uparrow}$ in 5.13 as an element of the 'matrix order parameter'

$$\hat{\Delta} = \begin{bmatrix}\Delta_s + \Delta_t & 0\\ 0 & \Delta_s - \Delta_t\end{bmatrix} = \begin{bmatrix}\Delta_+ & 0\\ 0 & \Delta_-\end{bmatrix} \tag{5.14}$$

The simplifying notation for the non-zero elements of $\hat{\Delta}$ introduced here will be frequently utilized in the following analysis. The elements Δ_+ and Δ_- have important physical meaning; this will be discussed in detail in section 5.5. Recognizing the second term on the RHS of 5.13 as the matrix

product of the diagonal matrices $\mathbf{G}^{21}$ and $\hat{\Delta}$, we obtain

$$\left(-\frac{\partial}{\partial\tau} - \xi_{\mathbf{k}} + \delta\mu\right)\mathcal{G}^{11}_{\uparrow\uparrow}(\mathbf{k},\tau) - \Delta_+\mathcal{G}^{21}_{\uparrow\uparrow}(\mathbf{k},\tau) \;=\; \delta(\tau) \tag{5.15}$$

Taking the Fourier transform of 5.15, we obtain the simple algebraic equation

$$(i\omega_n - \xi_{\mathbf{k}} + \delta\mu)\,\mathcal{G}^{11}_{\uparrow\uparrow}(\mathbf{k},\omega_n) - \Delta_+\mathcal{G}^{21}_{\uparrow\uparrow}(\mathbf{k},\omega_n) \;=\; 1 \tag{5.16}$$

An essentially identical analysis for the interband Green's function $\mathcal{G}^{21}$ gives

$$(i\omega_n + \xi_{\mathbf{k}} + \delta\mu)\,\mathcal{G}^{21}_{\uparrow\uparrow}(\mathbf{k},\omega_n) - \Delta_+\mathcal{G}^{11}_{\uparrow\uparrow}(\mathbf{k},\omega_n) \;=\; 0 \tag{5.17}$$

The equations of motion for $\mathcal{G}^{11}_{\downarrow\downarrow}$ and $\mathcal{G}^{21}_{\downarrow\downarrow}$ are identical to 5.16 and 5.17, with the replacement of Δ_+ by Δ_-. We may without difficulty also construct similar expressions connecting $\mathcal{G}^{22}_{\alpha\beta}$ and $\mathcal{G}^{12}_{\alpha\beta}$. Solving these equations, we obtain the Green's functions of the system in the conjugate ω-space:

$$\mathcal{G}^{jj}_{\alpha\beta}(\mathbf{k},\omega_n) \;=\; \delta_{\alpha\beta}\frac{i\omega_n + (-1)^{j-1}\xi_{\mathbf{k}} + \delta\mu}{(i\omega_n + \delta\mu)^2 - {\xi_{\mathbf{k}}}^2 - \Delta^2_{\alpha\beta}} \tag{5.18}$$

$$\mathcal{G}^{21}_{\alpha\beta}(\mathbf{k},\omega_n) \;=\; \mathcal{G}^{12}_{\alpha\beta}(\mathbf{k},\omega_n) \;=\; \delta_{\alpha\beta}\frac{\Delta_{\alpha\beta}}{(i\omega_n + \delta\mu)^2 - {\xi_{\mathbf{k}}}^2 - \Delta^2_{\alpha\beta}} \tag{5.19}$$

where $j = 1, 2$ in 5.18.

5.4 The Excitonic Insulator

We examine first the case where only one species of exciton is present in the system. For definiteness, we shall only consider a singlet excitonic insulator (sEI) in detail. The analysis for the triplet excitonic insulator (tEI) is identical *mutatis mutandis*.

The Green's functions of the sEI are given by

$$\mathcal{G}^{jj}_{\alpha\beta}(\mathbf{k},\omega_n) \;=\; \delta_{\alpha\beta}\frac{i\omega_n + (-1)^{j-1}\xi_{\mathbf{k}} + \delta\mu}{(i\omega_n + \delta\mu)^2 - E^2_{\mathbf{k}}} \tag{5.20}$$

$$\mathcal{G}^{21}_{\alpha\beta}(\mathbf{k},\omega_n) \;=\; \mathcal{G}^{12}_{\alpha\beta}(\mathbf{k},\omega_n) \;=\; \delta_{\alpha\beta}\frac{\Delta_s}{(i\omega_n + \delta\mu)^2 - E^2_{\mathbf{k}}} \tag{5.21}$$

where $j = 1, 2$ in 5.20. For the tEI, Δ_s is simply replaced by Δ_t in the expression for E, and the interband Green's functions acquire σ^z spin-structure:

$$\mathcal{G}^{21}_{\alpha\beta}(\mathbf{k},\omega_n) \;=\; \mathcal{G}^{12}_{\alpha\beta}(\mathbf{k},\omega_n) \;=\; \sigma^z_{\alpha\beta}\frac{\Delta_t}{(i\omega_n + \delta\mu)^2 - E^2_{\mathbf{k}}} \tag{5.22}$$

From the spin structure of the interband Green's functions, it is straightforward to verify that the RHS of the expression for the triplet order parameter vanishes in the sEI state and *vice versa*.

The poles of the Green's functions define the electron excitation spectra:

$$-\delta\mu \pm E_{\mathbf{k}} \;=\; -\delta\mu \pm \sqrt{\xi^2_{\mathbf{k}} + \Delta^2_s} \tag{5.23}$$

where the 'rebuilt' conduction (valence) band is defined by $+E_{\mathbf{k}}$ ($-E_{\mathbf{k}}$) in equation 5.23. The 'rebuilt' band structure is plotted in figure 5.2. We see that the exciton condensation dramatically alters the excitation spectrum of the system - the nested bands are hybridized and an 'insulating' gap $2\Delta_s \ll E_G$ is opened. Like the BCS superconductor, the sEI phase also exhibits a square-root divergence in the DOS η_{EI} at the edge of the insulating gap:

$$\eta_{\text{EI}} \;=\; \eta_{\text{N}}\frac{E}{\sqrt{E^2 - \Delta^2}} \tag{5.24}$$

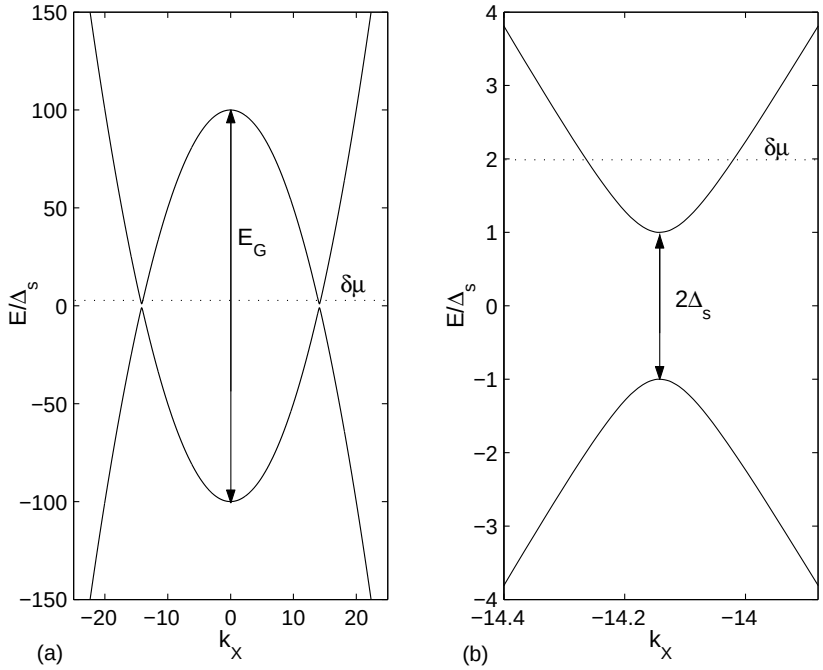

Figure 5.2: (a) The form of the 'rebuilt' spectrum: note the band hybridization and the opening of the gap $\Delta_s = 0.005 E_G$. We note that the 'rebuilt' valence band is to be translated by an amount $\mathbf{Q}$ in the reciprocal space, as in figure 5.1. (b) Detail of figure 5.2(a) illustrating the region in $\mathbf{k}$-space of least separation of the hybridized bands. Note the chemical potential $\delta\mu$ due to doping with excess electrons.

where η_N is the DOS in the normal phase. This is illustrated in figure 6.1(b).

Due to the obvious parallels in our treatment of the EI phase with the calculation for the BCS superconductor presented in chapter 3, it is interesting to consider whether or not the EI phase exhibits any kind of 'superphenomena'. In particular, the importance of excitons to energy transport in normal condensed-matter systems has lead some authors to suggest that the EI phase might display "super-thermal-conductivity" [48]. The apparent similarity to the BCS system is, however, misleading. The exciton condensate is an example of so-called Diagonal Long-Range Order (DLRO) as opposed to the Off-Diagonal Long-Range Order (ODLRO) that characterizes superfluid systems. As such, it may be unambiguously demonstrated that the EI phase displays no 'superphenomena' [51, 52].

Before deriving an expression for the singlet order parameter Δ_s, we relate the shift in the Fermi level $\delta\mu$ to the (constant) difference in the concentration of conduction band electrons and valence band holes and the form of the 'rebuilt' excitation spectrum. The concentration of electrons in the conduction band, n_e, is given by

$$n_e = \frac{1}{\beta V}\sum_{\mathbf{k},\alpha}\langle \hat{a}^\dagger_{1\mathbf{k}\alpha}\hat{a}_{1\mathbf{k}\alpha}\rangle = \lim_{\beta\to\infty}\frac{1}{\beta V}\sum_{\mathbf{k},n}\mathrm{Tr}\{\mathbf{G}^{11}(\mathbf{k},\omega_n)\}e^{-i\omega_n 0^-} \tag{5.25}$$

and similarly for the valence-band hole concentration n_h

$$n_h = \frac{1}{\beta V}\sum_{\mathbf{k},\alpha}\langle \hat{a}_{2\mathbf{k}\alpha}\hat{a}^\dagger_{2\mathbf{k}\alpha}\rangle = \lim_{\beta\to\infty} -\frac{1}{\beta V}\sum_{\mathbf{k},n}\mathrm{Tr}\{\mathbf{G}^{22}(\mathbf{k},\omega_n)\}e^{-i\omega_n 0^+} \tag{5.26}$$

We therefore have for δn

$$\delta n = n_e - n_h = \lim_{\beta\to\infty}\frac{1}{\beta V}\sum_{\mathbf{k},n}\sum_{j=1,2}\mathrm{Tr}\{\mathbf{G}^{jj}(\mathbf{k},\omega_n)\}e^{-(-1)^j i\omega_n 0^+} \tag{5.27}$$

Evaluating the Matsubara sums and converting the sum over $\mathbf{k}$ to an integral with respect to the semimetal energy spectrum ξ, we obtain

$$\begin{aligned}\delta n &= 2\eta_{\mathrm{N}}(0)\int_0^{\varpi} d\xi \left[\lim_{\beta\to\infty}\tanh\left(\frac{\beta(\delta\mu+E)}{2}\right)+\lim_{\beta\to\infty}\tanh\left(\frac{\beta(\delta\mu-E)}{2}\right)\right] \\ &= 2\eta_{\mathrm{N}}(0)\int_0^{\varpi} d\xi \left[1+\lim_{\beta\to\infty}\tanh\left(\frac{\beta(\delta\mu-E)}{2}\right)\right] \end{aligned} \tag{5.28}$$

The 'cut-off' ϖ is assumed much larger than either Δ_s or $\delta\mu$. The $\beta\to\infty$ (zero temperature) limit in 5.28 allows us to distinguish two cases

- $\delta\mu < \Delta_s$: the Fermi energy lies within the insulating gap.
- $\delta\mu > \Delta_s$: the Fermi energy lies in the 'rebuilt' conduction band.

In the former case, the limit of the hyperbolic tangent in 5.28 evaluates to -1 for all $\xi > 0$. The integrand of 5.28 therefore vanishes and we have $\delta n = 0$, i.e. equal electron and hole concentrations. It is convenient to assume that $\delta\mu = 0$ in this case. When the Fermi energy lies within the 'rebuilt' conduction band, however, the $\beta\to\infty$ limit of the hyperbolic tangent in 5.28 has a discontinuity at $E = \delta\mu$:

$$\lim_{\beta\to\infty}\tanh\left(\frac{\beta(\delta\mu-E)}{2}\right) = \begin{cases} -1 & \delta\mu - E < 0 \\ 1 & \delta\mu - E > 0 \end{cases} \tag{5.29}$$

The integrand of 5.28 is easily seen to vanish for $\xi^2 < \delta\mu^2 - {\Delta_s}^2$; we hence have for δn

$$\delta n = 4\eta_{\mathrm{N}}(0)\int_0^{\sqrt{\delta\mu^2-{\Delta_s}^2}} d\xi = 4\eta_{\mathrm{N}}(0)\sqrt{\delta\mu^2-{\Delta_s}^2} \tag{5.30}$$

It is conventional to express the concentration difference δn in 'energy units' [53]

$$n = \frac{\delta n}{4\eta_{\mathrm{N}}(0)}$$

The quantity n is the Fermi energy in the semimetal (normal) phase due to doping. Rearranging in equation 5.30 for the Fermi level $\delta\mu$ in the 'rebuilt' sEI phase, we thus obtain

$$\delta\mu = \sqrt{{\Delta_s}^2+n^2} \tag{5.31}$$

We now proceed to examine the expression for the singlet order parameter, equation 5.8. Expressed as an integral with respect to ξ, we obtain the self-consistency equation

$$\Delta_s = -\frac{g_s\eta_{\mathrm{N}}(0)}{2}\int_0^{\varpi} d\xi\frac{\Delta_s}{E}\left[1-\lim_{\beta\to\infty}\tanh\left(\frac{\beta(\delta\mu-E)}{2}\right)\right] \tag{5.32}$$

When $\delta\mu = 0$ (equal electron and hole concentrations), we may evaluate the integral

$$\Delta_s = -g_s\eta_{\mathrm{N}}(0)\Delta_s\ln\left(\frac{2\varpi}{\Delta_s}\right) \tag{5.33}$$

Ignoring the trivial solution, we solve for Δ_s:

$$\Delta_s = \Delta_{s0} \equiv 2\varpi\exp\left(\frac{1}{g_s\eta_{\mathrm{N}}(0)}\right) \tag{5.34}$$

The constant Δ_{s0} and the triplet equivalent Δ_{t0} (obtained via the replacement $g_s\to g_t$ in 5.34) provide useful energy parameters for the description of the EI and related phases. As will be shown below, they are the maximum value of the energy gap for any particular choice of coupling constants g_s and g_t.

In the case of unequal electron and hole concentrations ($\delta\mu > \Delta_s$), we have from 5.29

$$\Delta_s = -g_s\eta_{\rm N}(0)\Delta_s\int_{\sqrt{\delta\mu^2-{\Delta_s}^2}}^{\varpi}\frac{d\xi}{\sqrt{\xi^2+{\Delta_s}^2}} = -g_s\eta_{\rm N}(0)\Delta_s\ln\left(\frac{2\varpi}{\delta\mu+\sqrt{\delta\mu^2-{\Delta_s}^2}}\right) \quad (5.35)$$

Using the relations 5.31 and 5.34, we easily solve 5.35 for Δ_s

$${\Delta_s}^2 = \Delta_{s0}(\Delta_{s0}-2n) \quad (5.36)$$

We see that by increasing n from zero, we decrease the value of Δ_s from its maximum of Δ_{s0}. At a critical electron-hole concentration difference

$$n_c = \frac{\Delta_{s0}}{2} \quad (5.37)$$

the order parameter Δ_s vanishes. Since we assume that Δ_s is real, we see that for $n \geq n_c$ the formation of the sEI phase must be forbidden. This result illustrates the importance of the closeness to 'perfect' nesting for the appearance of the sEI phase. The sensitive dependence upon the nesting imperfection explains the scarcity of known excitonic insulators.

Finally, we consider the energetic stability of the excitonic state relative to the normal phase. By an identical analysis to that performed for the BCS superconductor, we find that the free energy change per unit volume upon entering the sEI state $\delta F_{\rm sEI}$ is given by

$$\delta F_{\rm sEI} = \int_0^{g_s}\frac{\Delta_s^2}{{g_s'}^2}dg_s' = -\frac{1}{2}\eta_{\rm N}(0)\left[\Delta_{s0}-2n\right]^2 \quad (5.38)$$

Since $\delta F_{\rm sEI} < 0$, the transition to the sEI phase liberates free energy. As such, the sEI phase is energetically stable relative to the normal phase below the critical doping concentration.

5.4.1 Density Waves in the Excitonic Insulator

The appearance of a density wave in a condensed-matter system implies a phase transition to a new state characterized by a periodic spatial modulation of the electron density of the normal phase. Density waves can be classified as either charge-density waves (CDWs) or spin-density waves (SDWs). In a system displaying a CDW, the total electron density displays a spatial modulation on top of that in the normal phase (figure 5.3(a)). In a real system, this change in the electron density is accompanied by a deformation of the lattice, perhaps leading to ferroelectricity. In the SDW state, each electron spin species exhibits a periodic modulation of its density such that the total electron density remains unchanged; this causes the appearance of antiferromagnetic ordering of the band electrons (figure 5.3(b)).

Nesting of a portion of the Fermi surface is essential for the realization of a density wave state [54]. In particular, the simple model of the excitonic insulator considered above is an important example of a system displaying a density wave, providing a successful quantitative description of many materials exhibiting a CDW or SDW state (see section 5.6). As we demonstrate below, the important distinction between the singlet and triplet EI phases is the appearance of a CDW and SDW in these systems respectively.

We define $\varphi_{j\mathbf{k}}(\mathbf{r})$ to be the Bloch function of an electron in the j-band with momentum $\mathbf{k}$, and define the electron-density corresponding to this state to be $\rho_{j\mathbf{k}}(\mathbf{r}) = |\varphi_{j\mathbf{k}}(\mathbf{r})|^2$. The local charge density $Q(\mathbf{r})$ and the local magnetic moment $M(\mathbf{r})$ may then be written as

$$Q(\mathbf{r}) = -\frac{e}{\beta}\sum_{\mathbf{k}}\left[2{\rm Re}\left(\varphi_{1\mathbf{k}}(\mathbf{r})\bar{\varphi}_{2\mathbf{k}}(\mathbf{r})\right){\rm Tr}\left\{\mathbf{G}^{21}(\mathbf{k},0^+)\right\} + \sum_{j=1,2}\rho_{j\mathbf{k}}(\mathbf{r}){\rm Tr}\left\{\mathbf{G}^{jj}(\mathbf{k},0^+)\right\}\right] \quad (5.39)$$

$$M(\mathbf{r}) = -\frac{\mu_B}{\beta}\sum_{\mathbf{k}}2{\rm Re}\left(\varphi_{1\mathbf{k}}(\mathbf{r})\bar{\varphi}_{2\mathbf{k}}(\mathbf{r})\right){\rm Tr}\left\{\sigma^z\mathbf{G}^{21}(\mathbf{k},0^+)\right\} \quad (5.40)$$

where μ_B is the Bohr magneton and e the charge on the electron [55]. The matrix Green's functions

are in their τ-representation. In the normal phase, the local magnetic moment is always zero, and the expression for the local charge density involves a sum over the densities $\rho_{j\mathbf{k}}(\mathbf{r})$ only. We see that the presence of the interband Green's functions in the EI phase introduces 'interference' terms of the form $\varphi_{1\mathbf{k}}(\mathbf{r})\bar{\varphi}_{2\mathbf{k}}(\mathbf{r})$ into the expressions for $Q(\mathbf{r})$ and $M(\mathbf{r})$. These 'interference' terms are indicative of the formation of a density wave in the system [48, 49]. Referring to equations 5.21 and 5.22, we see that in the sEI phase the 'interference' terms appear only in the expression for the local charge density; in the tEI phase they are only present in the local magnetic moment. Thus, the transition into the sEI state involves the formation of a CDW, whereas the tEI state is characterized by the appearance of a SDW.

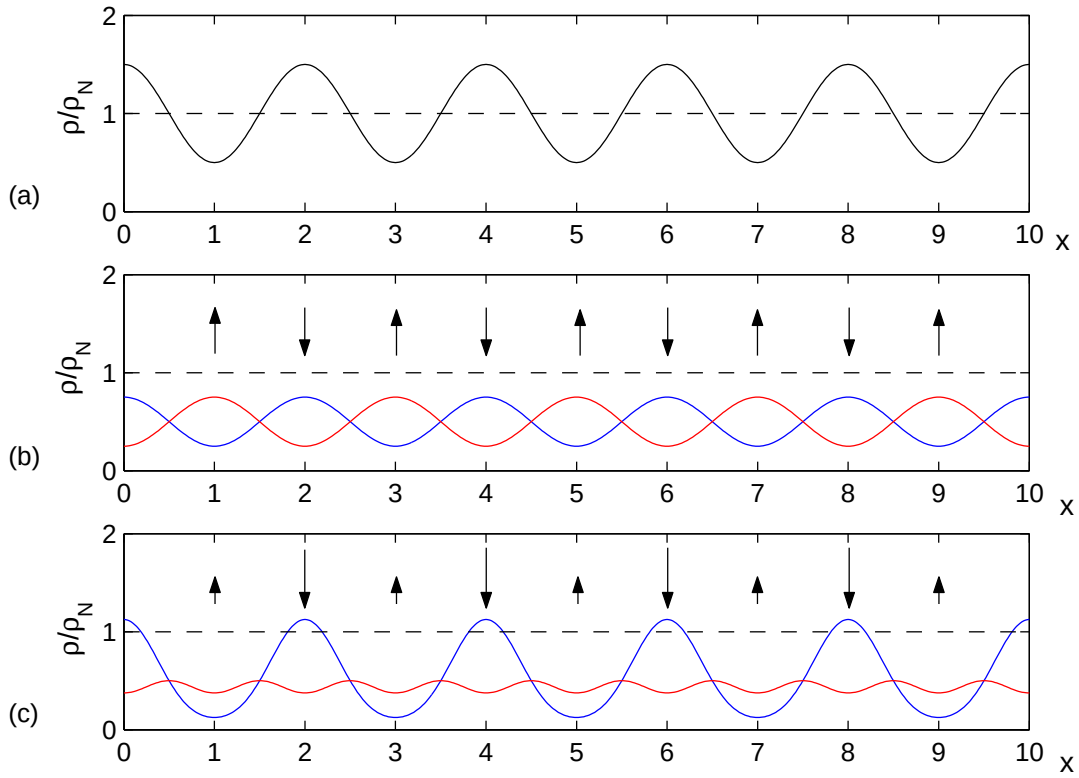

Figure 5.3: (a) The CDW state in a one-dimensional system: the normal state electron density ρ_N (dashed line) undergoes a periodic modulation (solid line). (b) The SDW state: the spin-down and spin-up electron densities (blue and red respectively) exhibit a periodic modulation such that the total electron density remains as in the normal phase. The local spin-density is indicated by the arrows: note the appearance of antiferromagnetic order. (c) Interference of CDW and SDW: the local spin-density exhibits ferromagnetic order.

5.5 The Excitonic Ferromagnet

It has been demonstrated by Volkov *et al.* that when both singlet and triplet electron-hole pairing occurs in the system, the spin-degeneracy of the excitation spectrum is lifted leading to a ferromagnetic state [55–57]. This may be qualitatively understood by the interference of the CDW and SDW associated with the singlet- and triplet-pairing respectively. As illustrated in figure 5.3(c), this interference produces a spin-up and spin-down density wave of differing amplitudes, thus leading to a partial polarization of the band-electrons in the system. The resulting ferromagnetic state is referred to as the excitonic ferromagnet (EF).

In the EF phase, the singlet and triplet order parameters Δ_s and Δ_t are simultaneously present

in the system. From 5.18 and 5.19 we therefore have the Green's functions in the EF phase

$$\mathcal{G}^{jj}_{\alpha\beta}(\mathbf{k},\omega_n) = \delta_{\alpha\beta}\frac{i\omega_n + (-1)^{j-1}\xi_{\mathbf{k}} + \delta\mu}{(i\omega_n+\delta\mu)^2 - {E_{\mathbf{k}\sigma}}^2} \tag{5.41}$$

$$\mathcal{G}^{21}_{\alpha\beta}(\mathbf{k},\omega_n) = \mathcal{G}^{12}_{\alpha\beta}(\mathbf{k},\omega_n) = \delta_{\alpha\beta}\frac{\Delta_\sigma}{(i\omega_n+\delta\mu)^2 - {E_{\mathbf{k}\sigma}}^2} \tag{5.42}$$

where $j = 1,2$ in 5.41. The label σ is either $+$ or $-$ corresponding to $\alpha\beta = \uparrow\uparrow$ and $\alpha\beta = \downarrow\downarrow$ respectively. The poles of the Green's functions define the 'rebuilt' electron excitation spectra, with different expressions for the two spin-species:

$$-\delta\mu \pm E_{\mathbf{k}\sigma} = -\delta\mu \pm \sqrt{{\xi_{\mathbf{k}}}^2 + \Delta_\sigma^2} \tag{5.43}$$

where the subscript σ is $+$ for spin-up electrons and $-$ for spin-down electrons and the sign of $E_{\mathbf{k}}$ defines the 'rebuilt' valence and conduction bands as before. The presence of both singlet and triplet order parameters therefore lifts the spin-degeneracy of the 'rebuilt' spectrum 5.23 by opening different insulating gaps Δ_+ and $|\Delta_-|$ in the spin-up and spin-down subbands respectively (figure 5.4(a)). The DOS of the 'rebuilt' excitation spectrum for spin-σ electrons is

$$\eta_{\mathrm{EF}\sigma} = \eta_{\mathrm{N}\sigma}\frac{E}{\sqrt{E^2 - \Delta_\sigma^2}} \tag{5.44}$$

where $\eta_{\mathrm{N}\sigma} = \frac{1}{2}\eta_{\mathrm{N}}$ is the spin-σ DOS in the normal phase. The DOS in the EF phase is plotted in figure 5.4(b). We note that $\eta_{\mathrm{EF}+}$ is higher near the edge of the spin-up gap than $\eta_{\mathrm{EF}-}$ a comparable distance from the edge of the spin-down gap.

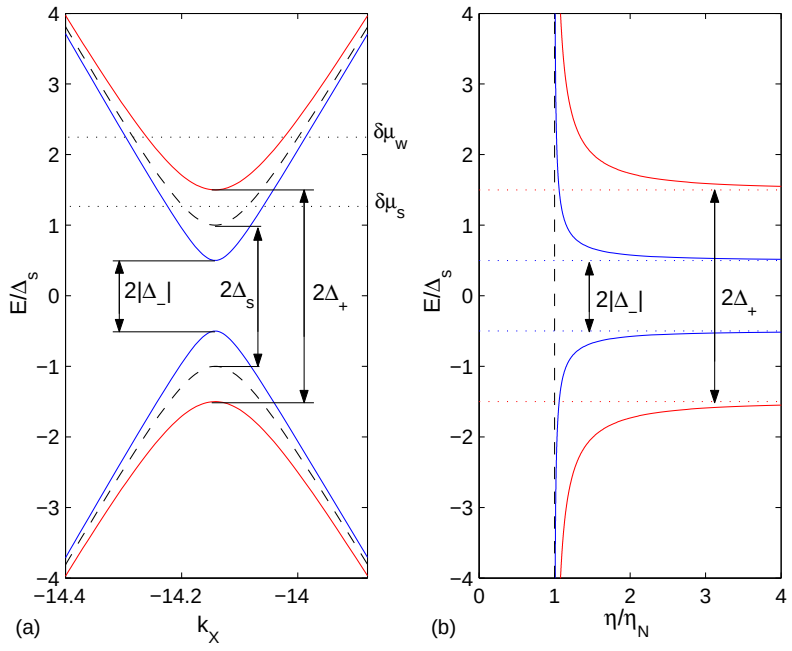

Figure 5.4: (a) Comparison of the excitation spectrum in the EF phase (red line spin-up, blue-line spin-down) to the EI phase (black dashed line) over the same range as in figure 5.2(b). In the EF phase we take $\Delta_s = 2\Delta_t = 0.005E_G$. Note the position of the chemical potential for weak ferromagnetism $\delta\mu_{\mathrm{w}}$ and strong ferromagnetism $\delta\mu_{\mathrm{s}}$. The rest of the excitation spectrum does not significantly differ from that for the EI phase (figure 5.2(a)). (b) The DOS of the spin-up and spin-down excitation spectra, compared to the DOS in the normal phase for one spin-species η_{N}. Note the enhancement of the spin-up DOS relative to the spin-down.

We obtain the self-consistency equations for Δ_s and Δ_t from the definitions 5.8 and 5.9 respectively; we present them in integral form:

$$\Delta_s = -\frac{g_s\eta_{\rm N}(0)}{4}\sum_{\sigma=-,+}\int_0^{\varpi} d\xi\frac{\Delta_\sigma}{E_\sigma}\left[1-\lim_{\beta\to\infty}\tanh\left(\frac{\beta(\delta\mu-E_\sigma)}{2}\right)\right] \tag{5.45}$$

$$\Delta_t = -\frac{g_t\eta_{\rm N}(0)}{4}\sum_{\sigma=-,+}\sigma\int_0^{\varpi} d\xi\frac{\Delta_\sigma}{E_\sigma}\left[1-\lim_{\beta\to\infty}\tanh\left(\frac{\beta(\delta\mu-E_\sigma)}{2}\right)\right] \tag{5.46}$$

The difference in electron and hole concentrations in energy units is also readily obtained:

$$n = \frac{1}{4}\sum_{\sigma=-,+}\int_0^{\varpi} d\xi\left[1+\lim_{\beta\to\infty}\tanh\left(\frac{\beta(\delta\mu-E_\sigma)}{2}\right)\right] \tag{5.47}$$

We see by reference to equation 5.29 that the $\beta\to\infty$ limit in 5.47 defines three distinct cases:

- $\delta\mu < |\Delta_-|, \Delta_+$: the Fermi energy lies within the insulating gap for both spin subbands. As for the EI phase, this corresponds to zero doping.
- $|\Delta_-| < \delta\mu < \Delta_+$: the Fermi energy lies inside the spin-down conduction band but also within the spin-up insulating gap. As such, the conduction-band electron population is completely spin-polarized, so-called strong ferromagnetism.
- $|\Delta_-|, \Delta_+ < \delta\mu$: the Fermi energy lies inside both the spin-down and spin-up conduction bands, and so the conduction band electron population is only partially spin-polarized. This is referred to as weak ferromagnetism.

We shall consider the case of the doped and undoped systems separately.

The ferromagnetic state is characterized by the appearance of a spontaneous magnetization M, here defined

$$M = \mu_B(n^1_{e\uparrow}+n^2_{e\uparrow}-n^1_{e\downarrow}-n^2_{e\downarrow}) \tag{5.48}$$

where $n^i_{e\sigma}$ is the concentration of j-band electrons with spin σ and μ_B is the Bohr magneton. We therefore have for M in integral form

$$M = 2\mu_B\eta_{\rm N}(0)\sum_{\sigma=-,+}\sigma\int_0^{\varpi} d\xi\left[1+\lim_{\beta\to\infty}\tanh\left(\frac{\beta(\delta\mu-E_\sigma)}{2}\right)\right] \tag{5.49}$$

It is curious to note that for $\delta\mu = 0$, the system exhibits no magnetization. This is due to the enhanced DOS at the edge of the filled spin-up valence band, which compensates for the spin-splitting. Therefore, in the model considered we only obtain a ferromagnetic state if $\Delta_s, \Delta_t \neq 0$ simultaneously in the presence of impurity doping. We shall continue, however, to refer to the coexistence of the two order parameters at zero doping as the EF phase.

5.5.1 The $n = 0$ System

At equal electron and hole concentrations, the equations 5.45 and 5.46 may be evaluated

$$\Delta_s = -\frac{g_s\eta_{\rm N}(0)}{2}\left[\Delta_+\ln\left(\frac{2\varpi}{\Delta_+}\right)+\Delta_-\ln\left(\frac{2\varpi}{|\Delta_-|}\right)\right] \tag{5.50}$$

$$\Delta_t = -\frac{g_t\eta_{\rm N}(0)}{2}\left[\Delta_+\ln\left(\frac{2\varpi}{\Delta_+}\right)-\Delta_-\ln\left(\frac{2\varpi}{|\Delta_-|}\right)\right] \tag{5.51}$$

To consider the coexistence phase (i.e. $\Delta_s, \Delta_t \neq 0$), it is convenient, however, to recast the equations 5.50 and 5.51 in the form

$$\ln\left(\frac{\Delta_{t0}}{\Delta_{s0}}\right) = \frac{1-z^2}{2z}\ln\left|\frac{1+z}{1-z}\right|, \qquad 2\ln\left(\frac{\Delta_{s0}}{\Delta_s}\right) = \ln|1-z^2|+z\ln\left|\frac{1+z}{1-z}\right| \tag{5.52}$$

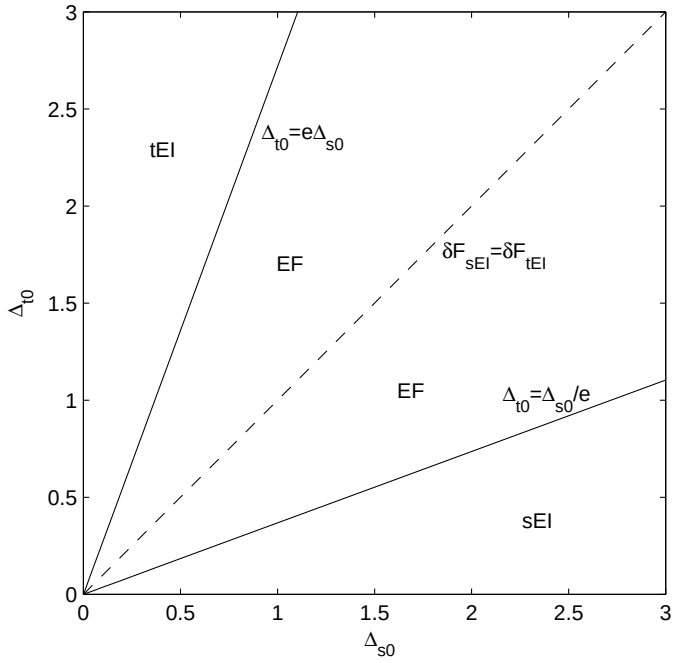

Figure 5.5: The phase diagram of the system at equal electron and hole concentrations. The EF phase is metastable, with the boundary between the tEI and sEI phases given by $\delta F_{\rm sEI} = \delta F_{\rm tEI}$.

where $z = \Delta_t/\Delta_s$ is a parameter which takes all values in the range $(0, \infty)$. The system of equations 5.52 only has a nontrivial solution when the condition $|\ln(\Delta_{t0}/\Delta_{s0})| < 1$ is fulfilled. This corresponds to the region between the lines

$$\Delta_{t0} = e\Delta_{s0}, \qquad \Delta_{t0} = e^{-1}\Delta_{s0} \tag{5.53}$$

in the $(\Delta_{s0}, \Delta_{t0})$-plane. These boundaries correspond to the limits $z \to 0$ $(\Delta_t \to 0)$ and $z \to \infty$ $(\Delta_s \to 0)$ respectively. The remaining regions of the phase diagram (figure 5.5) correspond to the sEI and tEI phases, determined by energetic stability analysis.

The behaviour of the singlet and triplet gaps in the coexistence regime found above exhibit a curious dependence upon the coupling constants g_s and g_t respectively: as the magnitude of the coupling constant increases, the value of the corresponding gap decreases. Indeed, the singlet (triplet) order parameter vanishes as the boundary with the sEI (tEI) phase is approached, precisely the opposite of what is expected (see section 2.5). This 'anomalous' behaviour suggests that the coexistence regime only occurs as a metastable state, i.e. it liberates less free energy upon formation than the pure EI phases [9, 53].

This is confirmed by calculating the free energy per unit volume of the EF phase relative to the normal phase, $\delta F_{\rm EF}$. By a straightforward generalization of the Feynman-Pauli theorem to the case where two interactions are present, we have for the free energy per unit volume of the EF phase for some point $(\Delta'_{s0}, \Delta'_{t0})$ within the region of predicted coexistence

$$\delta F_{\rm EF} = \int_C \frac{{\Delta_s}^2}{{g_s}^2} dg_s + \frac{{\Delta_t}^2}{{g_t}^2} dg_t \tag{5.54}$$

The contour C joins the given point $(\Delta'_{s0}, \Delta'_{t0})$ with the origin, and lies entirely within the region of coexistence. It is convenient to choose a contour such that the ratio z is constant along the path of integration. After lengthy calculation (summarized in section A.3 of the mathematical

appendix), we have

$$\delta F_{\rm EF} \;=\; f(z)\delta F_{\rm sEI} \;=\; f(z^{-1})\delta F_{\rm tEI} \tag{5.55}$$

where

$$\ln\left(f(z)\right) \;=\; \ln\left|\frac{1+z^2}{1-z^2}\right| - z\ln\left|\frac{1+z}{1-z}\right| \tag{5.56}$$

and z is as defined above. It may be shown that $\ln\left(f(z)\right) < 0$ for all $z > 0$. Therefore $0 > \delta F_{\rm EF} > \delta F_{\rm tEI}, \delta F_{\rm sEI}$ in the region of coexistence, and so we conclude that the coexistence phase is always unstable towards the pure phases at zero doping. Thus, only the sEI and tEI phases are present in the phase diagram at $\delta\mu = 0$, separated by the line $\delta F_{\rm sEI} = \delta F_{\rm tEI}$.

5.5.2 The $n \neq 0$ System

Weak Ferromagnetism

The weak ferromagnetic regime (Δ_+, $|\Delta_-| < \delta\mu$), is characterized by the equations

$$\Delta_s \;=\; -\frac{g_s\eta_{\rm N}(0)}{2}\left[\Delta_+\ln\left(\frac{2\varpi}{\delta\mu+\sqrt{\delta\mu^2-\Delta_+^2}}\right)+\Delta_-\ln\left(\frac{2\varpi}{\delta\mu+\sqrt{\delta\mu^2-\Delta_-^2}}\right)\right] \tag{5.57}$$

$$\Delta_t \;=\; -\frac{g_t\eta_{\rm N}(0)}{2}\left[\Delta_+\ln\left(\frac{2\varpi}{\delta\mu+\sqrt{\delta\mu^2-\Delta_+^2}}\right)-\Delta_-\ln\left(\frac{2\varpi}{\delta\mu+\sqrt{\delta\mu^2-\Delta_-^2}}\right)\right] \tag{5.58}$$

$$n \;=\; \frac{1}{2}\left(\sqrt{\delta\mu^2-\Delta_+^2}+\sqrt{\delta\mu^2-\Delta_-^2}\right) \tag{5.59}$$

$$M \;=\; 2\mu_B\eta_{\rm N}(0)\left(\sqrt{\delta\mu^2-\Delta_+^2}-\sqrt{\delta\mu^2-\Delta_-^2}\right) \tag{5.60}$$

Strong Ferromagnetism

The strongly ferromagnetic regime ($\Delta_+ > \delta\mu > |\Delta_-|$) is specified by the equations

$$\Delta_s \;=\; -\frac{g_s\eta_{\rm N}(0)}{2}\left[\Delta_+\ln\left(\frac{2\varpi}{\Delta_+}\right)+\Delta_-\ln\left(\frac{2\varpi}{\delta\mu+\sqrt{\delta\mu^2-\Delta_-^2}}\right)\right] \tag{5.61}$$

$$\Delta_t \;=\; -\frac{g_t\eta_{\rm N}(0)}{2}\left[\Delta_+\ln\left(\frac{2\varpi}{\Delta_+}\right)-\Delta_-\ln\left(\frac{2\varpi}{\delta\mu+\sqrt{\delta\mu^2-\Delta_-^2}}\right)\right] \tag{5.62}$$

$$n \;=\; \frac{1}{2}\sqrt{\delta\mu^2-\Delta_-^2} \tag{5.63}$$

$$M \;=\; -2\mu_B\eta_{\rm N}(0)\sqrt{\delta\mu^2-\Delta_-^2} \;=\; -4\mu_B\eta_{\rm N}(0)n \tag{5.64}$$

We see from 5.64 that in the strongly ferromagnetic regime, the excess electrons in the system are completely spin-polarized. For any choice of n, this is the maximum magnetization exhibited by the EF phase. Since n is limited by equation 5.37, this maximum magnetization is expected to be small.

The Phase Diagram

The phase diagram of the system is presented in figure 5.6. We have constructed it in terms of the dimensionless variables $\Delta_{s0}/2n$ and $\Delta_{t0}/2n$. We note that for $\Delta_{s0}, \Delta_{t0} < 2n$, the excitonic state is not possible, as the electron-hole concentration difference exceeds the critical level. Hence, the normal phase is realized in this region.

The boundary between the sEI and the EF phases is determined as follows. The transition into the EF phase from the EI phases is second order; therefore as the sEI-EF boundary is approached

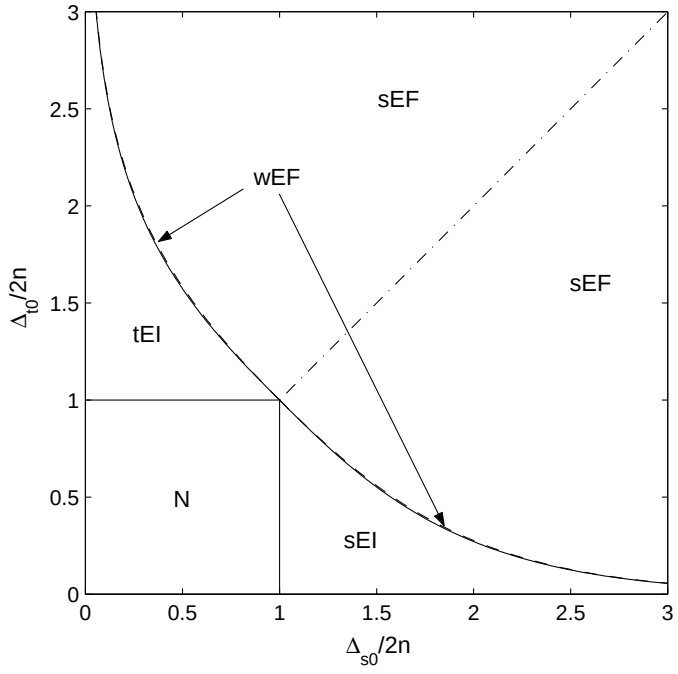

Figure 5.6: The phase diagram for the system at unequal electron and hole concentrations. Note the region of weak ferromagnetism wEF and strong ferromagnetism sEF. The boundary between the weak and strong ferromagnetic regimes is given by the dashed line; the diagonal $\Delta_{s0}/2n = \Delta_{t0}/2n$ by the dot-dashed line. Note that the normal (N) phase is realized for $\Delta_{s0},\ \Delta_{t0} \leq 2n$.

from inside the EF phase, the triplet order parameter $\Delta_t \to 0$ whilst Δ_s and $\delta\mu$ (continuously) approach their values in the sEI phase (equations 5.36 and 5.31 respectively). Sufficiently close to the boundary $\Delta_s \gg \Delta_t$: the EF phase near the boundary is in the weakly ferromagnetic regime. We consider the equation 5.58. Expanding the RHS as a Taylor series in Δ_t to first order, and setting $\delta\mu$ and Δ_s to their values in the sEI phase, we obtain

$$\Delta_t \left[\frac{1}{g_s \eta_{\rm N}(0)} - \frac{1}{g_t \eta_{\rm N}(0)} - \frac{\Delta_{s0}(\Delta_{s0} - 2n)}{n\left(n + \sqrt{\Delta_{s0}^2 - 2n\Delta_{s0} + n^2}\right)} \right] = 0 \tag{5.65}$$

Ignoring the trivial solution $\Delta_t = 0$, equation 5.65 implies the relation

$$\Delta_{t0} = \Delta_{s0} \exp\left(2 - \frac{\Delta_{s0}}{n}\right) \tag{5.66}$$

where $\Delta_{s0} > 2n$. The relation 5.66 thus defines the boundary between the weakly-ferromagnetic regime of the EF phase and the sEI phase . We similarly have for the boundary between the tEI and the weakly-ferromagnetic EF phases

$$\Delta_{s0} = \Delta_{t0} \exp\left(2 - \frac{\Delta_{t0}}{n}\right) \tag{5.67}$$

which holds for $\Delta_{t0} > 2n$. A more sophisticated analysis shows that the region where the EF phase occurs is defined by replacing the equality with $\geq$ in equations 5.66 and 5.67 [55].

The boundary between the weak and strong regimes is defined by the equality $\delta\mu = |\Delta_+|$. Referring to equations 5.59 and 5.63, this allows us to define the spin-up and spin-down insulating

gaps in terms of a real parameter ϕ:

$$\Delta_+ = 2n\cosh(\phi), \qquad \Delta_- = 2n\sinh(\phi) \tag{5.68}$$

where $-\infty < \phi < \infty$. Using 5.68, we may obtain parametric equations in ϕ for the boundary between weak and strong ferromagnetism on the phase diagram:

$$\begin{aligned} \frac{\Delta_{s0}}{2n} &= \exp\left(e^{\phi}\left(\cosh(\phi)\ln\left(\cosh(\phi)\right) + \sinh(\phi)\ln\left(\cosh(\phi)+1\right)\right)\right) \\ \frac{\Delta_{t0}}{2n} &= \exp\left(e^{-\phi}\left(\cosh(\phi)\ln\left(\cosh(\phi)\right) - \sinh(\phi)\ln\left(\cosh(\phi)+1\right)\right)\right) \end{aligned} \tag{5.69}$$

We note the dependence of $\Delta_{s0}/2n$ upon the parameter $\phi \geq 0$ in the limits $\phi \to 0, \infty$:

$$\frac{\Delta_{s0}}{2n} = \begin{cases} 1 + \ln(2)\phi + \mathcal{O}(\phi^2) & 0 < \phi \ll 1 \\ \frac{1}{2}e^{\phi} + \frac{1}{2} + \mathcal{O}(e^{-\phi}) & \phi \gg 1 \end{cases} \tag{5.70}$$

An identical expansion is obtained for $\Delta_{t0}/2n$ for $\phi \leq 0$. The point $\Delta_{s0}/2n = \Delta_{t0}/2n = 1$ therefore corresponds to $\phi = 0$; as ϕ is increased (decreased), we move along the weak-strong boundary close to the sEI-EF (tEI-EF) phase boundary (see figure 5.6).

The free energy per unit volume released upon entering the EF state is calculated using the formula 5.54. Instead of taking the contour $\mathcal{C}$ from the origin as in the undoped case, however, it is more convenient to start from the point $\Delta_{s0}/2n = \Delta_{t0}/2n = 1$ on the phase diagram figure 5.6, where all phases are equally stable. Using standard methods [58], we have the result

$$\delta F_{\text{EF}} = -\frac{1}{2}\eta_{\text{N}}(0)\left[\Delta_+^2 + \Delta_-^2 - 4\delta\mu n + 4n^2\right] \tag{5.71}$$

It has been demonstrated numerically that the EF phase is more stable than the EI phases in the region where it is predicted to occur by the self-consistency equations [55].

Two Analytic Solutions

In general, it is not possible to derive an analytic expression for the value of the order parameters Δ_s and Δ_t for given Δ_{s0}, Δ_{t0} and n. There are, however, two important cases where an analytic solution is possible: the solution on the boundary between the weak and strong ferromagnetic regimes, and along the diagonal $\Delta_{s0}/2n = \Delta_{t0}/2n$ (see figure 5.6). We examine these solutions in detail below.

The solution on the boundary separating the weak and strong ferromagnetic regimes has already been stated (5.68). Because of the proximity of the line 5.69 to the boundary of the EF and EI phases, it is interesting to compare the behaviour of the two phases along this line on the phase diagram. We consider the case $\phi \geq 0$, so that we examine the behaviour of the EF phase close to the boundary with the sEI phase. In figure 5.7(a) we plot the gaps Δ_+ and Δ_- as defined by 5.68, as well as Δ_s in the sEI phase for the given values of $\Delta_{s0}/2n$.

Approaching the point $\Delta_{s0}/2n = \Delta_{t0}/2n = 1$, we see that the difference between Δ_+ and Δ_s becomes increasingly pronounced. Since the increase in Δ_+ over its value in the sEI phase (Δ_s) occurs within the small region where the weak regime is realized, the change in its value is very rapid upon entry into the EF phase from the sEI. Similar considerations apply for Δ_-. An interesting feature of the solution 5.68 is the $\phi \to 0$ limit. We see from 5.68 that at $\Delta_{s0}/2n = \Delta_{t0}/2n = 1$, the spin-down gap $|\Delta_-|$ vanishes whilst $\Delta_+ = 2n$. This is the only point on the EF boundary where the order parameters do not converge to their values in the EI phases.

On the boundary between the weak and strong regimes, the free energy per unit volume of the EF phase relative to the normal may be expressed in terms of the parameter ϕ as

$$\delta F_{\text{EF}} = -2n^2\eta_{\text{N}}(0)\cosh(\phi)\left(\cosh(\phi) - 1\right) \tag{5.72}$$

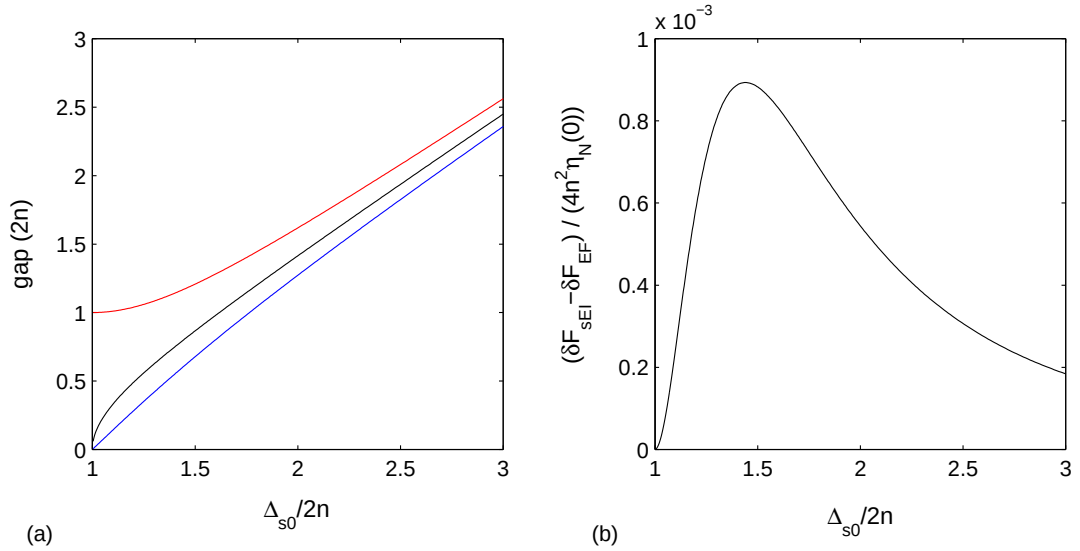

Figure 5.7: (a) The variation of the gaps along the $\phi \geq 0$ branch of the weak-strong boundary. The red line is Δ_+, the blue Δ_-. The black line is Δ_s in the sEI for the corresponding values of $\Delta_{s0}/2n$. All the gaps are expressed in multiples of $2n$. (b) The difference in free energy per unit volume between the sEI and EF phases along the $\phi \geq 0$ branch of the weak-strong boundary. Since $\delta F_{\rm sEI} - \delta F_{\rm EF} > 0$, the EF phase is the most stable for the given range of $\Delta_{s0}/2n$.

For $\phi \geq 0$, we plot in figure 5.7(b) the difference between the free energy per unit volume of the sEI and EF phases as a function of $\Delta_{s0}/2n$. For all $\phi \geq 0$, the EF phase is energetically favoured over the EI phases. This may be analytically verified in the limits $\phi \ll 1$ and $\phi \gg 1$ where we have the asymptotic expansions

$$\delta F_{\rm EI} - \delta F_{\rm EF} \quad = \quad \begin{cases} n^2\eta_{\rm N}(0)\left(1 - 2\left(\ln(2)\right)^2\right)\phi^2 + \mathcal{O}(\phi^3), & \phi \ll 1 \\ \\ \frac{1}{12}n^2\eta_{\rm N}(0)e^{-3\phi} + \mathcal{O}(e^{-4\phi}), & \phi \gg 1 \end{cases} \tag{5.73}$$

The EF phase is therefore realized everywhere along the weak-strong boundary.

The solution on the diagonal $\Delta_{s0}/2n = \Delta_{t0}/2n$ may be regarded as complementing the analysis on the boundary between the weak and strong regimes, affording an insight into the behaviour of the EF system far away from the boundary with the EI phases (see figure 5.6). The diagonal lies entirely within the strong regime; after some manipulation of equations 5.61 and 5.62, we find that the solution for the gaps Δ_+ and Δ_- is determined by the relations

$$\Delta_- \left[\ln\left(2n + \sqrt{4n^2 + \Delta_-^2}\right) - \ln(\Delta_{s0})\right] \quad = \quad 0, \qquad \Delta_+ \quad = \quad \Delta_{s0} \tag{5.74}$$

These equations exhibit two distinct solutions: for $\Delta_{s0}/2n \geq 1$,

$$\Delta_- \quad = \quad 0, \qquad \Delta_+ \quad = \quad \Delta_{s0}; \tag{5.75}$$

for $\Delta_{s0}/2n \geq 2$ the solution

$$\Delta_-^2 \quad = \quad \Delta_{s0}\left(\Delta_{s0} - 4n\right), \qquad \Delta_+ \quad = \quad \Delta_{s0} \tag{5.76}$$

is also possible. We note that for $\Delta_{s0}/2n \geq 2$, the solution is not unique. This is a characteristic feature of the system and occurs when the inequality $\Delta_{t0}\Delta_{s0} \geq 16n^2$ is satisfied [59]. The physically

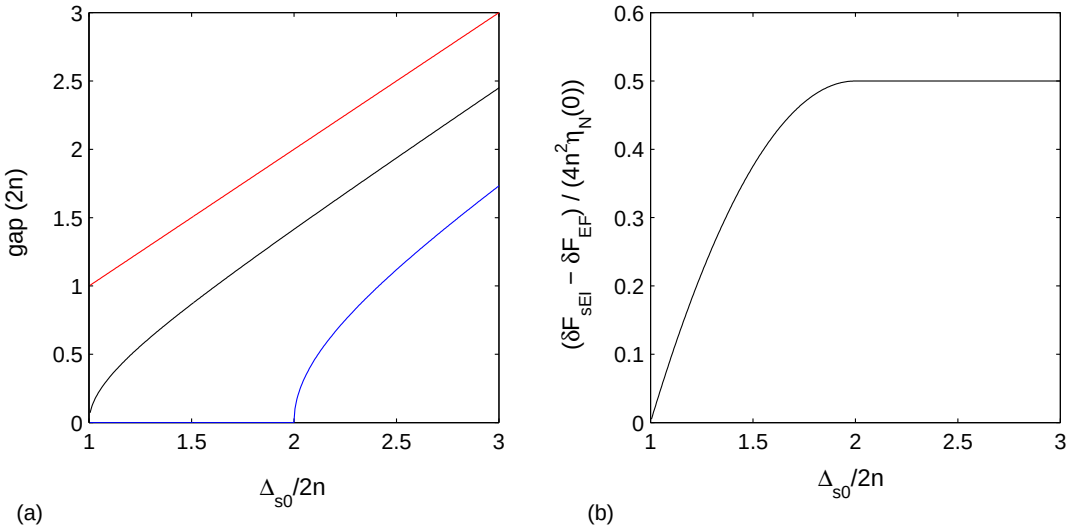

Figure 5.8: (a) The variation of the gaps along the diagonal. As in figure 5.7, the red line is Δ_+, the blue Δ_-, and the black line is Δ_s in the sEI for the corresponding values of $\Delta_{s0}/2n$. All the gaps are expressed in multiples of $2n$. (b) The difference in free energy per unit volume between the sEI and EF phases along the diagonal.

realized solution in this region is determined via appeal to energetic stability. We have for the free energy per unit volume relative to the normal phase for the two solutions 5.75 and 5.76

$$\begin{aligned} \delta F_{\text{EF}} &= -\tfrac{1}{2}\eta_{\text{N}}(0)\left[\Delta_{s0}^2 - 4n^2\right], && \tfrac{\Delta_{s0}}{2n} \geq 1 \\ \delta F_{\text{EF}} &= -\tfrac{1}{2}\eta_{\text{N}}(0)\left[(\Delta_{s0} - 2n)^2 + 2n^2\right], && \tfrac{\Delta_{s0}}{2n} \geq 2 \end{aligned} \tag{5.77}$$

It may be easily verified that for $\Delta_{s0}/2n \geq 2$ the solution 5.76 is the most stable.

In figure 5.8(a) we plot the solutions to the equations 5.74 and the value of Δ_s in the singlet EI phase for the corresponding values of $\Delta_{s0}/2n$. We note the absence of the spin-down gap for $2 \geq \Delta_{s0}/2n \geq 1$. In figure 5.8(b), we also plot the difference between the free energies of the EF and EI phases. It is clear that the EF phase is the most stable along the diagonal.

5.6 Experimental Evidence

The model of the nested semimetal considered here is much too simplistic to closely resemble any physical system; many improvements have accordingly been made upon it, most importantly the inclusion of non-nested portions of the Fermi surface which are not subject to the excitonic instability [60]. Although the qualitative picture of the EI phase as described above remains intact in such a system, the non-nested portions of the Fermi surface remain "ungapped" by the excitonic condensation, and so the system does not undergo a transition to an insulating state.

The topology of the Fermi surface in many physical systems displaying density wave phenomena is well-described in terms of a nested and a non-nested portion. An excellent example of this is provided by the itinerant antiferromagnetism of chromium and some of its alloys, which has attracted much interest since the mid-1960s (for reviews, see [61,62]). The basis for the theoretical description of these systems is the so-called Rice model, which attributes the SDW to an exciton-mediated hybridization of imperfectly nested portions of the Fermi surface. Notable examples of other systems to which the EI model has been applied with success are the vanadium dichalcogenides (in particular V_3S_4 and V_3Se_4) and the semiconductors of the A_4B_6 group (e.g. PbTe and SnTe) [61,63]. The latter systems are well modelled as nested semimetals in which the critical

temperature of the excitonic state lies above the melting point of the crystal itself.

The EI model has not been applied to any of these materials without reservation. Therefore, the discovery of what appears to be a pressure-driven transition to the 'classic' EI state in the narrow band-gap semiconductors $TmSe_{0.45}Te_{0.55}$ and $Sm_{0.75}La_{0.25}S$ came as an exciting development [64, 65]. The situation in $TmSe_{0.45}Te_{0.55}$ is of particular interest, as the temperature-pressure phase diagram has been determined, displaying an excellent agreement with the theoretical predictions [49]. Several other candidates for a realization of the EI phase have been identified, most recently FeSi and $CaPd_3O_4$; these interpretations are, however, still subject to dispute [66,67].

Experimental evidence for the EF phase has proved much more elusive. Although the original papers of Volkov *et al.* suggested that the magnetic behaviour of the narrow-band semiconductor HgTe could be explained in terms of the excitonic scenario, more convincing mechanisms which do not involve exciton condensation have since been proposed [57, 68]. A major reason for this rarity is the destructive effect that non-nested portions of the Fermi surface, which act like particle reservoirs, have been shown to exert upon the EF phase [69].

The EF scenario has most recently been invoked to explain the high-temperature weak ferromagnetism of the lanthanum- and vacancy-doped alkaline earth hexaborides $Ca_{1-x}La_xB_6$, $Ca_{1-x}B_6$, $Sr_{1-x}La_xB_6$ and $Ba_{1-x}La_xB_6$. When very weakly doped with lanthanum impurities or vacancies ($x \approx 0.005$), these materials have been found to exhibit a weak magnetization that persists up to remarkably high temperatures, often in excess of 700K [20,21,70]. Band structure calculations have revealed that the alkaline earth hexaborides are semimetals with very small band-overlap [71, 72]. This has led several authors to propose the alkaline earth hexaborides as examples of excitonic ferromagnets [22,23,73]. More recent experiments, however, have shed doubt upon this conclusion, and the situation is currently somewhat confused [24,74]. Nevertheless, the EF model remains the most convincing theoretical explanation for the exciting properties of these materials.

Superconductivity in Semimetals with an Excitonic Instability

In its original form, the BCS theory of superconductivity was explicitly formulated for a homogeneous electron gas. In the years following its publication, much work was devoted to the application of the BCS scheme to more realistic systems. The predictions of BCS theory were found to be in excellent qualitative (and sometimes even quantitative) agreement with experiment; in all extensions to the theory, the original concept of phonon-mediated electron-pairing was retained. The extraordinary success of their theory was recognized by the award of the 1972 Nobel Prize for Physics to Bardeen, Cooper and Schrieffer.

Part of the effort to verify the BCS scheme was directed towards the appearance of superconductivity in metals with overlapping bands [58, 75, 76]. Although for the majority of such systems the BCS theory was highly successful, surprisingly high critical temperatures ($T_{\rm S} > 10$K) were found in several compounds in which a density wave instability was known to occur. Indeed, the highest critical temperatures known prior to 1986 were found in the so-called A15 compounds (Laves phase), some of which exhibit a phase transition to a CDW at higher temperatures [10].

The possibility of raising $T_{\rm S}$ as a result of a transition to a density wave state naturally aroused much interest in the condensed-matter community [9, 44]. It was observed that the excitonic insulator model of the density wave state discussed in chapter 5 offered a natural mechanism for such an increase: the enhancement of the DOS about the insulating gap [77]. In the finite temperature BCS theory of superconductivity, the critical temperature is sensitively dependent upon the DOS near the Fermi energy, $\eta(0)$:

$$T_{\rm S} \;\propto\; \exp\left[(\lambda\eta(0))^{-1}\right] \tag{6.1}$$

The increased DOS around the insulating gap in the EI phase (see figure 6.1(b)) might therefore be able to support, and perhaps even enhance, Cooper-pairing. On the other hand, the presence of the insulating gap should be expected to have a negative impact upon the appearance of superconductivity in the EI phase. As the width of this gap is generally much smaller than the Debye energy, however, Cooper-pairing between electrons on both sides of the gap might still be possible (we assume $E_G \gg \omega_D \gg \Delta_{s0},\, \delta\mu$).

The results of theoretical studies have reflected this expected competition between the DOS enhancement and the opening of the insulating gap. The latter effect dominates for most choices of coupling parameters, leading to the suppression of Cooper-pairing in the system; modification of the normal BCS Hamiltonian in order to account for the exciton-mediated band hybridization, however, does allow an increase in $T_{\rm S}$ to be observed [12, 53, 78]. In both cases a new superconducting excitonic insulator (SEI) phase is predicted.

In the published literature, the situation where there is only one spin-species of exciton in the system is always assumed. In the following, we only consider the original case of spin singlet exciton-pairing (sSEI phase). The case of spin triplet exciton-pairing (the tSEI phase) has also been studied: neglecting the effects of the antiferromagnetic ordering, it is identical *mutatis mutandis* to the singlet case [79]. We shall follow closely the approach of Rusinov *et al.* in our analysis of

the sSEI phase [53]. After constructing the equations of motion for our model system (sections 6.1 and 6.2), we proceed to examine its predictions for two different choices of parameters (sections 6.3 and 6.4). These illustrate both the competition and co-operation between excitons and Cooper pairs in the system. We conclude with a brief review of density wave superconducting systems, and their relation to the model SEI state (section 6.5).

6.1 The Model Hamiltonian

The Hamiltonian describing the coexistence of Cooper-pairing with singlet exciton-binding in a semimetal with nested electron and hole Fermi surfaces is given by

$$\begin{aligned}\hat{K} &= \sum_{\mathbf{k}',\nu}\left[(\xi_{\mathbf{k}'}-\delta\mu)\,\hat{a}^{\dagger}_{1\mathbf{k}'\nu}\hat{a}_{1\mathbf{k}'\nu}+(-\xi_{\mathbf{k}'}-\delta\mu)\,\hat{a}^{\dagger}_{2\mathbf{k}'\nu}\hat{a}_{2\mathbf{k}'\nu}\right]\\ &+\frac{1}{2V}\sum_{\mathbf{k}',\mathbf{k}''}\sum_{\nu,\nu',\zeta,\zeta'} g_s\delta_{\nu\nu'}\delta_{\zeta\zeta'}\hat{a}^{\dagger}_{1\mathbf{k}'\nu}\hat{a}_{2\mathbf{k}'\nu'}\hat{a}^{\dagger}_{2\mathbf{k}''\zeta}\hat{a}_{1\mathbf{k}''\zeta'}\\ &+\frac{1}{2V}\sum_{\mathbf{k}',\mathbf{k}''}\sum_{\nu,\nu'}\sum_{i,j=1,2}\lambda_{ij}\hat{a}^{\dagger}_{i\mathbf{k}'\nu}\hat{a}^{\dagger}_{j-\mathbf{k}'\nu'}\hat{a}_{j\mathbf{k}''\nu'}\hat{a}_{i-\mathbf{k}''\nu}\end{aligned} \tag{6.2}$$

The first two terms we recognize as the Hamiltonian used to describe the sEI phase. The last term is a generalization of the BCS Hamiltonian to a two-band system, accounting for both intraband ($i=j$) and interband ($i\neq j$) Cooper-pairing. The intraband electron-electron coupling constants $\lambda_{ii}=\lambda$ are assumed to be negative, corresponding to a BCS-like attraction. The interband term accounts for the effect of the exciton-mediated band hybridization upon Cooper-pairing; the interaction constants $\lambda_{12}=\lambda_{21}$ may therefore be either positive or negative. In general the coupling constants g_s and λ_{ij} have different cut-offs, ϖ and ϖ' respectively. We shall assume for simplicity that they are equal. Relaxing this assumption does not introduce any essentially new physics, whilst significantly complicating our analysis.

There are 8 distinct Green's functions to consider in the description of the SEI phase. The necessary single-particle intraband and interband Green's functions $\mathcal{G}^{ij}_{\alpha\beta}$ were introduced in chapter 5. In order to describe the coupling to the Cooper pair reservoir, we define the Gor'kov Green's functions for the system:

$$\mathcal{F}^{ij}_{\alpha\beta}(\mathbf{k},\tau) = \langle[\hat{a}_{i\mathbf{k}\alpha}(\tau)\hat{a}_{j-\mathbf{k}\beta}(0)]\rangle \tag{6.3}$$

$$\mathcal{F}^{\dagger ij}_{\alpha\beta}(\mathbf{k},\tau) = \left\langle\left[\hat{a}^{\dagger}_{i-\mathbf{k}\alpha}(\tau)\hat{a}^{\dagger}_{j\mathbf{k}\beta}(0)\right]\right\rangle \tag{6.4}$$

where $i,j=1,2$ as above. The intraband Gor'kov Green's functions ($i=j$) are present both in the purely-superconducting semimetal (S phase) and SEI phase; the interband Gor'kov Green's functions ($i\neq j$) are only present in the SEI phase. They account for the effect of the exciton-mediated band hybridization. Both intraband and interband Gor'kov Green's functions are off-diagonal in their spin indices. We note the useful identities connecting the functions $\mathcal{F}^{ij}_{\alpha\beta}$ and $\mathcal{F}^{\dagger ij}_{\alpha\beta}$:

$$\begin{aligned}\mathcal{F}^{\dagger ij}_{\alpha\beta}(-\mathbf{k},0^+) &= \left\langle\hat{a}^{\dagger}_{i\mathbf{k}\alpha}\hat{a}^{\dagger}_{j-\mathbf{k}\beta}\right\rangle = -\left\langle\hat{a}^{\dagger}_{j-\mathbf{k}\beta}\hat{a}^{\dagger}_{i\mathbf{k}\alpha}\right\rangle = -\mathcal{F}^{\dagger ji}_{\beta\alpha}(\mathbf{k},0^+)\\ \mathcal{F}^{\dagger ij}_{\alpha\beta}(\mathbf{k},0^+) &= \left\langle\hat{a}^{\dagger}_{i-\mathbf{k}\alpha}\hat{a}^{\dagger}_{j\mathbf{k}\beta}\right\rangle = \langle\hat{a}_{j\mathbf{k}\beta}\hat{a}_{i-\mathbf{k}\alpha}\rangle^* = \left(\mathcal{F}^{ji}_{\beta\alpha}(\mathbf{k},0^+)\right)^*\end{aligned} \tag{6.5}$$

These are generalizations of the identities 3.11 to a two-band system. As in chapter 3, they are useful in the construction of the equations of motion for the Green's functions.

To describe the Cooper-pairing, we have four order parameters Σ_{11}, Σ_{22}, Σ_{12} and Σ_{21}, defined

$$\Sigma_{ij} = -\frac{1}{2V}\sum_{\mathbf{k}'}\left[\lambda_{ij}\mathcal{F}^{ij}_{\uparrow\downarrow}(\mathbf{k}',0^+)-\lambda_{ji}\mathcal{F}^{ji}_{\downarrow\uparrow}(\mathbf{k}',0^+)\right] \tag{6.6}$$

The order parameter for the singlet exciton binding, Δ_s, is as defined in chapter 5. For our simple analysis, we adopt the standard assumption that all the order parameters are real. The gaps of the S phase and the sEI phase at perfect nesting,

$$\Sigma_0 \;=\; 2\varpi \exp\left(\frac{1}{\lambda\eta_{\rm N}(0)}\right), \qquad \Delta_{s0} \;=\; 2\varpi \exp\left(\frac{1}{g_s\eta_{\rm N}(0)}\right) \tag{6.7}$$

respectively, are frequently used in the following analysis as characteristic energy parameters.

6.2 The Equations of Motion

We consider the equations of motion of the Green's functions of the system. We present the detailed calculations for $\mathcal{G}^{11}_{\uparrow\uparrow}$ only; the calculations for the other Green's functions differ in minor details only and so are not presented here.

After tedious and unenlightening calculation, the equation of motion for the intraband single-particle Green's function $\mathcal{G}^{11}_{\uparrow\uparrow}$ is given by

$$\begin{aligned}
-\frac{\partial}{\partial\tau}\mathcal{G}^{11}_{\uparrow\uparrow}(\mathbf{k},\tau) \;=\;& \delta(\tau) + (\xi_{\mathbf{k}} - \delta\mu)\mathcal{G}^{11}_{\uparrow\uparrow}(\mathbf{k},\tau) - \frac{g_s}{2V}\sum_{\mathbf{k}',\nu}\left\langle T_\tau\left[\hat{a}_{2\mathbf{k}\uparrow}(\tau)\hat{a}^\dagger_{2\mathbf{k}'\nu}(\tau)\hat{a}_{1\mathbf{k}'\nu}(\tau)\hat{a}^\dagger_{1\mathbf{k}\uparrow}(0)\right]\right\rangle \\
&+ \frac{\lambda_{11}}{2V}\sum_{\mathbf{k}'\nu}\left\{\left\langle T_\tau\left[\hat{a}^\dagger_{1-\mathbf{k}\nu}(\tau)\hat{a}_{1-\mathbf{k}'\uparrow}(\tau)\hat{a}_{1\mathbf{k}'\nu}(\tau)\hat{a}^\dagger_{1\mathbf{k}\uparrow}(0)\right]\right\rangle\right. \\
&\qquad\left. - \left\langle T_\tau\left[\hat{a}^\dagger_{1-\mathbf{k}\nu}(\tau)\hat{a}_{1-\mathbf{k}'\nu}(\tau)\hat{a}_{1\mathbf{k}'\uparrow}(\tau)\hat{a}^\dagger_{1\mathbf{k}\uparrow}(0)\right]\right\rangle\right\} \\
&+ \frac{1}{2V}\sum_{\mathbf{k}',\nu}\left\{\lambda_{21}\left\langle T_\tau\left[\hat{a}^\dagger_{2-\mathbf{k}\nu}(\tau)\hat{a}_{1-\mathbf{k}'\uparrow}(\tau)\hat{a}_{2\mathbf{k}'\nu}(\tau)\hat{a}^\dagger_{1\mathbf{k}\uparrow}(0)\right]\right\rangle\right. \\
&\qquad\left. - \lambda_{12}\left\langle T_\tau\left[\hat{a}^\dagger_{2-\mathbf{k}\nu}(\tau)\hat{a}_{2-\mathbf{k}'\nu}(\tau)\hat{a}_{1\mathbf{k}'\uparrow}(\tau)\hat{a}^\dagger_{1\mathbf{k}\uparrow}(0)\right]\right\rangle\right\}
\end{aligned} \tag{6.8}$$

We decompose the τ-products in 6.8 using Wick's theorem, keeping only terms that describe the coupling to the Cooper pair and exciton reservoirs as in chapters 3 and 5. We thus have for $\mathcal{G}^{11}_{\uparrow\uparrow}$'s equation of motion

$$\begin{aligned}
&\left(-\frac{\partial}{\partial\tau} - \xi_{\mathbf{k}} + \delta\mu\right)\mathcal{G}^{11}_{\uparrow\uparrow}(\mathbf{k},\tau) \\
&= \delta(\tau) + \frac{g_s}{2V}\sum_{\mathbf{k}',\nu}\mathcal{G}^{12}_{\nu\nu}(\mathbf{k}',0^+)\mathcal{G}^{21}_{\uparrow\uparrow}(\mathbf{k},\tau) + \frac{\lambda_{11}}{2V}\sum_{\mathbf{k}'}\left\{\mathcal{F}^{11}_{\uparrow\downarrow}(\mathbf{k}',0^+) - \mathcal{F}^{11}_{\downarrow\uparrow}(\mathbf{k}',0^+)\right\}\mathcal{F}^{\dagger 11}_{\downarrow\uparrow}(\mathbf{k},\tau) \\
&\quad + \frac{1}{2V}\sum_{\mathbf{k}'}\left\{\lambda_{12}\mathcal{F}^{12}_{\uparrow\downarrow}(\mathbf{k}',0^+) - \lambda_{21}\mathcal{F}^{21}_{\downarrow\uparrow}(\mathbf{k}',0^+)\right\}\mathcal{F}^{\dagger 21}_{\downarrow\uparrow}(\mathbf{k},\tau) \qquad (6.9) \\
&= \delta(\tau) + \Delta_s\mathcal{G}^{21}_{\uparrow\uparrow}(\mathbf{k},\tau) - \Sigma_{11}\mathcal{F}^{\dagger 11}_{\downarrow\uparrow}(\mathbf{k},\tau) - \Sigma_{12}\mathcal{F}^{\dagger 21}_{\downarrow\uparrow}(\mathbf{k}',0^+) \qquad (6.10)
\end{aligned}$$

where we have used the definition of the order parameters to obtain 6.10 from 6.9. By entirely similar arguments, we obtain the equation of motion of $\mathcal{G}^{21}_{\uparrow\uparrow}$, $\mathcal{F}^{\dagger 11}_{\downarrow\uparrow}$ and $\mathcal{F}^{\dagger 21}_{\downarrow\uparrow}$:

$$\left(-\frac{\partial}{\partial\tau} + \xi_{\mathbf{k}} + \delta\mu\right)\mathcal{G}^{21}_{\uparrow\uparrow}(\mathbf{k},\tau) \;=\; \Delta_s\mathcal{G}^{11}_{\uparrow\uparrow}(\mathbf{k},\tau) - \Sigma_{21}\mathcal{F}^{\dagger 11}_{\downarrow\uparrow}(\mathbf{k},\tau) - \Sigma_{22}\mathcal{F}^{\dagger 21}_{\downarrow\uparrow}(\mathbf{k},\tau) \tag{6.11}$$

$$\left(-\frac{\partial}{\partial\tau} + \xi_{\mathbf{k}} - \delta\mu\right)\mathcal{F}^{\dagger 11}_{\downarrow\uparrow}(\mathbf{k},\tau) \;=\; -\Delta_s\mathcal{F}^{\dagger 21}_{\downarrow\uparrow}(\mathbf{k},\tau) - \Sigma_{11}\mathcal{G}^{11}_{\uparrow\uparrow}(\mathbf{k},\tau) - \Sigma_{21}\mathcal{G}^{21}_{\uparrow\uparrow}(\mathbf{k},\tau) \tag{6.12}$$

$$\left(-\frac{\partial}{\partial\tau} - \xi_{\mathbf{k}} - \delta\mu\right)\mathcal{F}^{\dagger 21}_{\downarrow\uparrow}(\mathbf{k},\tau) \;=\; -\Delta_s\mathcal{F}^{\dagger 11}_{\downarrow\uparrow}(\mathbf{k},\tau) - \Sigma_{12}\mathcal{G}^{11}_{\uparrow\uparrow}(\mathbf{k},\tau) - \Sigma_{22}\mathcal{G}^{21}_{\uparrow\uparrow}(\mathbf{k},\tau) \tag{6.13}$$

To obtain the equations of motion of $\mathcal{F}^{\dagger 11}_{\downarrow\uparrow}$ and $\mathcal{F}^{\dagger 21}_{\downarrow\uparrow}$, the identities 6.5 and the assumption that the order parameters are real are utilized in much the same way as in the chapter 3. We may

similarly derive the equations of motion for $\mathcal{G}^{11}_{\downarrow\downarrow}$, $\mathcal{G}^{21}_{\downarrow\downarrow}$, $\mathcal{F}^{\dagger 11}_{\uparrow\downarrow}$ and $\mathcal{F}^{\dagger 21}_{\uparrow\downarrow}$. These may be obtained with the replacement of Σ_{ij} by $-\Sigma_{ji}$ in equations 6.10, 6.11, and 6.13 respectively.

In order to solve the system of equations 6.10, 6.11, 6.12 and 6.13, we take their Fourier transforms into the conjugate ω-space to obtain an algebraic system. It is convenient to express this algebraic system in matrix form:

$$\begin{bmatrix} i\omega_n - \zeta_{1\mathbf{k}} & -\Delta_s & \Sigma_{11} & \Sigma_{12} \\ -\Delta_s & i\omega_n - \zeta_{2\mathbf{k}} & \Sigma_{21} & \Sigma_{22} \\ \Sigma_{11} & \Sigma_{21} & i\omega_n + \zeta_{1\mathbf{k}} & \Delta_s \\ \Sigma_{12} & \Sigma_{22} & \Delta_s & i\omega_n + \zeta_{2\mathbf{k}} \end{bmatrix} \begin{bmatrix} \mathcal{G}^{11}_{\uparrow\uparrow}(\mathbf{k},\omega_n) \\ \mathcal{G}^{21}_{\uparrow\uparrow}(\mathbf{k},\omega_n) \\ \mathcal{F}^{\dagger 11}_{\downarrow\uparrow}(\mathbf{k},\omega_n) \\ \mathcal{F}^{\dagger 21}_{\downarrow\uparrow}(\mathbf{k},\omega_n) \end{bmatrix} = \begin{bmatrix} 1 \\ 0 \\ 0 \\ 0 \end{bmatrix} \tag{6.14}$$

$$\begin{bmatrix} i\omega_n - \zeta_{1\mathbf{k}} & -\Delta_s & -\Sigma_{11} & -\Sigma_{21} \\ -\Delta_s & i\omega_n - \zeta_{2\mathbf{k}} & -\Sigma_{12} & -\Sigma_{22} \\ -\Sigma_{11} & -\Sigma_{12} & i\omega_n + \zeta_{1\mathbf{k}} & \Delta_s \\ -\Sigma_{21} & -\Sigma_{22} & \Delta_s & i\omega_n + \zeta_{2\mathbf{k}} \end{bmatrix} \begin{bmatrix} \mathcal{G}^{11}_{\downarrow\downarrow}(\mathbf{k},\omega_n) \\ \mathcal{G}^{21}_{\downarrow\downarrow}(\mathbf{k},\omega_n) \\ \mathcal{F}^{\dagger 11}_{\uparrow\downarrow}(\mathbf{k},\omega_n) \\ \mathcal{F}^{\dagger 21}_{\uparrow\downarrow}(\mathbf{k},\omega_n) \end{bmatrix} = \begin{bmatrix} 1 \\ 0 \\ 0 \\ 0 \end{bmatrix} \tag{6.15}$$

where $\zeta_{j\mathbf{k}} = (-1)^{j-1}\xi_{\mathbf{k}} - \delta\mu$. Similar matrix equations of motion can be obtained for the other Green's functions $\mathcal{G}^{22}_{\alpha\beta}$, $\mathcal{G}^{12}_{\alpha\beta}$, $\mathcal{F}^{\dagger 22}_{\alpha\beta}$ and $\mathcal{F}^{\dagger 12}_{\alpha\beta}$ by making the replacements $\zeta_{1\mathbf{k}} \leftrightarrow \zeta_{2\mathbf{k}}$, $\Sigma_{11} \leftrightarrow \Sigma_{22}$ and $\Sigma_{12} \leftrightarrow \Sigma_{21}$ in 6.14 and 6.15.

The solutions of these equations were classified in [53,80]. These authors made the simplifying assumptions that $|\Sigma_{11}| = |\Sigma_{22}|$ and $|\Sigma_{12}| = |\Sigma_{21}|$. The former condition follows from the assumption that the difference from perfect nesting is small: the superconducting gaps in the two bands do not therefore appreciably differ. There appears to be no physical situation under which the latter condition would be violated. It may be shown that there are only two solutions of the above matrix equations satisfying these criteria:

- 'antisymmetric' solution: $\Sigma_{11} = -\Sigma_{22} = \Sigma$ and $\Sigma_{12} = 0$.
- 'symmetric' solution: $\Sigma_{11} = \Sigma_{22} = \Sigma$ and $\Sigma_{12} = \Sigma_{21} = \Sigma_2$.

We shall consider the antisymmetric and symmetric solutions separately. We note that $\Sigma_{12} = 0$ in the antisymmetric case does not imply that the interband Gor'kov Green's functions are also vanishing.

6.3 The Antisymmetric Solution

For the antisymmetric solution, the matrix equations of motion are re-written

$$\begin{bmatrix} i\omega_n - \zeta_{1\mathbf{k}} & -\Delta_s & \Sigma & 0 \\ -\Delta_s & i\omega_n - \zeta_{2\mathbf{k}} & 0 & -\Sigma \\ \Sigma & 0 & i\omega_n + \zeta_{1\mathbf{k}} & \Delta_s \\ 0 & -\Sigma & \Delta_s & i\omega_n + \zeta_{2\mathbf{k}} \end{bmatrix} \begin{bmatrix} \mathcal{G}^{11}_{\uparrow\uparrow}(\mathbf{k},\omega_n) \\ \mathcal{G}^{21}_{\uparrow\uparrow}(\mathbf{k},\omega_n) \\ \mathcal{F}^{\dagger 11}_{\downarrow\uparrow}(\mathbf{k},\omega_n) \\ \mathcal{F}^{\dagger 21}_{\downarrow\uparrow}(\mathbf{k},\omega_n) \end{bmatrix} = \begin{bmatrix} 1 \\ 0 \\ 0 \\ 0 \end{bmatrix} \tag{6.16}$$

$$\begin{bmatrix} i\omega_n - \zeta_{1\mathbf{k}} & -\Delta_s & -\Sigma & 0 \\ -\Delta_s & i\omega_n - \zeta_{2\mathbf{k}} & 0 & \Sigma \\ -\Sigma & 0 & i\omega_n + \zeta_{1\mathbf{k}} & \Delta_s \\ 0 & \Sigma & \Delta_s & i\omega_n + \zeta_{2\mathbf{k}} \end{bmatrix} \begin{bmatrix} \mathcal{G}^{11}_{\downarrow\downarrow}(\mathbf{k},\omega_n) \\ \mathcal{G}^{21}_{\downarrow\downarrow}(\mathbf{k},\omega_n) \\ \mathcal{F}^{\dagger 11}_{\uparrow\downarrow}(\mathbf{k},\omega_n) \\ \mathcal{F}^{\dagger 21}_{\uparrow\downarrow}(\mathbf{k},\omega_n) \end{bmatrix} = \begin{bmatrix} 1 \\ 0 \\ 0 \\ 0 \end{bmatrix} \tag{6.17}$$

Solving these equations, we obtain

$$\mathcal{G}^{11}_{\alpha\beta}(\mathbf{k},\omega_n) = \delta_{\alpha\beta}\frac{((i\omega_n)^2 - (\zeta_{2\mathbf{k}})^2)(i\omega_n + \zeta_{1\mathbf{k}}) - \Sigma^2(i\omega_n + \zeta_{1\mathbf{k}}) - \Delta_s^2(i\omega_n - \zeta_{2\mathbf{k}})}{((i\omega_n)^2 - \omega_{\mathbf{k}}^{+\,2})((i\omega_n)^2 - \omega_{\mathbf{k}}^{-\,2})} \tag{6.18}$$

$$\mathcal{G}^{21}_{\alpha\beta}(\mathbf{k},\omega_n) = \delta_{\alpha\beta}\frac{\Delta_s\left((i\omega_n - \delta\mu)^2 - \xi_{\mathbf{k}}^2 - \Delta_s^2 + \Sigma^2\right)}{((i\omega_n)^2 - \omega_{\mathbf{k}}^{+\,2})((i\omega_n)^2 - \omega_{\mathbf{k}}^{-\,2})} \tag{6.19}$$

$$\mathcal{F}^{\dagger 11}_{\alpha\beta}(\mathbf{k},\omega_n) = -i\sigma^y_{\alpha\beta}\frac{\Sigma\left(\Sigma^2-\Delta_s^2-(i\omega_n)^2+\zeta_{2\mathbf{k}}^2\right)}{((i\omega_n)^2-\omega_{\mathbf{k}}^{+\,2})((i\omega_n)^2-\omega_{\mathbf{k}}^{-\,2})} \tag{6.20}$$

$$\mathcal{F}^{\dagger 21}_{\alpha\beta}(\mathbf{k},\omega_n) = -i\sigma^y_{\alpha\beta}\frac{2\Delta_s\Sigma(i\omega_n+\zeta_{1\mathbf{k}}+\delta\mu)}{((i\omega_n)^2-\omega_{\mathbf{k}}^{+\,2})((i\omega_n)^2-\omega_{\mathbf{k}}^{-\,2})} \tag{6.21}$$

The poles of the Green's functions give the electron and hole excitation spectra; when both Σ and Δ_s are non-zero, there are four distinct poles at the points $i\omega_n = \pm\omega_{\mathbf{k}}^{+}$, $\pm\omega_{\mathbf{k}}^{-}$. For perfect nesting ($\delta\mu = 0$), the poles are defined

$$\omega_{\mathbf{k}}^{\pm\,2} = \xi_{\mathbf{k}}^2 + (\Sigma \pm \Delta_s)^2 \tag{6.22}$$

Note that this excitation spectrum is identical to the undoped excitonic ferromagnet with the replacement $\Delta_t \to \Sigma$. For the case of imperfect nesting, the poles have the form

$$\omega_{\mathbf{k}}^{\pm\,2} = (E_{\mathbf{k}} \pm \delta\mu)^2 + \widetilde{\Sigma}^2, \qquad E_{\mathbf{k}}^2 = \xi_{\mathbf{k}}^2 + \widetilde{\Delta}_s^2 \tag{6.23}$$

where the so-called 'effective' gaps $\widetilde{\Sigma}$, $\widetilde{\Delta}_s$ are defined

$$\widetilde{\Sigma}^2 = \Sigma^2\left(1-\frac{\Delta_s^2}{\delta\mu^2}\right), \qquad \widetilde{\Delta}_s^2 = \Delta_s^2\left(1+\frac{\Sigma^2}{\delta\mu^2}\right) \tag{6.24}$$

We plot the electron excitation spectrum for imperfect nesting about the insulating gap (figure 6.1(a)); the rest of the EI spectrum is only insignificantly affected by the appearance of Cooper-pairing. Note the opening of the superconducting gap about the Fermi energy and the role of the 'effective' gaps.

The Green's functions $\mathcal{G}^{22}_{\alpha\beta}$, $\mathcal{G}^{12}_{\alpha\beta}$, $\mathcal{F}^{\dagger 22}_{\alpha\beta}$ and $\mathcal{F}^{\dagger 12}_{\alpha\beta}$ are obtained from the expressions for $\mathcal{G}^{11}_{\alpha\beta}$, $\mathcal{G}^{21}_{\alpha\beta}$, $\mathcal{F}^{\dagger 11}_{\alpha\beta}$ and $\mathcal{F}^{\dagger 21}_{\alpha\beta}$ respectively with the replacement $\zeta_{1\mathbf{k}} \leftrightarrow \zeta_{2\mathbf{k}}$; the Gor'kov Green's functions $\mathcal{F}^{\dagger 22}_{\alpha\beta}$ and $\mathcal{F}^{\dagger 12}_{\alpha\beta}$ also acquire a factor of -1.

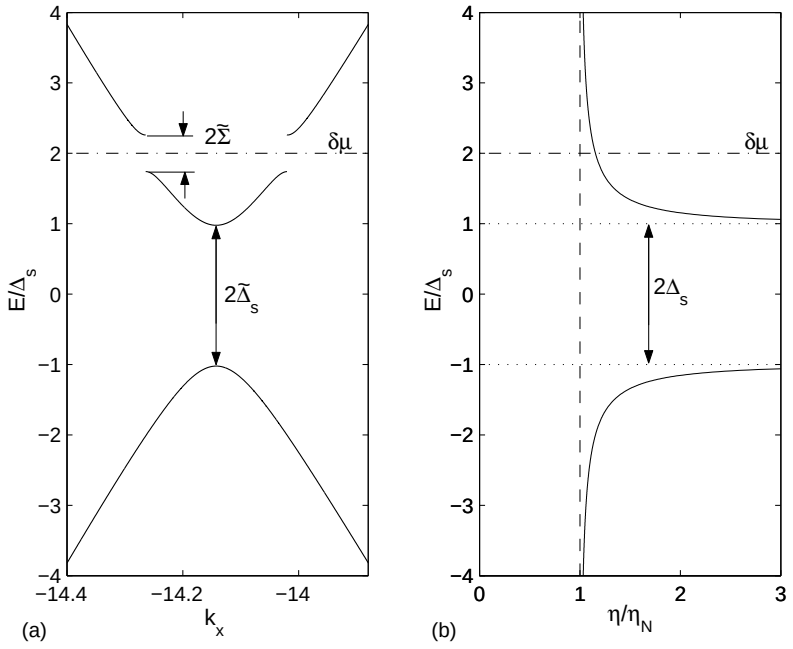

Figure 6.1: (a) Detail of the 'rebuilt' electron excitation spectrum in the sSEI phase, over the same range as in 5.2(b). The rest of the excitation spectrum does not significantly differ from that plotted in figure 5.2(a). We took $\Sigma = 0.3\Delta_s$ in this plot. (b) The DOS in the sEI phase: note the increase in η near the edge of the band gap. The sensitive dependence of T_S upon $\eta(0)$ means that even a modest change (as at $\delta\mu$) can cause a significant increase in the critical temperature.

6.3.1 Important Integrals

We introduce some important integrals which will frequently appear in the following analysis:

$$\mathcal{I}_1(\widetilde{\Delta}_s,\widetilde{\Sigma},\delta\mu) = \lim_{\beta\to\infty}\int_0^{\varpi}\frac{d\xi}{2E}\left[\frac{E+\delta\mu}{\omega^+}\tanh\left(\frac{\beta\omega^+}{2}\right)+\frac{E-\delta\mu}{\omega^-}\tanh\left(\frac{\beta\omega^-}{2}\right)\right] \quad (6.25)$$

$$\mathcal{I}_2(\widetilde{\Delta}_s,\widetilde{\Sigma},\delta\mu) = \lim_{\beta\to\infty}\int_0^{\varpi}\frac{d\xi}{2E}\left[\frac{1}{\omega^-}\tanh\left(\frac{\beta\omega^-}{2}\right)-\frac{1}{\omega^+}\tanh\left(\frac{\beta\omega^+}{2}\right)\right] \quad (6.26)$$

$$\mathcal{I}_3(\widetilde{\Delta}_s,\widetilde{\Sigma},\delta\mu) = \lim_{\beta\to\infty}\int_0^{\varpi}\frac{d\xi}{2E}\left[\frac{E+\delta\mu}{\omega^+}\tanh\left(\frac{\beta\omega^+}{2}\right)-\frac{E-\delta\mu}{\omega^-}\tanh\left(\frac{\beta\omega^-}{2}\right)\right] \quad (6.27)$$

For the sake of clarity, we shall use the abbreviated expressions $\mathcal{I}_j$ instead of explicitly writing the integrals. The important properties of these integrals are presented in section A.4 of the mathematical appendix, to which we shall often refer the reader. A particularly important property is the asymptotic form of the integral $\mathcal{I}_2$ in the limit $\Sigma\to 0$:

$$\mathcal{I}_2(\widetilde{\Delta}_s,\widetilde{\Sigma}\to 0,\delta\mu) \approx \frac{1}{\sqrt{\delta\mu^2-\Delta_s^2}}\ln\left|\frac{4\delta\mu\sqrt{\delta\mu^2-\Delta_s^2}}{\Sigma\left(\delta\mu+\sqrt{\delta\mu^2-\Delta_s^2}\right)}\right| \quad (6.28)$$

We shall frequently utilize this expression in the following analysis.

6.3.2 The Self-Consistency Equations

Using the derived expressions for the Green's functions, we obtain for the equations for the order parameters

$$\Sigma = -\lambda\eta_{\rm N}(0)\Sigma\left[\mathcal{I}_1(\widetilde{\Delta}_s,\widetilde{\Sigma},\delta\mu)+\left(\delta\mu-\frac{\Delta_s^2}{\delta\mu^2}\right)\mathcal{I}_2(\widetilde{\Delta}_s,\widetilde{\Sigma},\delta\mu)\right] \quad (6.29)$$

$$\Delta_s = -g_s\eta_{\rm N}(0)\Delta_s\left[\mathcal{I}_1(\widetilde{\Delta}_s,\widetilde{\Sigma},\delta\mu)-\frac{\Sigma^2}{\delta\mu}\mathcal{I}_2(\widetilde{\Delta}_s,\widetilde{\Sigma},\delta\mu)\right] \quad (6.30)$$

The trivial solution ($\Sigma=\Delta_s=0$) to the self-consistency equations 6.29 and 6.30 is ignored in the following analysis.

As in the EI and EF phases studied in chapter 5, the chemical potential $\delta\mu$ is determined by the structure of the 'rebuilt' spectrum and the impurity doping. Thus, in order to derive the self-consistent solution to equations 6.29 and 6.30 for a fixed electron-hole concentration difference, it is necessary to determine the relationship between the nesting imperfection $\delta\mu$ and the electron-hole concentration difference n. We have

$$n = \frac{\delta n}{4\eta_{\rm N}(0)} = \lim_{\beta\to\infty}\frac{1}{4\eta_{\rm N}(0)}\frac{1}{\beta V}\sum_{\mathbf{k},n}\sum_{j=1,2}\mathrm{Tr}\left\{\mathbf{G}^{jj}(\mathbf{k},\omega_n)\right\}e^{-(-1)^j i\omega_n 0^+}$$

$$= \mathcal{I}_3(\widetilde{\Delta}_s,\widetilde{\Sigma},\delta\mu)+\left(\frac{\Delta_s\Sigma}{\delta\mu}\right)^2\mathcal{I}_2(\widetilde{\Delta}_s,\widetilde{\Sigma},\delta\mu) \quad (6.31)$$

It is straightforward to verify that the integrals $\mathcal{I}_2$ and $\mathcal{I}_3$ are always nonnegative for $\delta\mu\geq 0$. For $\Sigma\neq 0$, substitution of the $\delta\mu$ Laurent-series expansions of the integrals (see mathematical appendix) into 6.31 demonstrates that $n\sim\delta\mu$ as $\delta\mu\to 0$. Thus, when the superconducting order parameter is nonzero, strict equality of electron and hole concentrations is only realized for $\delta\mu=0$. This condition allows us to easily discuss the coexistence regime in both the absence and presence of impurity-doping. The general relationship between $\delta\mu$ and n in the coexistence regime does not admit an analytic expression.

6.3.3 The $n = 0$ System

In the limit $\delta\mu = 0$, the gap equations 6.29 and 6.30 have the analytic form

$$\Sigma = -\frac{\lambda\eta_{\rm N}(0)}{2}\left[(\Sigma+\Delta_s)\ln\left(\frac{2\varpi}{\Delta_s+\Sigma}\right)+(\Sigma-\Delta_s)\ln\left(\frac{2\varpi}{|\Delta_s-\Sigma|}\right)\right] \tag{6.32}$$

$$\Delta_s = -\frac{g_s\eta_{\rm N}(0)}{2}\left[(\Delta_s+\Sigma)\ln\left(\frac{2\varpi}{\Delta_s+\Sigma}\right)+(\Delta_s-\Sigma)\ln\left(\frac{2\varpi}{|\Delta_s-\Sigma|}\right)\right] \tag{6.33}$$

where we assume that $\Delta_s,\ \Sigma > 0$. Referring to the gap equations for the EF phase at equal electron and hole concentrations, we see that they are identical to the system 6.32 and 6.33 upon the replacement of Δ_t by Σ. All the results of subsection 5.5.1 are therefore readily applicable here upon making this replacement. In summary, the gap equations predict the existence of a sSEI phase in the region of the (Δ_{s0},Σ_0)-plane between the lines

$$\Delta_{s0} = e\Sigma_0, \qquad \Delta_{s0} = e^{-1}\Sigma_0 \tag{6.34}$$

In this sSEI phase, however, the order parameters exhibit 'anomalous' dependence upon the coupling constants, indicating that the sSEI phase is metastable. This may be directly verified by calculating the free energy per unit volume relative to the normal phase: although more stable than the normal phase, the sSEI phase is less stable than the sEI and S phases.

6.3.4 The $n \neq 0$ System

In the case of unequal electron and hole concentrations, the self-consistency equations 6.29, 6.30 and 6.31 cannot be solved to obtain an analytic expression for the parameters Δ_s, Σ and $\delta\mu$ in the sSEI phase. In the limit of weak Cooper-pairing ($\Sigma_0 \ll \Delta_{s0}$), however, an expression for the variation of Σ in the sSEI phase of asymptotic validity may be derived. We are also able to obtain the phase diagram of the system.

In the SCHF approximation considered here, the critical temperatures of the S and sEI phases, $T_{\rm S}$ and $T_{\rm sEI}$ respectively, are related to the gaps Σ_0 and Δ_{s0} by the ratio

$$\frac{T_{\rm S}}{T_{\rm sEI}} \approx \frac{\Sigma_0}{\Delta_{s0}} \tag{6.35}$$

Typically, $T_{\rm S}$ ranges between $0.01 - 1$K. The EI phase is generally much more robust, with $T_{\rm EI}$ lying between $10 - 1000$K. The study of the system when the inequality $\Sigma_0 \ll \Delta_{s0}$ is satisfied is therefore most relevant to physical reality. This is, of course, the weak Cooper-pairing regime.

In the weak Cooper-pairing regime, the integral $\mathcal{I}_2$ has a logarithmic divergence (see equation 6.28). Thus, the RHS of the self-consistency equation 6.29 is of order $\ln|\Sigma|$, and so has no solutions for $\Sigma = 0$ when $\lambda \neq 0$. Thus, the presence of excess electrons or holes in the system always makes the sEI phase unstable to arbitrarily weak attractive electron-electron interactions. We may regard this as evidence that the DOS increase near the edge of the insulating gap allows the sEI phase to support Cooper-pairing.

For the integrals $\mathcal{I}_1$ and $\mathcal{I}_3$, the lowest order corrections to their $\Sigma = 0$ values are $\sim \Sigma\ln|\Sigma|$ (see section A.4 of the mathematical appendix). To first order in Σ, therefore, we may neglect the influence of the Cooper-pairing on the insulating state: that is, for $\Sigma \to 0$, we may approximate Δ_s and n by their values in the equilibrium EI phase (refer to section 5.4). Using the expression for Σ_0, we therefore have for 6.29 in the limit of weak Cooper-pairing

$$\ln\left(\frac{2\varpi}{\Sigma_0}\right) \approx \ln\left(\frac{2\varpi}{\Delta_{s0}}\right)+\frac{n}{\Delta_{s0}-n}\ln\left(\frac{4n(\Delta_{s0}-n)}{|\Sigma|\Delta_{s0}}\right) \tag{6.36}$$

Solving for Σ (assumed positive), we have

$$\Sigma = \frac{4n(\Delta_{s0}-n)}{\Delta_{s0}}\exp\left[-\frac{\Delta_{s0}-n}{n}\ln\left(\frac{\Delta_{s0}}{\Sigma_0}\right)\right] \tag{6.37}$$

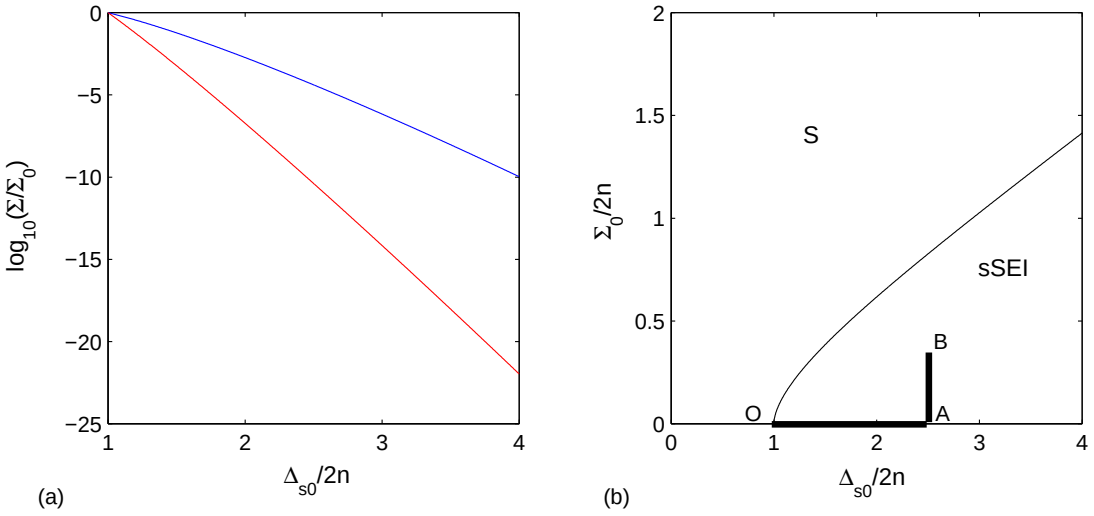

Figure 6.2: (a) The variation of Σ with $\Delta_{s0}/2n$ in the weak Cooper-pairing regime. The blue line is for $\Sigma_0/2n = 0.1$, the red line for $\Sigma_0/2n = 0.001$. (b) The phase diagram for the antisymmetric solution. The bold line OAB is the contour used for the evaluation of the free energy.

This expression is valid provided that $\Sigma \ll 4n(\Delta_{s0} - n)/\Delta_{s0}$: in this limit, the second term on the RHS of 6.36 dominates the other small-Σ corrections. In figure 6.2(a), we plot the variation of Σ inside the sSEI phase for two values of $\Sigma_0/2n$. We note that the rapidity of the decrease in Σ in the sSEI phase increases with decreasing Σ_0.

The result 6.37 illustrates the importance of a non-zero electron-hole concentration difference to the appearance of superconductivity in the sEI phase: for $n \ll \Delta_{s0}$, the superconducting order parameter Σ is exponentially small. This is consistent with the conclusions of subsection 6.3.3 that demonstrated the impossibility of an equilibrium coexistence phase in the absence of electron doping. Treated as a function of Δ_{s0}, the expression for Σ also evidences the inhibiting effect that the insulating gap has on Cooper-pairing, with Σ vanishing as $\Delta_{s0} \to \infty$.

The above results for the weak Cooper-pairing regime indicate that although Cooper-pairing is never completely extinguished by the appearance of an insulating gap, it is, however, strongly suppressed. This evidences the competition between the two effects of DOS enhancement and energy gap opening. The deleterious effect that the insulating gap has upon Cooper-pairing is clearly demonstrated by 6.37; it is apparently mitigated, however, by the increase in the DOS near the edge of the band gap, so that Cooper-pairing is always possible for $\lambda < 0$.

This competitive coexistence between the S and sEI phases is also characteristic of the general case ($\Sigma \not\ll \Delta_s$). This is demonstrated by the phase diagram in the $(\Delta_{s0}/2n, \Sigma_0/2n)$-plane. It is clear from the above discussion that only two phases will be realized on a set of nonzero measure: (i) the S phase ($\Sigma = \Sigma_0$, $n = \delta\mu$, $\Delta_s = 0$) and (ii) the sSEI phase (Σ, Δ_s, $\delta\mu \neq 0$). The boundary between these two phases is obtained by expanding the RHS of 6.30 to zeroth order in Δ_s:

$$\begin{aligned} -\frac{1}{g_s \eta_{\rm N}(0)} &= \mathcal{I}_1(0, \Sigma_0, n) - \frac{\Sigma_0^2}{n}\mathcal{I}_2(0, \Sigma_0, n) \\ &= \ln\left(\frac{2\varpi}{\Sigma_0}\right) - \frac{\sqrt{n^2+\Sigma_0^2}}{n}\ln\left(\frac{n+\sqrt{n^2+\Sigma_0^2}}{\Sigma_0}\right) \end{aligned} \tag{6.38}$$

Using the relations 6.7, we may, after some re-arrangement, place these equations in the form

$$\ln(x) = \ln(y) + \sqrt{1+4y^2}\ln\left(\frac{1+\sqrt{1+4y^2}}{2y}\right) \tag{6.39}$$

where the variables $x = \Delta_{s0}/2n$ and $y = \Sigma_0/2n$. This line is plotted in figure 6.2(b). For fixed concentration difference between the conduction band electrons and valence band holes, we see that as Σ_0 increases, the value of Δ_{s0} for which the sSEI phase is possible increases monotonically. That is, as the interaction responsible for Cooper-pairing becomes stronger, the minimum value of $|g_s|$ required for simultaneous electron-hole binding also increases. Thus, the presence of Cooper-pairing in the system tends to impair the formation of excitons. The reverse conclusion can also be drawn from this result.

We conclude the analysis of the antisymmetric solution by calculating its energetic stability. Relative to the normal phase, the free energy per unit volume of the sSEI state, δF_{sSEI}, is for some choice of parameters $\Delta'_{s0}, \Sigma'_0, n'$ given by the expression

$$\delta F_{\text{sSEI}} = \int_{\mathcal{C}} \frac{\Delta_s^2}{{g_s}^2} dg_s + \frac{\Sigma^2}{\lambda^2} d\lambda \tag{6.40}$$

where $\mathcal{C}$ is a contour joining the point $(\Delta'_{s0}/2n', \Sigma'_0/2n')$ to the point $(1,0)$ where all the possible phases are equally stable energetically. An analytic expression for δF_{sSEI} may be obtained in the weak Cooper-pairing limit. It is particularly convenient to choose $\mathcal{C}$ to be the line OAB (see figure 6.2(b)). Integrating along OA, we obtain the free energy per unit volume of the sEI phase for the given values of Δ_{s0} and n. Continuing the integration along AB, we need only consider the integral with respect to λ: using the expression 6.37 we obtain after lengthy calculation

$$\delta F_{\text{sSEI}} = \delta F_{\text{sEI}} - \frac{1}{2}\eta_{\text{N}}(0)\frac{n'}{\Delta'_{s0} - n'}{\Sigma'}^2 < \delta F_{\text{sEI}} \tag{6.41}$$

where δF_{sEI} is the free energy per unit volume of the sEI phase relative to the normal phase and Σ' is the value of the superconducting order parameter at the point $(\Delta'_{s0}/2n', \Sigma'_0/2n')$. We see that the sSEI phase is therefore always stable towards the sEI phase. This confirms the earlier result that the sEI phase is unstable to arbitrarily weak attractive electron interactions. Numerical calculations confirm that the sSEI phase is also more stable than the S phase [53].

6.4 The Symmetric Solution

The matrix equations of motion for the symmetric solution are written as

$$\begin{bmatrix} i\omega_n - \zeta_{1\mathbf{k}} & -\Delta_s & \Sigma & \Sigma_2 \\ -\Delta_s & i\omega_n - \zeta_{2\mathbf{k}} & \Sigma_2 & \Sigma \\ \Sigma & \Sigma_2 & i\omega_n + \zeta_{1\mathbf{k}} & \Delta_s \\ \Sigma_2 & \Sigma & \Delta_s & i\omega_n + \zeta_{2\mathbf{k}} \end{bmatrix} \begin{bmatrix} \mathcal{G}^{11}_{\uparrow\uparrow}(\mathbf{k},\omega_n) \\ \mathcal{G}^{21}_{\uparrow\uparrow}(\mathbf{k},\omega_n) \\ \mathcal{F}^{\dagger 11}_{\downarrow\uparrow}(\mathbf{k},\omega_n) \\ \mathcal{F}^{\dagger 21}_{\downarrow\uparrow}(\mathbf{k},\omega_n) \end{bmatrix} = \begin{bmatrix} 1 \\ 0 \\ 0 \\ 0 \end{bmatrix} \tag{6.42}$$

$$\begin{bmatrix} i\omega_n - \zeta_{1\mathbf{k}} & -\Delta_s & -\Sigma & -\Sigma_2 \\ -\Delta_s & i\omega_n - \zeta_{2\mathbf{k}} & -\Sigma_2 & -\Sigma \\ -\Sigma & -\Sigma_2 & i\omega_n + \zeta_{1\mathbf{k}} & \Delta_s \\ -\Sigma_2 & -\Sigma & \Delta_s & i\omega_n + \zeta_{2\mathbf{k}} \end{bmatrix} \begin{bmatrix} \mathcal{G}^{11}_{\downarrow\downarrow}(\mathbf{k},\omega_n) \\ \mathcal{G}^{21}_{\downarrow\downarrow}(\mathbf{k},\omega_n) \\ \mathcal{F}^{\dagger 11}_{\uparrow\downarrow}(\mathbf{k},\omega_n) \\ \mathcal{F}^{\dagger 21}_{\uparrow\downarrow}(\mathbf{k},\omega_n) \end{bmatrix} = \begin{bmatrix} 1 \\ 0 \\ 0 \\ 0 \end{bmatrix} \tag{6.43}$$

Solving these equations, we obtain

$$\mathcal{G}^{11}_{\alpha\beta}(\mathbf{k},\omega_n) = \delta_{\alpha\beta}\frac{((i\omega_n)^2 - (\zeta_{2\mathbf{k}})^2)(i\omega_n + \zeta_{1\mathbf{k}}) + 2\Sigma_2\Sigma\Delta_s - \Sigma^2(i\omega_n + \zeta_{1\mathbf{k}}) - \Sigma_2^2(i\omega_n + \zeta_{2\mathbf{k}}) - \Delta_s^2(i\omega_n - \zeta_{2\mathbf{k}})}{\left((i\omega_n)^2 - {\omega_{\mathbf{k}}^+}^2\right)\left((i\omega_n)^2 - {\omega_{\mathbf{k}}^-}^2\right)} \tag{6.44}$$

$$\mathcal{G}^{21}_{\alpha\beta}(\mathbf{k},\omega_n) = \delta_{\alpha\beta}\frac{\Delta_s\left((i\omega_n - \delta\mu)^2 - \xi_{\mathbf{k}}^2 - \Delta_s^2 - \Sigma^2 - \Sigma_2^2\right) + 2\Sigma\Sigma_2(i\omega_n - \delta\mu)}{\left((i\omega_n)^2 - {\omega_{\mathbf{k}}^+}^2\right)\left((i\omega_n)^2 - {\omega_{\mathbf{k}}^-}^2\right)} \tag{6.45}$$

$$\mathcal{F}^{\dagger 11}_{\alpha\beta}(\mathbf{k},\omega_n) = -i\sigma^y_{\alpha\beta}\frac{\Sigma\left(\Sigma^2 + \Delta_s^2 - \Sigma_2^2 - (i\omega_n)^2 - \zeta_{2\mathbf{k}}^2\right) + 2\Sigma_2\Delta_s\zeta_{2\mathbf{k}}}{\left((i\omega_n)^2 - {\omega_{\mathbf{k}}^+}^2\right)\left((i\omega_n)^2 - {\omega_{\mathbf{k}}^-}^2\right)} \tag{6.46}$$

$$\mathcal{F}^{\dagger 21}_{\alpha\beta}(\mathbf{k},\omega_n) = -i\sigma^y_{\alpha\beta}\frac{\Sigma_2\left(\Sigma_2^2+\Delta_s^2-\Sigma^2-(i\omega_n+\xi_{\mathbf{k}})^2+\delta\mu^2\right)-2\Delta_s\Sigma\delta\mu}{\left((i\omega_n)^2-\omega_{\mathbf{k}}^{+\,2}\right)\left((i\omega_n)^2-\omega_{\mathbf{k}}^{-\,2}\right)} \tag{6.47}$$

The poles of the Green's functions $i\omega_n = \pm\omega^+_{\mathbf{k}},\ \pm\omega^-_{\mathbf{k}}$ define the 'rebuilt' electron and hole excitation spectra. These excitation spectra are identical in form to those for the antisymmetric case:

$$\omega_{\mathbf{k}}^{\pm\,2} = \left(E^2_{\mathbf{k}} \pm \delta\widetilde{\mu}\right)^2 + \widetilde{\Sigma}^2, \qquad E^2_{\mathbf{k}} = \xi^2_{\mathbf{k}} + \widetilde{\Delta}_s^2 \tag{6.48}$$

where the effective gaps $\widetilde{\Delta}_s$, $\widetilde{\Sigma}$ and chemical potential $\delta\widetilde{\mu}$ are defined

$$\widetilde{\Delta}_s = \frac{\delta\mu\Delta_s+\Sigma\Sigma_2}{\delta\widetilde{\mu}}, \quad \widetilde{\Sigma} = \frac{\delta\mu\Sigma-\Delta_s\Sigma_2}{\delta\widetilde{\mu}}, \quad \delta\widetilde{\mu}^2 = \delta\mu^2+\Sigma_2^2 \tag{6.49}$$

The Green's functions $\mathcal{G}^{22}_{\alpha\beta}$, $\mathcal{G}^{12}_{\alpha\beta}$, $\mathcal{F}^{\dagger 22}_{\alpha\beta}$ and $\mathcal{F}^{\dagger 12}_{\alpha\beta}$ are obtained by the replacement $\zeta_{1\mathbf{k}} \leftrightarrow \zeta_{2\mathbf{k}}$ in the expressions for $\mathcal{G}^{11}_{\alpha\beta}$, $\mathcal{G}^{21}_{\alpha\beta}$, $\mathcal{F}^{\dagger 11}_{\alpha\beta}$ and $\mathcal{F}^{\dagger 21}_{\alpha\beta}$ respectively.

6.4.1 Important Integrals

As for the antisymmetric case, it will frequently be impossible to analytically evaluate the integrals occurring in the gap equations. These integrals are of the same form as those introduced in subsection 6.3.1 but with the symmetric solution's definition of E and $\omega^{\pm}$, and the chemical potential $\delta\mu$ replaced by the effective chemical potential $\delta\widetilde{\mu} \geq 0$. We shall therefore employ the notation $\mathcal{I}_1$, $\mathcal{I}_2$ and $\mathcal{I}_3$ in what follows, but will regard these integrals as functions of the effective gaps and the effective chemical potential defined in 6.49. We note that in the limit $\widetilde{\Sigma} \to 0$, the integral $\mathcal{I}_2$ has the asymptotic form as given by equation 6.28

6.4.2 The Self-Consistency Equations

From the expressions for the Green's functions, we obtain the equations for the order parameters Σ, Σ_2 and Δ_s and the electron-hole concentration difference n

$$-\frac{\Sigma}{\lambda\eta_{\mathrm{N}}(0)} = \Sigma\mathcal{I}_1\left(\widetilde{\Delta}_s,\widetilde{\Sigma},\delta\widetilde{\mu}\right)+\delta\mu\widetilde{\Sigma}\mathcal{I}_2\left(\widetilde{\Delta}_s,\widetilde{\Sigma},\delta\widetilde{\mu}\right) \tag{6.50}$$

$$\frac{\Sigma_2}{\lambda_{12}\eta_{\mathrm{N}}(0)} = -\frac{\Sigma_2}{\delta\widetilde{\mu}}\mathcal{I}_3\left(\widetilde{\Delta}_s,\widetilde{\Sigma},\delta\widetilde{\mu}\right)+\frac{\delta\mu}{\delta\widetilde{\mu}}\widetilde{\Sigma}\widetilde{\Delta}_s\mathcal{I}_2\left(\widetilde{\Delta}_s,\widetilde{\Sigma},\delta\widetilde{\mu}\right) \tag{6.51}$$

$$-\frac{\Delta_s}{g_s\eta_{\mathrm{N}}(0)} = \Delta_s\mathcal{I}_1\left(\widetilde{\Delta}_s,\widetilde{\Sigma},\delta\widetilde{\mu}\right)-\Sigma_2\widetilde{\Sigma}\mathcal{I}_2\left(\widetilde{\Delta}_s,\widetilde{\Sigma},\delta\widetilde{\mu}\right) \tag{6.52}$$

$$n = \frac{\delta\mu}{\delta\widetilde{\mu}}\left[\mathcal{I}_3\left(\widetilde{\Delta}_s,\widetilde{\Sigma},\delta\widetilde{\mu}\right)+\left(\Sigma^2-\widetilde{\Sigma}^2\right)\mathcal{I}_2\left(\widetilde{\Delta}_s,\widetilde{\Sigma},\delta\widetilde{\mu}\right)\right] \tag{6.53}$$

The doping n must be an odd function of $\delta\mu$ and *vice versa*. Therefore, the term in square brackets in equation 6.53 must be an even function of $\delta\mu$; it is clear that this requires the integrals $\mathcal{I}_2$ and $\mathcal{I}_3$ to be even in $\delta\mu$. Studying the form of the integrands, the only place where a sign change in $\delta\mu$ could make an important difference is in the values of the effective gaps $\widetilde{\Sigma}$ and $\widetilde{\Delta}_s$: for the integrands to be even in $\delta\mu$, these must either be even or odd. If we assume that Σ and Δ_s are both even in $\delta\mu$, whilst Σ_2 is an odd function of $\delta\mu$, the effective gaps are then odd functions of $\delta\mu$. It is easily verifiable that this is consistent with the gap equations 6.50, 6.51 and 6.52, as the integral $\mathcal{I}_1$ is therefore also even in $\delta\mu$. We hence see that when Σ is non-zero, the condition $\delta\widetilde{\mu} = 0$ guarantees equal electron and hole concentrations in the system. Again, therefore, it is straightforward to discuss the coexistence in both the presence and absence of impurity-doping.

6.4.3 The $n = 0$ System

Setting $\delta\widetilde{\mu} = 0$, the Green's functions take the simplified form

$$\mathcal{G}^{jj}_{\alpha\beta}(\mathbf{k},\omega_n) = \delta_{\alpha\beta}\frac{i\omega_n - (-1)^{j-1}\xi_{\mathbf{k}}}{(i\omega_n)^2 - \omega^2} \tag{6.54}$$

$$\mathcal{G}^{12}_{\alpha\beta}(\mathbf{k},\omega_n) = \mathcal{G}^{21}_{\alpha\beta}(\mathbf{k},\omega_n) = \delta_{\alpha\beta}\frac{\Delta_s}{(i\omega_n)^2 - \omega^2} \tag{6.55}$$

$$\mathcal{F}^{\dagger 11}_{\alpha\beta}(\mathbf{k},\omega_n) = \mathcal{F}^{\dagger 22}_{\alpha\beta}(\mathbf{k},\omega_n) = -i\sigma^y_{\alpha\beta}\frac{\Sigma}{(i\omega_n)^2 - \omega^2} \tag{6.56}$$

where $j = 1,\ 2$ in the expression for the intraband Green's functions. The interband Gor'kov Green's functions are zero. Unlike the general case, the Green's functions have only two simple poles at the points $\pm\omega$, where

$$\omega = \sqrt{\xi^2_{\mathbf{k}} + \Delta_s^2 + \Sigma^2} \tag{6.57}$$

Note that the general form of the 'rebuilt' spectrum is identical to that characterizing the sEI or S phases, with effective gap $\sqrt{\Delta_s^2 + \Sigma^2}$.

In the limit of zero doping, the gap equations 6.50 and 6.52 may be placed in the simple form

$$\Sigma = -\lambda\eta_{\text{N}}(0)\Sigma\ln\left(\frac{2\varpi}{\sqrt{\Delta_s^2 + \Sigma^2}}\right), \qquad \Delta_s = -g_s\eta_{\text{N}}(0)\Delta_s\ln\left(\frac{2\varpi}{\sqrt{\Delta_s^2 + \Sigma^2}}\right) \tag{6.58}$$

When $\Delta_s,\ \Sigma \neq 0$, we may with the aid of the definitions 6.7 rewrite the self-consistency equations

$$2\ln(\Delta_{s0}) = 2\ln(\Sigma_0) = \ln\left(\Delta_s^2 + \Sigma^2\right) \tag{6.59}$$

It is clear that the coexistence occurs only upon the line $\Sigma_0 = \Delta_{s0}$ in the (Δ_{s0}, Σ_0)-plane. On this line, the order parameters Δ_s and Σ are connected by the relationship

$$\Delta_s^2 + \Sigma^2 = \Sigma_0^2 = \Delta_{s0}^2 \tag{6.60}$$

The free energy change per unit volume upon formation of the sSEI phase is easily calculated by the methods outlined in the mathematical appendix (section A.3) to be

$$\delta F_{\text{sSEI}} = -\frac{1}{2}\eta_{\text{N}}(0)\left(\Delta_s^2 + \Sigma^2\right) \tag{6.61}$$

From the relation 6.60, we observe that the S, sEI and sSEI phases are all equally stable upon the line $\Sigma_0 = \Delta_{s0}$. These results were originally arrived at in [81].

We plot the phase diagram of the $n = 0$ system, including the metastable antisymmetric solution, in figure 6.3. The physicality of the solution 6.60 is apparently questionable, as it would appear to be destabilized by small perturbations. This is, however, an artifact of the simplistic model adopted here: the inclusion of interband transition terms in the Hamiltonian 6.2 or alternatively the relaxation of the condition that the exciton-binding and Cooper-pairing cut-offs are equal yields a coexistence region on a set of non-zero measure in the (Δ_{s0}, Σ_0)-plane [9, 82].

6.4.4 The $n \neq 0$ System

As for the antisymmetric solution in the case of unequal electron and hole concentrations, the self-consistency equations for the symmetric solution cannot be solved to yield analytic expressions for the parameters Δ_s, Σ, Σ_2 and $\delta\mu$ in the sSEI phase. As before, however, we are able to study the system in the physical limit of weak Cooper-pairing, although the analysis is complicated by the presence of Σ_2. We may also utilize the self-consistency equations to obtain the general phase diagram of the system.

The equation for Σ_2 only involves the integrals $\mathcal{I}_2$ and $\mathcal{I}_3$; unlike $\mathcal{I}_1$, their integrands do not diverge for large values of ξ. Referring to 6.51, this implies that in the physical 'weak coupling'

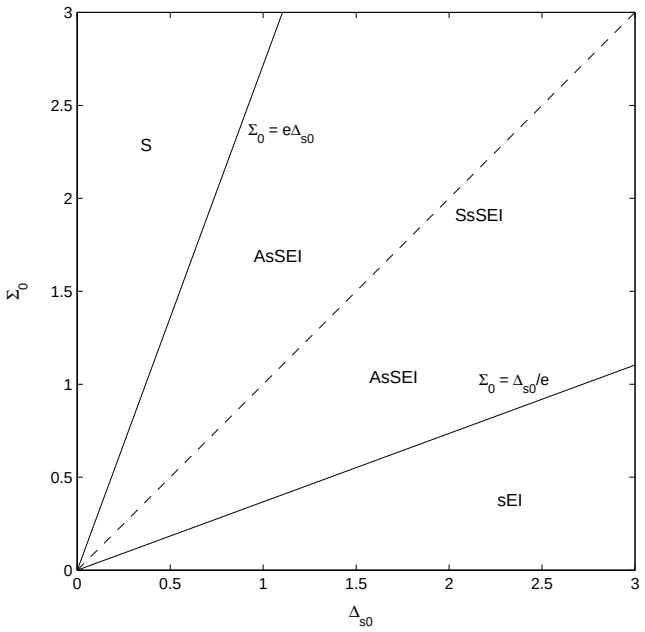

Figure 6.3: The phase diagram in the absence of doping. Between the two solid lines $\Sigma_0 = e\Delta_{s0}$ and $\Sigma_0 = \Delta_{s0}/e$ a metastable antisymmetric sSEI (AsSEI) phase is predicted. A stable symmetric sSEI (SsSEI) phase is realized along the dotted line ($\Sigma_0 = \Delta_{s0}$).

limit $|\lambda_{12}|\eta_N(0) \ll 1$, we have $\Sigma_2 \sim \lambda_{12}\eta_N(0)$. Thus, for $\lambda,\ g_s \gg \lambda_{12}$, we may regard Σ_2 as vanishing. In the limit of weak Cooper-pairing, however, this simplification is inappropriate. We demonstrate the failure of this assumption by expanding the RHS of 6.51 to zeroth order in Σ_2 and letting $\Sigma \to 0$. Using the asymptotic expression for $\mathcal{I}_2$, we have

$$\frac{\Sigma_2}{\Sigma} \sim -\lambda_{12}\eta_N(0)\frac{\Delta_{s0}}{\sqrt{\delta\mu^2 - \Delta_s^2}} \ln\left[\frac{4(\delta\mu^2 - \Delta_s^2)}{\Sigma\left(\delta\mu + \sqrt{\delta\mu^2 - \Delta_s^2}\right)}\right] \tag{6.62}$$

Due to the diverging logarithm, the RHS of this expression may not be small when $\Sigma \ll \Delta_s,\ \delta\mu$. This result demonstrates the necessity of including Σ_2 in the analysis of the weak Cooper-pairing regime.

As for the antisymmetric case, in the limit of weak Cooper-pairing the parameters Δ_s and $\delta\mu$ are, up to corrections of order $\Sigma \ln|\Sigma|$, equal to their values in the EI phase. As before, we consider only the limit $|\widetilde{\Sigma}| \ll 4n^2/\Delta_{s0}$: thus, the RHS of the equations 6.50 and 6.51 are dominated by the integral $\mathcal{I}_2$. Letting $\widetilde{\Delta}_s \approx \Delta_s$ and $\delta\widetilde{\mu} \approx \delta\mu$, we have for the asymptotic form of the equations for the gaps Σ and Σ_2

$$\Sigma \approx \frac{\Delta_{s0} - n}{n\ln(\Delta_{s0}/\Sigma_0)}\widetilde{\Sigma}\ln\left(\frac{4n^2}{|\widetilde{\Sigma}|\Delta_{s0}}\right) \tag{6.63}$$

$$\Sigma_2 \approx \lambda_{12}\eta_N(0)\frac{\sqrt{\Delta_{s0}(\Delta_{s0} - 2n)}}{n}\widetilde{\Sigma}\ln\left(\frac{4n^2}{|\widetilde{\Sigma}|\Delta_{s0}}\right) \tag{6.64}$$

In the weak coupling limit, the effective superconducting gap $\widetilde{\Sigma}$ is related to the gaps Σ and Σ_2 by

$$\widetilde{\Sigma} \approx \Sigma - \frac{\sqrt{\Delta_{s0}(\Delta_{s0} - 2n)}}{\Delta_{s0} - n}\Sigma_2 \tag{6.65}$$

Substituting 6.63 and 6.64 into this expression and solving for $\widetilde{\Sigma} \neq 0$, we have

$$|\widetilde{\Sigma}| = \frac{4n^2}{\Delta_{s0}} \exp\left[-\frac{n}{\Delta_{s0}-n} g^*\right] \tag{6.66}$$

$$g^* = \ln\left(\frac{\Delta_{s0}}{\Sigma_0}\right)\left[1 - \lambda_{12}\eta_{\rm N}(0)\frac{\Delta_{s0}(\Delta_{s0}-2n)}{(\Delta_{s0}-n)^2}\ln\left(\frac{\Delta_{s0}}{\Sigma_0}\right)\right]^{-1} \tag{6.67}$$

Examining 6.67, we see that if $\lambda_{12} > 0$, (repulsive interband electron interactions), the denominator of g^* has a zero for the values of $\Delta_{s0}/2n = x$ and $\Sigma_0/2n = y$ satisfying the relation

$$y = x \exp\left[-\frac{1}{\lambda_{12}\eta_{\rm N}(0)}\frac{(2x-1)^2}{4x(x-1)}\right] \tag{6.68}$$

Approaching this line on the (x, y)-plane, the argument of the exponential in 6.66 diverges toward $-\infty$: the effective gap $\widetilde{\Sigma}$ therefore vanishes. The line 6.68 is thus the boundary between the sSEI and sEI phases. In this region, therefore, the interband electron-electron interactions are more important to Cooper-pairing than the intraband: since for $\lambda_{12} > 0$ these interband interactions are repulsive, Cooper-pairing in the system vanishes.

Away from the line 6.68, we may neglect the term in g^* involving λ_{12}, i.e. we have $g^* \sim \ln(\Delta_{s0}/\Sigma_0)$. Regarded as a function of the concentration difference n, the effective superconducting gap $|\widetilde{\Sigma}|$ then has a maximum at

$$\frac{2n_{\rm max}}{\Delta_{s0}} = 2 + \ln\left(\frac{\Delta_{s0}}{\Sigma_0}\right) - \sqrt{\ln\left(\frac{\Delta_{s0}}{\Sigma_0}\right)\left[2 + \frac{1}{4}\ln\left(\frac{\Delta_{s0}}{\Sigma_0}\right)\right]} \tag{6.69}$$

For $e\Delta_{s0} \geq \Sigma_0$, this maximum lies in the physical region ($\Delta_{s0} \geq 2n$). In the weak Cooper-pairing limit considered (i.e. $\Delta_{s0}/\Sigma_0 \gg 1$), $|\widetilde{\Sigma}|$ exceeds the value of the S-phase gap Σ_0 at this point by

$$\frac{|\widetilde{\Sigma}|_{\rm max}}{\Sigma_0} \approx \left(\frac{4}{e\ln\left(\frac{\Delta_{s0}}{\Sigma_0}\right)}\right)^2 \frac{\Delta_{s0}}{\Sigma_0} \gg 1 \tag{6.70}$$

We see that the increase in $|\widetilde{\Sigma}|$ over its value in the equilibrium S-phase can apparently become arbi-

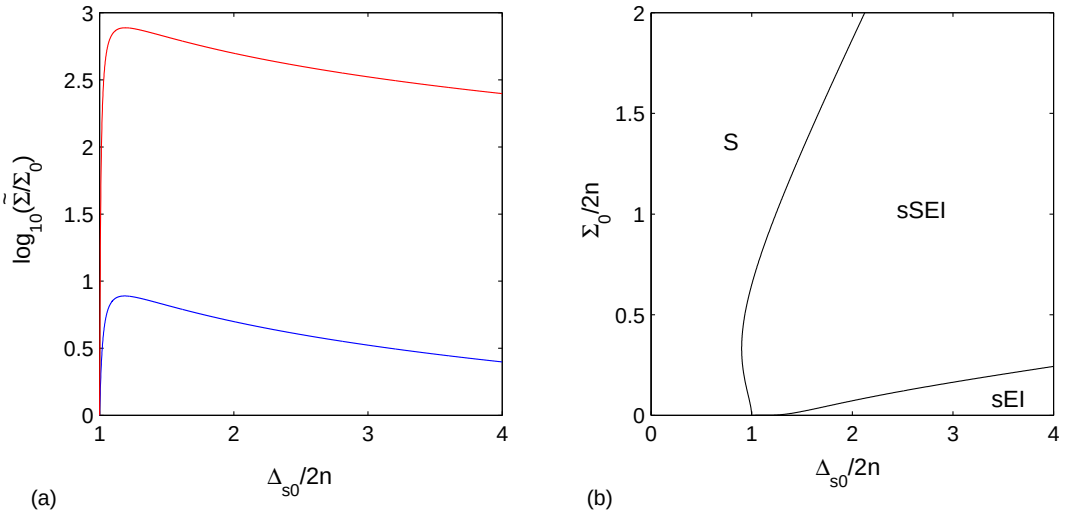

Figure 6.4: (a) The variation of Σ with $\Delta_{s0}/2n$ in the weak Cooper-pairing regime. The blue line is for $\Sigma_0/2n = 0.1$, the red line for $\Sigma_0/2n = 0.001$. (b) The phase diagram for the symmetric solution. The sEI phase only appears for $\lambda_{12} > 0$. We took $\lambda_{12}\eta_{\rm N}(0) = 0.2$; for clarity, the line 6.68 is multiplied by 10.

trarily large as Σ_0 decreases. For $\lambda_{12} > 0$, this increase saturates for $\Sigma_0 \sim \Delta_{s0} \exp[-(\lambda_{12}\eta_N(0))^{-1}]$; there is no apparent limit to this growth for $\lambda_{12} < 0$. We plot the variation of $|\widetilde{\Sigma}|$ in the sSEI phase in figure 6.4(a). We note that the superconducting critical temperature is directly dependent upon $\widetilde{\Sigma}$: this behaviour is therefore indicative of a significant T_S increase. Unfortunately, these results have been arrived at using the weak Cooper-pairing approximation; they therefore should be regarded not as rigorous but rather as suggestive of the actual behaviour of the system. Numerical methods are required for the study of the co-operative coexistence [12, 78].

The co-operative coexistence found above is actually rather robust and extends outside of the weak Cooper-pairing regime. We consider the phase diagram in the $(\Delta_{s0}/2n, \Sigma_0/2n)$-plane. By an analysis entirely identical to that performed for the antisymmetric case above, we find the boundary between the SEI and S phases:

$$\ln(x) = \ln(y) + \frac{1}{\sqrt{1+4y^2}} \ln\left(\frac{1+\sqrt{1+4y^2}}{2y}\right) \tag{6.71}$$

The lines 6.68 and 6.71 thus determine the phase diagram (figure 6.4(b)). We note an important change in the behaviour of the line 6.71 at $\Sigma_0 \approx 0.66n$: for $\Sigma_0 > 0.66n$, equation 6.71 defines a monotonic increasing function of Δ_{s0}; for $\Sigma_0 < 0.66n$, the opposite is true. In this latter region, the co-operative coexistence occurs: near the boundary 6.71 there is an increase in $\widetilde{\Sigma}$ over its value in the S phase. This has been rigorously confirmed by a "very cumbersome" calculation of the variation of $\widetilde{\Sigma}$ to second order in $\widetilde{\Delta}_s$ [53].

6.5 Density Waves in Superconductors

Superconductivity has been found to coexist with both SDWs and CDWs in a wide variety of substances, ranging from metallic alloys to organic salts [10, 83]. In many of these systems, the density wave is believed to be driven by an excitonic-instability of nested portions of the Fermi surface. We give a brief survey of these materials below.

The A15 and C15 compounds (Laves phases) are the most well-known examples of a CDW-superconductivity coexistence. The remarkably high critical superconducting temperatures of some of these materials (e.g. Nb_3Sn where $T_S = 18$K) is thought to be connected with a coexisting CDW phase which induces a lattice instability. The theory of these compounds is based upon the Bilbro-McMillan model, which is closely related to the SEI state studied here [11]. Similar models have also been applied to several superconducting organic salts [9].

The appearance of superconductivity in the alloys $Cr_{1-x}Re_x$ for $x > 0.18$ is a good example of the SDW-superconductivity coexistence in which the SDW state arises from an excitonic instability (Rice model). In spite of the significant differences between the Rice model and the EI state studied in chapter 5, it is interesting to note that the triplet version of the SEI phase studied above gives good qualitative agreement with the observed Re doping-T_S curve [79]. The recently discovered SDW-superconductivity coexistence in the quaternary borocarbides RNi_2B_2C where R = Lu, Y, Tb, Er, Ho, Gd and Tm offers the exciting prospect of the study of the coexistence when the SDW critical temperature is $\sim T_S$, i.e. outside the weak Cooper-pairing regime [84].

The near-equiatomic vanadium-ruthenium alloys, although not known to exhibit density wave phenomena, are also examples of systems in which an excitonic instability is thought to coexist with superconductivity. Of particular interest is the apparent correlation between the superconducting and excitonic-instability transition temperatures, perhaps indicating a co-operative coexistence over a very narrow composition range [12, 85].

In concluding, we note the coexistence of SDWs and superconductivity in both the heavy-fermion and high-temperature superconductors. The relationship between the SDW state and the superconductivity in these materials is currently unclear, although some authors have suggested that it is of great importance to the physics of these systems [44]. It is also interesting to note the possible role of Fermi surface nesting in the recently discovered (traditional) superconductor MgB_2, which has the incredibly high critical temperature $T_S = 39$K [86, 87].

Coexistence of Superconductivity and Excitonic Ferromagnetism

The model of the SEI state discussed in chapter 6 has been considerably extended and embellished. For example, the coexistence of Cooper pairs and triplet excitons has been studied [79]; the effects of non-nested portions of the Fermi surface have been taken into account [11]; the coexistence in a non-homogeneous system (i.e. **k**-dependent excitonic and superconducting order parameters) has been examined [88, 89]; and the possibility of Cooper-pairing in the spin-triplet configuration investigated [90].

A natural generalization of the SEI model is the inclusion of both singlet and triplet electron-hole binding. In chapter 5, it was shown that the simultaneous presence of both singlet and triplet excitons in the EI phase may cause the system to exhibit ferromagnetic ordering of the band electrons. From the remarks at the end of chapter 4, the appearance of Cooper-pairing in such a system may seem unlikely. The exotic properties of the EF phase, however, makes such a judgement premature:

- magnetization: the magnetization displayed by our simple model of the EF phase is strictly limited by the critical excess-electron concentration. As this must be very small, the magnetization of the system is unlikely to exceed the critical field.

- spin-splitting: the objection to superconductivity in a Stoner ferromagnet does not apply here, as the spin-splitting of the bands is comparable to the insulating gap in the EI phase, and so is much smaller than ω_D. This should be expected to impede Cooper-pairing in the system, but not prevent it.

Although not ruled out by 'traditional' reasons, the appearance of superconductivity in an excitonic ferromagnet should also be hindered by the presence of the insulating gap. We note, however, that the increase in the DOS at the edge of this gap might, as in the EI phase, allow the coexistence of the two phenomena. As was found in the symmetric solution studied in section 6.4, the increased DOS of the EI phase can actually lead to an enhancement of Cooper-pairing in the system. The possibility of a similar situation in the coexistence of excitonic ferromagnetism with superconductivity provides strong motivation for the study of this system.

In the following analysis, we neglect the coupling of the Cooper pairs to the magnetic field produced by the partial spin-polarization of the band electrons in the EF phase. Rigorously accounting for this effect requires an extremely sophisticated treatment of the system, which does not introduce any physics peculiar to the EF state. Rather, we concentrate our attention upon the effect that the unique excitation spectrum of the EF phase has upon the appearance of Cooper-pairing.

We begin by presenting an extension of the simple model outlined in chapter 6 to include both singlet and triplet electron-hole binding (section 7.1). By constructing the equations of motion of the Green's functions, we demonstrate that the classification of the solutions of the SEI model may be adopted here (section 7.2). We proceed to examine these solutions in sections 7.3 and 7.4 for both equal and unequal electron-hole concentrations. For the antisymmetric solution at unequal electron and hole concentrations, we demonstrate the existence of a coexistence between

superconductivity and excitonic ferromagnetism at zero temperature. We refer to this as the SEF phase. In section 7.5 we conclude with an evaluation of experimental evidence for this new phase.

7.1 The Model Hamiltonian

In order to describe the coexistence of excitonic ferromagnetism with superconductivity, we simply add a triplet electron-hole coupling term to the Hamiltonian utilized in the description of superconductivity in the sEI phase (equation 6.2):

$$\begin{aligned}\hat{K} &= \sum_{\mathbf{k}',\nu}\left[(\xi_{\mathbf{k}'}-\delta\mu)\,\hat{a}^{\dagger}_{1\mathbf{k}'\nu}\hat{a}_{1\mathbf{k}'\nu}+(-\xi_{\mathbf{k}'}-\delta\mu)\,\hat{a}^{\dagger}_{2\mathbf{k}'\nu}\hat{a}_{2\mathbf{k}'\nu}\right]\\ &\quad+\frac{1}{2V}\sum_{\mathbf{k}',\mathbf{k}''}\sum_{\nu,\nu',\zeta,\zeta'}\left(g_s\delta_{\nu\nu'}\delta_{\zeta\zeta'}+g_t\sigma^z_{\nu\nu'}\sigma^z_{\zeta\zeta'}\right)\hat{a}^{\dagger}_{1\mathbf{k}'\nu}\hat{a}_{2\mathbf{k}'\nu'}\hat{a}^{\dagger}_{2\mathbf{k}''\zeta}\hat{a}_{1\mathbf{k}''\zeta'}\\ &\quad+\frac{1}{2V}\sum_{\mathbf{k}',\mathbf{k}''}\sum_{\nu,\nu'}\sum_{i,j=1,2}\lambda_{ij}\hat{a}^{\dagger}_{i\mathbf{k}'\nu}\hat{a}^{\dagger}_{j-\mathbf{k}'\nu'}\hat{a}_{j\mathbf{k}''\nu'}\hat{a}_{i-\mathbf{k}''\nu}\end{aligned}\tag{7.1}$$

The first two terms are recognizable as the Hamiltonian used to describe the (perhaps simultaneous) appearance of singlet and triplet exciton binding in an impurity-doped semimetal; the last term is the BCS Hamiltonian for a two-band system.

We do not introduce any new Green's functions to describe the system, requiring only those appearing in chapter 6. Nor is it necessary to define any new order parameters. We also retain the simplifying assumptions that $|\Sigma_{11}| = |\Sigma_{22}| = \Sigma$ and $\Sigma_{21} = \Sigma_{12} = \Sigma_2$. The former is again a statement of our assumption that the difference from perfect nesting is small. When the singlet and triplet order parameters are simultaneously nonzero, it will be convenient to utilize the notation $\Delta_{\pm} = \Delta_s \pm \Delta_t$ for the spin-up and spin-down insulating gaps as introduced in the description of the EF phase.

We will frequently use the pure phase gaps

$$\Delta_{s0} = 2\varpi\exp\left(\frac{1}{g_s\eta_{\mathrm{N}}(0)}\right),\quad \Delta_{t0} = 2\varpi\exp\left(\frac{1}{g_t\eta_{\mathrm{N}}(0)}\right),\quad \Sigma_0 = 2\varpi\exp\left(\frac{1}{\lambda\eta_{\mathrm{N}}(0)}\right)$$

in our analysis. We remind the reader that the coupling constants g_s, g_t and λ are supposed negative; the cut-off energy ϖ is assumed equal for all coupling constants.

7.2 The Equations of Motion

The only difference between the calculations of the equations of motion in chapter 6 and here is the simple necessity of taking triplet electron-hole pairing into account. With only very minor modification of the procedure outlined above, we obtain the system of differential equations for the Green's functions $\mathcal{G}^{11}_{\uparrow\uparrow}$, $\mathcal{G}^{21}_{\uparrow\uparrow}$, $\mathcal{F}^{\dagger 11}_{\downarrow\uparrow}$ and $\mathcal{F}^{\dagger 21}_{\downarrow\uparrow}$

$$\left(-\frac{\partial}{\partial\tau}-\xi_{\mathbf{k}}+\delta\mu\right)\mathcal{G}^{11}_{\uparrow\uparrow}(\mathbf{k},\tau) = \delta(\tau)+\Delta_+\mathcal{G}^{21}_{\uparrow\uparrow}(\mathbf{k},\tau)-\Sigma_{11}\mathcal{F}^{\dagger 11}_{\downarrow\uparrow}(\mathbf{k},\tau)-\Sigma_{12}\mathcal{F}^{\dagger 21}_{\downarrow\uparrow}(\mathbf{k},\tau)\tag{7.2}$$

$$\left(-\frac{\partial}{\partial\tau}+\xi_{\mathbf{k}}+\delta\mu\right)\mathcal{G}^{21}_{\uparrow\uparrow}(\mathbf{k},\tau) = \Delta_+\mathcal{G}^{11}_{\uparrow\uparrow}(\mathbf{k},\tau)-\Sigma_{21}\mathcal{F}^{\dagger 11}_{\downarrow\uparrow}(\mathbf{k},\tau)-\Sigma_{22}\mathcal{F}^{\dagger 21}_{\downarrow\uparrow}(\mathbf{k},\tau)\tag{7.3}$$

$$\left(-\frac{\partial}{\partial\tau}+\xi_{\mathbf{k}}-\delta\mu\right)\mathcal{F}^{\dagger 11}_{\downarrow\uparrow}(\mathbf{k},\tau) = -\Delta_+\mathcal{F}^{\dagger 21}_{\downarrow\uparrow}(\mathbf{k},\tau)-\Sigma_{11}\mathcal{G}^{11}_{\uparrow\uparrow}(\mathbf{k},\tau)-\Sigma_{21}\mathcal{G}^{21}_{\uparrow\uparrow}(\mathbf{k},\tau)\tag{7.4}$$

$$\left(-\frac{\partial}{\partial\tau}-\xi_{\mathbf{k}}-\delta\mu\right)\mathcal{F}^{\dagger 21}_{\downarrow\uparrow}(\mathbf{k},\tau) = -\Delta_+\mathcal{F}^{\dagger 11}_{\downarrow\uparrow}(\mathbf{k},\tau)-\Sigma_{12}\mathcal{G}^{11}_{\uparrow\uparrow}(\mathbf{k},\tau)-\Sigma_{22}\mathcal{G}^{21}_{\uparrow\uparrow}(\mathbf{k},\tau)\tag{7.5}$$

The equations of motion for $\mathcal{G}^{11}_{\downarrow\downarrow}$, $\mathcal{G}^{21}_{\downarrow\downarrow}$, $\mathcal{F}^{\dagger 11}_{\uparrow\downarrow}$ and $\mathcal{F}^{\dagger 21}_{\uparrow\downarrow}$ may be obtained by the replacement of Δ_+ with Δ_- and Σ_{ij} with $-\Sigma_{ji}$ in equations 7.2, 7.3, 7.4 and 7.5 respectively.

As usual, we solve the above system of equations by taking the Fourier transforms into the conjugate ω-space. In matrix form, we have

$$\begin{bmatrix} i\omega_n - \zeta_{1\mathbf{k}} & -\Delta_+ & \Sigma_{11} & \Sigma_{12} \\ -\Delta_+ & i\omega_n - \zeta_{2\mathbf{k}} & \Sigma_{21} & \Sigma_{22} \\ \Sigma_{11} & \Sigma_{21} & i\omega_n + \zeta_{1\mathbf{k}} & \Delta_+ \\ \Sigma_{12} & \Sigma_{22} & \Delta_+ & i\omega_n + \zeta_{2\mathbf{k}} \end{bmatrix} \begin{bmatrix} \mathcal{G}^{11}_{\uparrow\uparrow}(\mathbf{k},\omega_n) \\ \mathcal{G}^{21}_{\uparrow\uparrow}(\mathbf{k},\omega_n) \\ \mathcal{F}^{\dagger 11}_{\downarrow\uparrow}(\mathbf{k},\omega_n) \\ \mathcal{F}^{\dagger 21}_{\downarrow\uparrow}(\mathbf{k},\omega_n) \end{bmatrix} = \begin{bmatrix} 1 \\ 0 \\ 0 \\ 0 \end{bmatrix} \tag{7.6}$$

$$\begin{bmatrix} i\omega_n - \zeta_{1\mathbf{k}} & -\Delta_- & -\Sigma_{11} & -\Sigma_{21} \\ -\Delta_- & i\omega_n - \zeta_{2\mathbf{k}} & -\Sigma_{12} & -\Sigma_{22} \\ -\Sigma_{11} & -\Sigma_{12} & i\omega_n + \zeta_{1\mathbf{k}} & \Delta_- \\ -\Sigma_{21} & -\Sigma_{22} & \Delta_- & i\omega_n + \zeta_{2\mathbf{k}} \end{bmatrix} \begin{bmatrix} \mathcal{G}^{11}_{\downarrow\downarrow}(\mathbf{k},\omega_n) \\ \mathcal{G}^{21}_{\downarrow\downarrow}(\mathbf{k},\omega_n) \\ \mathcal{F}^{\dagger 11}_{\uparrow\downarrow}(\mathbf{k},\omega_n) \\ \mathcal{F}^{\dagger 21}_{\uparrow\downarrow}(\mathbf{k},\omega_n) \end{bmatrix} = \begin{bmatrix} 1 \\ 0 \\ 0 \\ 0 \end{bmatrix} \tag{7.7}$$

We recall that $\zeta_{j\mathbf{k}} = (-1)^{j-1}\xi_{\mathbf{k}} - \delta\mu$. The equations for $\mathcal{G}^{22}_{\alpha\beta}$, $\mathcal{G}^{12}_{\alpha\beta}$, $\mathcal{F}^{\dagger 22}_{\alpha\beta}$ and $\mathcal{F}^{\dagger 12}_{\alpha\beta}$ are obtained by making the replacements $\zeta_{1\mathbf{k}} \leftrightarrow \zeta_{2\mathbf{k}}$, $\Sigma_{11} \leftrightarrow \Sigma_{22}$ and $\Sigma_{12} \leftrightarrow \Sigma_{21}$ in equations 7.6 and 7.7 . From the form of the matrix equations of motion, it is clear that the classification of the solutions to the equations of motion for the sSEI phase still holds. We shall therefore investigate the equations in the two cases

- antisymmetric coexistence: $\Sigma_{11} = -\Sigma_{22} = \Sigma$; $\Sigma_{12} = \Sigma_{21} = 0$
- symmetric coexistence: $\Sigma_{11} = \Sigma_{22} = \Sigma$; $\Sigma_{12} = \Sigma_{21} = \Sigma_2$.

As in chapter 6, we shall allow Σ_2 to be either vanishing or non-vanishing in the symmetric coexistence phase. We note that the sign of the triplet order parameter in the matrix equations of motion 7.6 and 7.7 is consistent with previous studies of the tSEI phase [79].

For our purposes, the most important feature of the matrix equations of motion is that different spin-components of the same Green's function are defined in terms of different insulating gaps $\Delta_\pm$. This implies that when $|\Delta_+| \neq |\Delta_-|$, the poles of the different spin-components will not coincide, leading to spin-splitting of the excitation spectrum as seen previously in the EF phase.

7.3 The Antisymmetric Solution

Solving the equations of motion 7.6 in the antisymmetric case, we have for the Green's functions

$$\mathcal{G}^{11}_{\alpha\beta}(\mathbf{k},\omega_n) = \delta_{\alpha\beta}\frac{((i\omega_n)^2 - (\zeta_{2\mathbf{k}})^2)(i\omega_n + \zeta_{1\mathbf{k}}) - \Sigma^2(i\omega_n + \zeta_{1\mathbf{k}}) - \Delta_\sigma^2(i\omega_n - \zeta_{2\mathbf{k}})}{\left((i\omega_n)^2 - \omega^{+\,2}_{\mathbf{k}\sigma}\right)\left((i\omega_n)^2 - \omega^{-\,2}_{\mathbf{k}\sigma}\right)} \tag{7.8}$$

$$\mathcal{G}^{21}_{\alpha\beta}(\mathbf{k},\omega_n) = \delta_{\alpha\beta}\frac{\Delta_\sigma\left((i\omega_n - \delta\mu)^2 - \xi_{\mathbf{k}}^2 - \Delta_\sigma^2 + \Sigma^2\right)}{\left((i\omega_n)^2 - \omega^{+\,2}_{\mathbf{k}\sigma}\right)\left((i\omega_n)^2 - \omega^{-\,2}_{\mathbf{k}\sigma}\right)} \tag{7.9}$$

$$\mathcal{F}^{\dagger 11}_{\alpha\beta}(\mathbf{k},\omega_n) = -i\sigma^y_{\alpha\beta}\frac{\Sigma\left(\Sigma^2 - \Delta_\sigma^2 - (i\omega_n)^2 + \zeta_{2\mathbf{k}}^2\right)}{\left((i\omega_n)^2 - \omega^{+\,2}_{\mathbf{k}\sigma}\right)\left((i\omega_n)^2 - \omega^{-\,2}_{\mathbf{k}\sigma}\right)} \tag{7.10}$$

$$\mathcal{F}^{\dagger 21}_{\alpha\beta}(\mathbf{k},\omega_n) = -i\sigma^y_{\alpha\beta}\frac{2\Delta_\sigma\Sigma(i\omega_n + \zeta_{1\mathbf{k}} + \delta\mu)}{\left((i\omega_n)^2 - \omega^{+\,2}_{\mathbf{k}\sigma}\right)\left((i\omega_n)^2 - \omega^{-\,2}_{\mathbf{k}\sigma}\right)} \tag{7.11}$$

The subscript σ takes the value $+(-)$ for $\alpha\beta = \uparrow\uparrow\,(\downarrow\downarrow)$ in 7.8, 7.9 and $\alpha\beta = \downarrow\uparrow\,(\uparrow\downarrow)$ in 7.10, 7.11.

In the general case, the poles of the Green's functions are spin-dependent. This indicates that the spin-degeneracy of the excitation spectra is lifted in the 'rebuilt' system. For perfect nesting ($\delta\mu = 0$), the poles are

$$\omega^{\pm\,2}_{\mathbf{k}\sigma} = \xi_{\mathbf{k}}^2 + (\Sigma \pm \Delta_\sigma)^2 \tag{7.12}$$

In the general case $\delta\mu \neq 0$, the poles take the form

$$\omega^{\pm\,2}_{\mathbf{k}\sigma} = (E_{\mathbf{k}\sigma} \pm \delta\mu)^2 + \widetilde{\Sigma}_\sigma^2, \qquad E_{\mathbf{k}\sigma} = \xi_{\mathbf{k}}^2 + \widetilde{\Delta}_\sigma^2 \tag{7.13}$$

where the spin-dependent effective gaps are

$$\widetilde{\Sigma}_\sigma^2 = \Sigma^2\left(1-\frac{\Delta_\sigma^2}{\delta\mu^2}\right), \qquad \widetilde{\Delta}_\sigma^2 = \Delta_\sigma^2\left(1+\frac{\Sigma^2}{\delta\mu^2}\right) \tag{7.14}$$

It is easy to see that when one of the order parameters is vanishing, we recover the spectrum of either the sSEI, tSEI or EF phases. This is of course encouraging, as it implies that our calculations are consistent with previous work, as they should be. As in the sSEI phase, the eight poles define both the electron and hole excitation spectra.

The Green's functions $\mathcal{G}^{22}_{\alpha\beta}$, $\mathcal{G}^{12}_{\alpha\beta}$, $\mathcal{F}^{\dagger 22}_{\alpha\beta}$ and $\mathcal{F}^{\dagger 12}_{\alpha\beta}$ are obtained from the expressions for $\mathcal{G}^{11}_{\alpha\beta}$, $\mathcal{G}^{21}_{\alpha\beta}$, $\mathcal{F}^{\dagger 11}_{\alpha\beta}$ and $\mathcal{F}^{\dagger 21}_{\alpha\beta}$ by replacement $\zeta_{1\mathbf{k}} \leftrightarrow \zeta_{2\mathbf{k}}$; $\mathcal{F}^{\dagger 22}_{\alpha\beta}$ and $\mathcal{F}^{\dagger 12}_{\alpha\beta}$ also acquire a factor of -1.

7.3.1 The Self-Consistency Equations

Using the expressions for the Green's functions, we obtain after long calculation the self-consistency equations for the order parameters and the electron-hole concentration difference

$$\Sigma = -\frac{\lambda\eta_{\rm N}(0)}{2}\sum_{\sigma=-,+}\Sigma\left[\mathcal{I}_1(\widetilde{\Delta}_\sigma,\widetilde{\Sigma},\delta\mu)+\left(\delta\mu-\frac{\Delta_\sigma^2}{\delta\mu}\right)\mathcal{I}_2(\widetilde{\Delta}_\sigma,\widetilde{\Sigma},\delta\mu)\right] \tag{7.15}$$

$$\Delta_s = -\frac{g_s\eta_{\rm N}(0)}{2}\sum_{\sigma=-,+}\Delta_\sigma\left[\mathcal{I}_1(\widetilde{\Delta}_\sigma,\widetilde{\Sigma},\delta\mu)-\frac{\Sigma^2}{\delta\mu}\mathcal{I}_2(\widetilde{\Delta}_\sigma,\widetilde{\Sigma},\delta\mu)\right] \tag{7.16}$$

$$\Delta_t = -\frac{g_t\eta_{\rm N}(0)}{2}\sum_{\sigma=-,+}\sigma\Delta_\sigma\left[\mathcal{I}_1(\widetilde{\Delta}_\sigma,\widetilde{\Sigma},\delta\mu)-\frac{\Sigma^2}{\delta\mu}\mathcal{I}_2(\widetilde{\Delta}_\sigma,\widetilde{\Sigma},\delta\mu)\right] \tag{7.17}$$

$$n = \frac{1}{2}\sum_{\sigma=-,+}\left[\mathcal{I}_3(\widetilde{\Delta}_\sigma,\widetilde{\Sigma},\delta\mu)+\left(\frac{\Delta_\sigma\Sigma}{\delta\mu}\right)^2\mathcal{I}_2(\widetilde{\Delta}_\sigma,\widetilde{\Sigma},\delta\mu)\right] \tag{7.18}$$

The integrals $\mathcal{I}_j$ where $j=1,2,3$ are as defined in subsection 6.3.1. Note that here their first argument is $\widetilde{\Delta}_\sigma$ as opposed to $\widetilde{\Delta}_s$.

Examining equations 7.15, 7.16, 7.17 and 7.18, we see that in the limit $|\Delta_+| = |\Delta_-|$ we recover the gap equations for the sSEI or tSEI phases. Thus, the derived gap equations are consistent with previous work. Referring to 7.18 we see that the conclusions drawn in section 6.3 regarding the relationship between the nesting imperfection $\delta\mu$ and the electron-hole concentration difference n in the sSEI phase are also applicable here. For $\Sigma \neq 0$, strict equality of the electron and hole concentrations is therefore only realized when $\delta\mu = 0$.

Since we shall be considering a system with spin-dependent excitation spectra, we may obtain a net magnetic moment M. This is defined

$$\begin{aligned} M &= \mu_B(n^1_{e\uparrow}+n^2_{e\uparrow}-n^1_{e\downarrow}-n^2_{e\downarrow}) \\ &= 2\mu_B\eta_{\rm N}(0)\sum_{\sigma=-,+}\sigma\left[\mathcal{I}_3(\widetilde{\Delta}_\sigma,\widetilde{\Sigma},\delta\mu)+\left(\frac{\Delta_\sigma\Sigma}{\delta\mu}\right)^2\mathcal{I}_2(\widetilde{\Delta}_\sigma,\widetilde{\Sigma},\delta\mu)\right] \end{aligned} \tag{7.19}$$

where $n^j_{e\sigma}$ is the concentration of j-band electrons with spin σ. We note immediately that in the case of equal electron and hole concentrations we have $M=0$. This is consistent with the earlier result for the EF phase (see section 5.5).

7.3.2 The $n=0$ System

In the special case of equal electron and hole concentrations (perfect nesting), the integrals in 7.15, 7.16 and 7.17 may be evaluated to yield the analytic forms

$$\Delta_s = -\frac{g_s\eta_{\rm N}(0)}{4}\left[(\Sigma-\Delta_+)\ln\left(\frac{2\varpi}{|\Sigma-\Delta_+|}\right)-(\Sigma+\Delta_+)\ln\left(\frac{2\varpi}{|\Sigma+\Delta_+|}\right)\right.$$

$$+(\Sigma-\Delta_-)\ln\left(\frac{2\varpi}{|\Sigma-\Delta_-|}\right)-(\Sigma+\Delta_-)\ln\left(\frac{2\varpi}{|\Sigma+\Delta_-|}\right)\Bigg] \tag{7.20}$$

$$\begin{aligned}\Delta_t &= -\frac{g_t\eta_{\rm N}(0)}{4}\Bigg[(\Sigma-\Delta_+)\ln\left(\frac{2\varpi}{|\Sigma-\Delta_+|}\right)-(\Sigma+\Delta_+)\ln\left(\frac{2\varpi}{|\Sigma+\Delta_+|}\right)\\ &\quad -(\Sigma-\Delta_-)\ln\left(\frac{2\varpi}{|\Sigma-\Delta_-|}\right)+(\Sigma+\Delta_-)\ln\left(\frac{2\varpi}{|\Sigma+\Delta_-|}\right)\Bigg] \end{aligned}\tag{7.21}$$

$$\begin{aligned}\Sigma &= \frac{\lambda\eta_{\rm N}(0)}{4}\Bigg[(\Sigma-\Delta_+)\ln\left(\frac{2\varpi}{|\Sigma-\Delta_+|}\right)+(\Sigma+\Delta_+)\ln\left(\frac{2\varpi}{|\Sigma+\Delta_+|}\right)\\ &\quad +(\Sigma-\Delta_-)\ln\left(\frac{2\varpi}{|\Sigma-\Delta_-|}\right)+(\Sigma+\Delta_-)\ln\left(\frac{2\varpi}{|\Sigma+\Delta_-|}\right)\Bigg] \end{aligned}\tag{7.22}$$

When all three order parameters are non-zero, we obtain after some rearrangement a simplified form of these equations

$$4\ln(z_1^0) = \left(z_1-\frac{1}{z_1}\right)\ln\left|\frac{(1-z_1)^2-z_2^2}{(1+z_1)^2-z_2^2}\right|+z_2\ln\left|\frac{(1-z_2)^2-z_1^2}{(1+z_2)^2-z_1^2}\right|-\frac{z_2}{z_1}\ln\left|\frac{(z_1-z_2)^2-1}{(z_1+z_2)^2-1}\right| \tag{7.23}$$

$$4\ln(z_2^0) = \left(z_2-\frac{1}{z_2}\right)\ln\left|\frac{(1-z_2)^2-z_1^2}{(1+z_2)^2-z_1^2}\right|+z_1\ln\left|\frac{(1-z_1)^2-z_2^2}{(1+z_1)^2-z_2^2}\right|-\frac{z_1}{z_2}\ln\left|\frac{(z_1-z_2)^2-1}{(z_1+z_2)^2-1}\right| \tag{7.24}$$

where the dimensionless parameters $0<z_1,z_1^0,z_2,z_2^0<\infty$ are defined

$$z_1 = \frac{\Delta_s}{\Sigma},\quad z_1^0 = \frac{\Delta_{s0}}{\Sigma_0},\quad z_2 = \frac{\Delta_t}{\Sigma}\quad z_2^0 = \frac{\Delta_{t0}}{\Sigma_0} \tag{7.25}$$

The equations 7.23 and 7.24 are in a particularly convenient form for the investigation of the phase diagram in the (z_1^0,z_2^0)-plane.

We consider first the boundary between the SEF and sSEI phases. Approaching this boundary, Δ_t vanishes whilst Δ_s and Σ remain non-zero. We must therefore take the limit $z_2\to 0$ in 7.23 and 7.24 with the condition $z_1\neq 0$. Taking this limit for the former equation is trivially easy; that for the latter involves several applications of l'Hôpital's rule (we refer the reader to section A.5 for several important limits utilized in this analysis). We then easily obtain parametric equations for the phase-boundary:

$$z_1^0=\exp\left(\frac{t^2-1}{2t}\ln\left|\frac{1-t}{1+t}\right|\right),\qquad z_2^0=\exp\left(1+\frac{t}{2}\ln\left|\frac{1-t}{1+t}\right|\right) \tag{7.26}$$

where $t=\Delta_s/\Sigma$. The argument is basically the same for the SEF and tSEI boundary, except that we let $z_1\to 0$ whilst $z_2\neq 0$. This gives the parametric equations

$$z_1^0=\exp\left(1+\frac{t}{2}\ln\left|\frac{1-t}{1+t}\right|\right),\qquad z_2^0=\exp\left(\frac{t^2-1}{2t}\ln\left|\frac{1-t}{1+t}\right|\right) \tag{7.27}$$

where $t=\Delta_t/\Sigma$. Approaching the boundary between the SEF and EF phases, we have $\Sigma\to 0$ whilst $\Delta_s,\ \Delta_t\neq 0$. Thus, in equations 7.23 and 7.24 we must let z_1 and z_2 simultaneously diverge such that their ratio z_1/z_2 is finite. We accordingly obtain a set of parametric equations describing the boundary:

$$z_1^0=\exp\left(-1-\frac{1}{2t}\ln\left|\frac{1-t}{1+t}\right|\right),\qquad z_2^0=\exp\left(-1-\frac{t}{2}\ln\left|\frac{1-t}{1+t}\right|\right) \tag{7.28}$$

with $t=\Delta_s/\Delta_t$. The gap equations 7.23 and 7.24 predict that the SEF phase nowhere borders upon the pure phases.

We complete the description of the phase diagram by stating the boundary between the double coexistence and pure phases in the (z_1^0,z_2^0)-plane. These are as follows: the sSEI phase is predicted

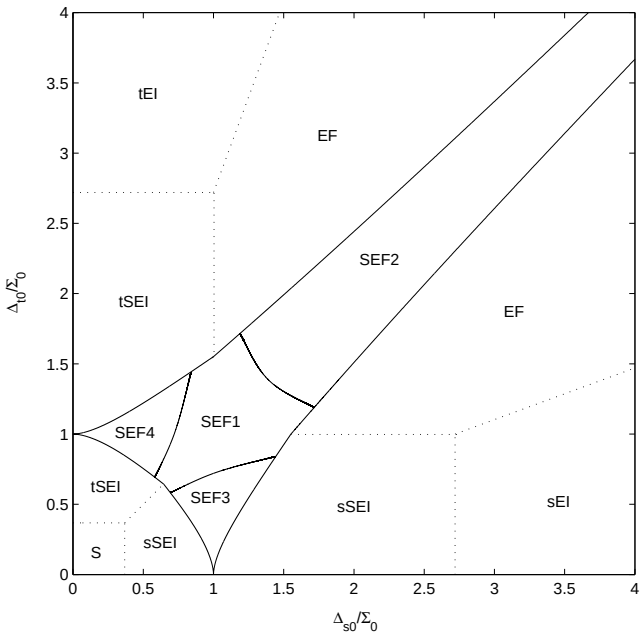

Figure 7.1: The phase diagram of the antisymmetric solution at equal electron and hole concentrations. The different phases are denoted using the standard abbreviations. The region where the SEF phase is predicted is divided into four distinct sections: SEF1 where the SEF phase is less stable than all 'pure' phases; SEF2 where the SEF phase is more stable than the S phase but less stable than the sEI and tEI phases; SEF3 where the SEF phase is more stable than the tEI phase, but less stable than the S and sEI phases; SEF4 where the SEF phase is more stable than the sEI phase but less stable than the S and tEI phases.

between the lines

$$z_1^0 = e, \qquad z_1^0 = e^{-1}; \tag{7.29}$$

the tSEI phase is bounded by

$$z_2^0 = e, \qquad z_2^0 = e^{-1}; \tag{7.30}$$

and the EF phase is possible only between

$$z_1^0 = e z_2^0, \qquad z_1^0 = e^{-1} z_2^0 \tag{7.31}$$

Using the above results, we draw the phase diagram as predicted by the gap equations 7.20, 7.21 and 7.22 in figure 7.1 We note that when two metastable double coexistence phases are possible, we only indicate the most stable phase as predicted by the calculated free energy change. In the interests of clarity, we also do not illustrate a double coexistence regime if it is possible in a region where neither coexisting phase is the most stable in its 'pure' form.

In order to evaluate the free energy per unit volume of the SEF phase relative to the normal phase, $\delta F_{\rm SEF}$, we employ the same basic method as utilized in subsection 5.5.1 to calculate $\delta F_{\rm EF}$. Generalizing equation 5.54 to the case of three order parameters, we have for the free energy per unit volume of the SEF phase for some choice of characteristic gaps Δ'_{s0}, Δ'_{t0}, Σ'_0

$$\delta F_{\rm SEF} = \int_{\mathcal{C}} \frac{\Delta_s^2}{{g_s}^2} dg_s + \frac{\Delta_t^2}{{g_t}^2} dg_t + \frac{\Sigma^2}{\lambda^2} d\lambda \tag{7.32}$$

where $\mathcal{C}$ is a contour joining the point $(\Delta'_{s0}, \Delta'_{t0}, \Sigma'_0)$ to the coordinate origin in $(\Delta_{s0}, \Delta_{t0}, \Sigma_0)$-

space, and lying entirely within the region of predicted SEF coexistence. It is convenient to choose a contour along which the ratios z_1 and z_2 are constant: referring to the gap equations 7.23 and 7.24, we see that this requires the ratios z_1^0 and z_2^0 to be constant, defining our path $\mathcal{C}$ as the straight line from the origin to $(\Delta'_{s0}, \Delta'_{t0}, \Sigma'_0)$. Integrating along this contour, we obtain the result

$$\delta F_{\text{SEF}} = f(z_1, z_2)\delta F_{\text{S}} = f\left(\frac{1}{z_1}, \frac{z_2}{z_1}\right)\delta F_{\text{sEI}} = f\left(\frac{1}{z_2}, \frac{z_1}{z_2}\right)\delta F_{\text{tEI}} < 0 \tag{7.33}$$

where the function $\infty > f(x, y) > 0$ is defined

$$\begin{aligned}\ln\left(f(x,y)\right) &= \ln(1+x^2+y^2) + \frac{1}{2}\left[(x+y)\ln\left|\frac{1-x-y}{1+x+y}\right|\right. \\ &\quad \left. + (x-y)\ln\left|\frac{1-x+y}{1+x-y}\right| - \ln\left|1-2x^2-2y^2+\left(x^2-y^2\right)^2\right|\right]\end{aligned} \tag{7.34}$$

where $x,\ y \geq 0$ are real. The important details of the calculation leading to the expression 7.33 are presented in section A.3 of the mathematical appendix.

From equation 7.33, we see that the SEF phase will be more stable than the S phase whenever $f(z_1, z_2) > 1$. This, however, is of significance only if the S phase is the most stable of the pure phases in this region: if the S phase is the most stable pure phase, then the SEF phase will be energetically favoured over all the other possible states of the system; if the S phase is not the most stable, then the SEF phase will only be realized as a stable state if the inequality $\delta F_{\text{SEF}} < \delta F_{\text{sEI}}, \delta F_{\text{tEI}}$ is also satisfied somewhere in this region. It is a simple task to show that for some (z_1, z_2), the relation $f(z_1, z_2) \geq 1$ is satisfied. Hence, there exists a region of the phase diagram in which the SEF phase is more stable than each of the pure phases. Further numerical analysis, however, reveals that these regions do not overlap (see the phase diagram figure 7.1). It is therefore clear that the SEF phase cannot be realized except perhaps as a metastable state.

7.3.3 The $n \neq 0$ System

In the presence of an excess electron population, the self-consistency equations cannot be analytically solved for the order parameters and $\delta\mu$. In particular, this prevents us from obtaining the phase diagram of the system. We may, however, utilize the $\Sigma \to 0$ asymptotic form of $\mathcal{I}_2$ to study the behaviour of the superconducting order parameter in the weak Cooper-pairing regime. We hence show that the EF phase is unstable in the presence of arbitrarily weak electron-electron interactions.

As in the sSEI analysis, the corrections to the $\lambda = 0$ values of the excitonic order parameters and $\delta\mu$ in the limit of weak Cooper-pairing may be disregarded to order $\Sigma \ln|\Sigma|$. This therefore requires us to distinguish between the two regimes of weak and strong ferromagnetism in the following analysis. We note that this also implies that the magnetization is therefore only slightly affected by the appearance of weak Cooper-pairing.

The general phase diagram of the system may be constructed in the $(\Delta_{s0}/2n, \Delta_{t0}/2n, \Sigma_0/2n)$-space. In the weak Cooper-pairing limit ($\Sigma_0/2n \ll 1$), we may take a "slice" through this phase diagram at constant $\Sigma_0/2n$; such a "slice" is presented in figure 7.3. In line with our assumption that the parameters Δ_s, Δ_t and $\delta\mu$ may be approximated by their $\lambda = 0$ values in the weak Cooper-pairing regime, the boundaries of the phases in this "slice" are defined by the boundaries of the corresponding phases at $\Sigma_0 = 0$ (i.e. figure 5.6).

The Weak Ferromagnet Regime

The weakly ferromagnetic EF phase is characterized by the inequality $\Delta_+, \Delta_- < \delta\mu$. When this condition is satisfied in the weak Cooper-pairing regime of the SEF phase, the excitation spectrum of the two spin-species each has the form of that for the sSEI phase, but with differing effective excitonic and superconducting gaps $\widetilde{\Delta}_\pm$ and $\widetilde{\Sigma}_\pm$. We note that in the limit $\Delta_+ \to \delta\mu^-$, the effective gap $\widetilde{\Sigma}_+$ vanishes; this is due to the disappearance of the spin-up Fermi surface. We consider this point further below. In figure 7.2(a), we plot the electron excitation spectra about the insulating

gap; the rest of the EF excitation spectrum is insignificantly affected by the appearance of Cooper-pairing in the system.

Since $\Delta_+, \Delta_- < \delta\mu$, the integral $\mathcal{I}_2(\Delta_\sigma, \Sigma, \delta\mu)$ has a logarithmic singularity for both Δ_- and Δ_+ with the asymptotic form as introduced in subsection 6.3.1. Thus, the system of equations 7.15, 7.16, 7.17 and 7.18 have no $\Sigma = 0$ solution when Δ_s, Δ_t, $\delta\mu$, and λ are all non-vanishing. That is, the presence of arbitrarily weak attractive electron-electron interactions causes the spontaneous formation of Cooper pairs in the weak EF phase. We may derive an expression for Σ of asymptotic validity in this regime. Disregarding the trivial solution to equation 7.15, we have in the limit of weak Cooper-pairing

$$2\ln\left(\frac{2\varpi}{\Sigma_0}\right) \approx \sum_{\sigma=-,+}\left[\ln\left(\frac{2\varpi}{\delta\mu+\sqrt{\delta\mu^2-\Delta_\sigma^2}}\right)+\frac{\sqrt{\delta\mu^2-\Delta_\sigma^2}}{\delta\mu}\ln\left|\frac{4\delta\mu\sqrt{\delta\mu^2-\Delta_\sigma^2}}{\Sigma\left(\delta\mu+\sqrt{\delta\mu^2-\Delta_\sigma^2}\right)}\right|\right] \tag{7.35}$$

Solving for Σ, we have

$$\begin{aligned}\Sigma \;=\; \exp\Bigg[&\frac{\delta\mu}{\sqrt{\delta\mu^2-\Delta_+^2}+\sqrt{\delta\mu^2-\Delta_-^2}}\ln\left(\frac{\Sigma_0^2}{\sqrt{\delta\mu^2-\Delta_+^2}\sqrt{\delta\mu^2-\Delta_-^2}}\right)\\ &+\sum_{\sigma=-,+}\frac{\sqrt{\delta\mu^2-\Delta_\sigma^2}}{\sqrt{\delta\mu^2-\Delta_+^2}+\sqrt{\delta\mu^2-\Delta_-^2}}\ln\left(\frac{4\delta\mu\sqrt{\delta\mu^2-\Delta_\sigma^2}}{\delta\mu+\sqrt{\delta\mu^2-\Delta_\sigma^2}}\right)\Bigg]\end{aligned} \tag{7.36}$$

Equation 7.36 reduces to the expression for the sSEI (tSEI) phase upon setting $\Delta_t = 0$ ($\Delta_s = 0$).

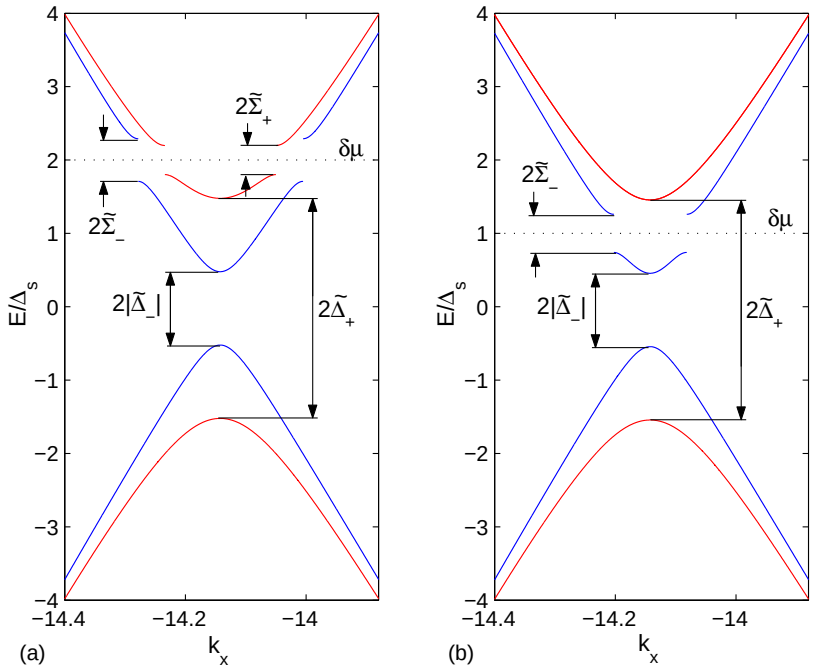

Figure 7.2: (a) Detail of the 'rebuilt' electron excitation spectrum in the weak ferromagnet regime, over the same range as in figure 5.2(b). The rest of the excitation spectrum does not differ significantly from that plotted in figure 5.2(a). As usual, the red line denotes the spin-up spectrum; the blue line the spin-down. Note the role of the effective gaps $\widetilde{\Sigma}_\sigma$ and $\widetilde{\Delta}_\sigma$. (b) Detail of the 'rebuilt' electron excitation spectrum in the strong ferromagnet regime. Note the absence of the superconducting gap in the spin-up spectrum. In both (a) and (b), Δ_s and Δ_t as in figure 5.4; $\Sigma = 0.3\Delta_s$.

The Strong Ferromagnet Regime

In the strong EF phase, the spin-down and spin-up insulating gaps satisfy the inequality $|\Delta_-| < \delta\mu < \Delta_+$. Referring to the expression for the effective gaps 7.14, we see that $\widetilde{\Sigma}_+^2$ is therefore negative. This does not imply a complex energy spectrum; rather, it indicates the disappearance of the spin-up Fermi surface. The resulting electron energy spectrum about the insulating gap is plotted in figure 7.2(b); note the absence of the superconducting gap in the spin-up spectrum.

The disappearance of the spin-up Fermi surface dramatically alters the asymptotic form of the integral $\mathcal{I}_2(\Delta_+, \Sigma, \delta\mu)$, as the integrand no longer has a singularity in the range of integration when $\Sigma = 0$ (see equation A.39). The $\Sigma \to 0$ behaviour of the integral $\mathcal{I}_2(\Delta_-, \Sigma, \delta\mu)$, however, remains unchanged: this ensures that a $\Sigma = 0$ solution is impossible in the strong regime so long as $\lambda \neq 0$. We therefore have in the limit of weak Cooper-pairing for equation 7.15

$$2\ln\left(\frac{2\varpi}{\Sigma_0}\right) \approx \ln\left(\frac{2\varpi}{\delta\mu + \sqrt{\delta\mu^2 - \Delta_-^2}}\right) + \ln\left(\frac{2\varpi}{\Delta_+}\right) + \frac{\sqrt{\delta\mu^2 - \Delta_-^2}}{\delta\mu}\ln\left(\frac{4\delta\mu\sqrt{\delta\mu^2 - \Delta_-^2}}{\Sigma\left(\delta\mu + \sqrt{\delta\mu^2 - \Delta_-^2}\right)}\right) - \frac{\sqrt{\Delta_+^2 - \delta\mu^2}}{\delta\mu}\left[\frac{\pi}{2} - \arctan\left(\frac{\sqrt{\Delta_+^2 - \delta\mu^2}}{\delta\mu}\right)\right] \tag{7.37}$$

Solving for Σ, we obtain

$$\Sigma = \frac{4\delta\mu\sqrt{\delta\mu^2 - \Delta_-^2}}{\delta\mu + \sqrt{\delta\mu^2 - \Delta_-^2}} \exp\left[\frac{\delta\mu}{\sqrt{\delta\mu^2 - \Delta_-^2}}\ln\left(\frac{\Sigma_0^2}{\Delta_+\left(\delta\mu + \sqrt{\delta\mu^2 - \Delta_-^2}\right)}\right) - \sqrt{\frac{\Delta_+^2 - \delta\mu^2}{\delta\mu^2 - \Delta_-^2}}\left(\frac{\pi}{2} - \arctan\left(\frac{\sqrt{\Delta_+^2 - \delta\mu^2}}{\delta\mu}\right)\right)\right] \tag{7.38}$$

We note that on the boundary between weak and strong ferromagnetism, $\delta\mu = \Delta_+$, the two expressions 7.36 and 7.38 are equal.

Energetic Stability

It is a simple task to calculate the free energy per unit volume of the SEF phase in the weak Cooper-pairing limit. We employ a simple generalization of the method adopted in subsection 6.3.4. We consider some set of parameters Σ_0', Δ_{s0}', Δ_{t0}' and n' such that $\Sigma_0'/2n' \ll \Delta_{s0}'/2n', \Delta_{t0}'/2n'$. We choose for the contour $\mathcal{C}$ in expression 7.32 the path OAB in $(\Delta_{t0}/2n, \Delta_{s0}/2n, \Sigma_0/2n)$-space. The segment OA lies in the $\Sigma_0/2n = 0$ plane joining the point $(1, 1, 0)$ to $(\Delta_{s0}'/2n', \Delta_{t0}'/2n', 0)$: it is the free energy per unit volume of the EF phase for these choice of parameters, δF_{EF}. The segment AB runs perpendicular to the $\Sigma_0/2n = 0$ plane, connecting $(\Delta_{s0}'/2n', \Delta_{t0}'/2n', 0)$ and $(\Delta_{s0}'/2n', \Delta_{t0}'/2n', \Sigma_0'/2n')$. We therefore have for 7.32

$$\begin{aligned}\delta F_{\text{SEF}} &= \int_{\text{OA}} \frac{\Delta_s^2}{g_s^2} dg_s + \frac{\Delta_t^2}{g_t^2} dg_t + \int_{\text{AB}} \frac{\Sigma^2}{\lambda^2} d\lambda \\ &= \delta F_{\text{EF}} - \begin{cases} \frac{1}{2}\eta_{\text{N}}(0)\frac{\sqrt{\delta\mu^2 - \Delta_+^2} + \sqrt{\delta\mu^2 - \Delta_-^2}}{\delta\mu}\Sigma^2 & \Delta_+, |\Delta_-| < \delta\mu \\ \frac{1}{2}\eta_{\text{N}}(0)\frac{\sqrt{\delta\mu^2 - \Delta_-^2}}{\delta\mu}\Sigma^2 & |\Delta_-| < \delta\mu < \Delta_+ \end{cases}\end{aligned} \tag{7.39}$$

It is clear that $\delta F_{\text{SEF}} < \delta F_{\text{EF}}$, confirming the instability of the EF phase towards the appearance of Cooper pairing when $\lambda \neq 0$. It is not obvious, however, that the SEF phase will always be more stable than the sSEI or tSEI phases.

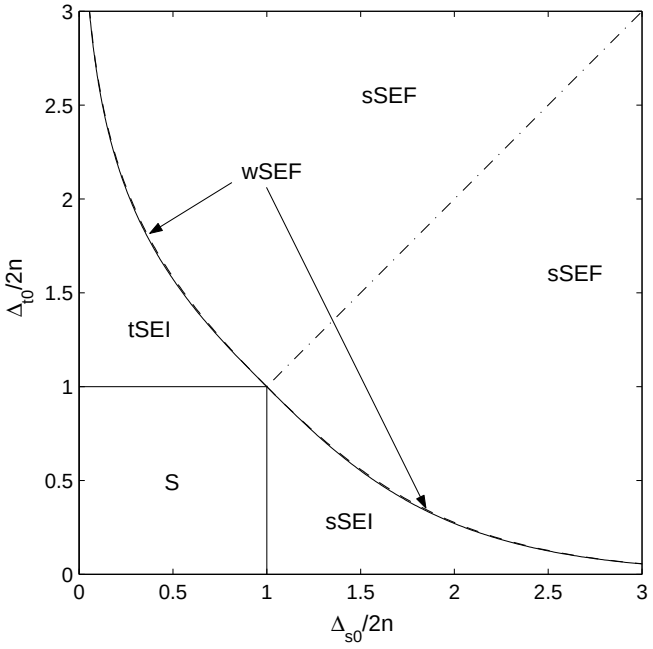

Figure 7.3: $\Sigma_0/2n$ = constant $\ll 1$ slice through the $n \neq 0$ phase diagram in the weak Cooper-pairing regime. The phase boundaries are identical to those in figure 5.6. The abbreviations wSEF and sSEF refer to the weak and strong SEF regimes respectively.

Two Analytic Solutions

It is interesting to study the above equations in the two cases where an analytic solution exists to the gap equations of the EF phase: on the boundary between the weak and strong ferromagnet regimes; and on the diagonal $\Delta_{s0}/2n = \Delta_{t0}/2n$. The details of these solutions were presented in subsection 5.5.2.

On the boundary between the weak and strong ferromagnet regimes, the spin-up and spin-down insulating gaps have the parametrization

$$\Delta_+ \;=\; 2n\cosh(\phi), \quad \Delta_- \;=\; 2n\sinh(\phi), \quad -\infty < \phi < \infty$$

Substituting these expressions into equation 7.36 or 7.38, we obtain for the variation of Σ along the boundary

$$\frac{\Sigma}{2n} \;=\; \frac{4\cosh(\phi)}{1+\cosh(\phi)} \exp\left[\cosh(\phi)\ln\left(\frac{(\Sigma_0/2n)^2}{\cosh(\phi)(1+\cosh(\phi))}\right)\right] \tag{7.40}$$

We plot $\log_{10}(\Sigma/\Sigma_0)$ for two values of $\Sigma_0/2n$as a function of $\Delta_{s0}/2n$ along the $\phi > 0$ branch of the curve defining the weak-strong boundary (figure 7.4). We compare with the results for the sSEI phase.

The most striking feature of figure 7.4(a) is the different behaviour of the two curves near $\Delta_{s0} = 2n$. This is to be explained in terms of the variation of the insulating gaps in the two phases along the weak-strong boundary. In the weak Cooper-pairing regime, the insulating gap Δ_s vanishes in the sSEI phase in the limit $\Delta_{s0} \to 2n$. Thus, Σ approaches its value in the pure S phase. For the SEF phase, we must consider the behaviour of the spin-up (spin-down) insulating gap in the EF phase as $\phi \to 0$: the significant increase (decrease) in its value over that in the EI phase was noted in chapter 5 (see figure 5.7(a)). Thus, in the weak Cooper-pairing limit, we expect a pronounced spin-splitting of the excitation spectrum of the SEF phase when $\Delta_{t0}/2n,\ \Delta_{s0}/2n \approx 1$. This has the expected effect upon Cooper-pairing, with the value of Σ in the SEF and sSEI phases differing by a factor $\sim \Sigma_0/2n \ll 1$ in this regime. Considering how close

the weak-strong boundary is to the boundary between the EF and EI phases, the large differences in Σ indicate a very rapid suppression of Cooper-pairing upon entry into the SEF phase from the SEI phases. This suppression increases with weakening Cooper-pairing.

The behaviour for $0 < \Delta_{s0}/2n - 1 \ll 1$ is, however, complicated by considerations of energetic stability. As $\phi \to 0$, the free energies per unit volume δF_{sEI} and δF_{EF} also vanish; the free energies per unit volume of the SEF and SEI phases will therefore be dominated by the contribution from Cooper-pairing for $\phi \ll 1$. Expanding the free energy per unit volume of the SEF and sSEI phases on the $\phi > 0$ weak-strong boundary to second order in ϕ, we have

$$-\frac{\delta F_{\text{SEF}}}{4n^2\eta_{\text{N}}(0)} = \frac{1}{2}\left(\frac{\Sigma_0}{2n}\right)^4 + \frac{1}{2}\left(\frac{\Sigma_0}{2n}\right)^4\left[1-\ln(2)+2\ln\left(\frac{\Sigma_0}{2n}\right)\right]\phi^2 + \mathcal{O}(\phi^4) \tag{7.41}$$

$$\begin{aligned}-\frac{\delta F_{\text{sSEI}}}{4n^2\eta_{\text{N}}(0)} = {} & \frac{1}{2}\left(\frac{\Sigma_0}{2n}\right)^2 + 2\ln(2)\left(\frac{\Sigma_0}{2n}\right)^2\ln\left(\frac{\Sigma_0}{2n}\right)\phi + \left[\frac{1}{2}\ln(2)^2 - \left(\frac{\Sigma_0}{2n}\right)^2\left[3\ln(2)^2 - \ln\left(\frac{\Sigma_0}{2n}\right)\right.\right. \\ & \left.\left. +2\ln(2)\ln\left(\frac{\Sigma_0}{2n}\right) - \ln(2)^2\ln\left(\frac{\Sigma_0}{2n}\right) - 4\ln(2)^2\ln\left(\frac{\Sigma_0}{2n}\right)^2\right]\right]\phi^2 + \mathcal{O}(\phi^3)\end{aligned} \tag{7.42}$$

We use equations 7.41 and 7.42 to solve $\delta F_{\text{SEF}} = \delta F_{\text{sSEI}}$ for ϕ to first order in $\Sigma_0/2n$. We find that equality obtains at

$$\phi = -\frac{\sqrt{2-4\ln(2)^2}}{1-2\ln(2)^2}\frac{\Sigma_0}{2n} + \ldots \approx 7.15\frac{\Sigma_0}{2n} \quad \Rightarrow \quad \frac{\Delta_{s0}}{2n} \approx 1 + 4.96\frac{\Sigma_0}{2n} \tag{7.43}$$

This result implies that just within the SEF phase and for $\Delta_{s0}/2n, \Delta_{t0}/2n \approx 1$, the SEI phases are actually more stable in the weak Cooper-pairing limit.

For $\Delta_{s0} \gg n$, the spin-splitting of the bands becomes increasingly unimportant, as is clearly evidenced by the apparent convergence of the sSEI and SEF curves in figure 7.4(a). For sufficiently large $\Delta_{s0}/2n$, the two curves actually intersect. We cannot offer a convincing explanation for this behaviour. We note that as $\Sigma \ll \Sigma_0$ in this region, its physical significance appears to be slight.

Along the diagonal $\Delta_{s0}/2n = \Delta_{t0}/2n$, the (energetically favourable) solution to the EF gap equations is

$$\begin{aligned}&\Delta_+ = \Delta_{s0}, \qquad \Delta_- = 0, \qquad 2n \le \Delta_{s0} \le 4n \\ &\Delta_+ = \Delta_{s0}, \quad \Delta_-^2 = \Delta_{s0}\left(\Delta_{s0} - 4n\right), \qquad 4n \le \Delta_{s0}\end{aligned} \tag{7.44}$$

Substituting these values of the spin-down and spin-up insulating gaps into 7.38, we obtain

$$\frac{\Sigma}{2n} = \begin{cases} 2\exp\left[\ln\left(\frac{\Sigma_0^2}{4n\Delta_{s0}}\right) - \sqrt{\left(\frac{\Delta_{s0}}{2n}\right)^2 - 1}\left(\frac{\pi}{2} - \arctan\left(\sqrt{\left(\frac{\Delta_{s0}}{2n}\right)^2 - 1}\right)\right)\right] & 1 \le \frac{\Delta_{s0}}{2n} \le 2 \\ \frac{4(\Delta_{s0}-2n)}{\Delta_{s0}}\exp\left[\frac{\Delta_{s0}-2n}{n}\ln\left(\frac{\Sigma_0}{\Delta_{s0}}\right) - \sqrt{\frac{\Delta_{s0}-n}{n}}\left(\frac{\pi}{2} - \arctan\left(\frac{2\sqrt{n(\Delta_{s0}-n)}}{\Delta_{s0}-2n}\right)\right)\right] & 2 \le \frac{\Delta_{s0}}{2n} \end{cases} \tag{7.45}$$

Using these results, we plot $\log_{10}(\Sigma/\Sigma_0)$ along the diagonal, comparing the SEF result (equation 7.45) with that already derived for the sSEI phase.

We consider first the behaviour of equation 7.45 for $1 \le \Delta_{s0}/2n \le 2$. Upon entry into the SEF phase, Σ discontinuously drops to a factor of $\Sigma_0/2n$ its value in the S phase, as predicted by the $\phi \to 0$ limit of equation 7.40. After this initial drop, however, Σ decreases less rapidly in the SEF than in the sSEI phase. The two curves eventually intersect at some point $2 > \Delta_{s0}/2n > 1.5$, beyond which Σ is always larger in the SEF phase than in the sSEI. The spin-splitting of the SEF spectrum makes this an unexpected result. We tentatively interpret the variation of Σ as demonstrating the central role that the insulating gap plays in suppressing Cooper-pairing: in contrast to the sSEI phase, there is no insulating gap in the the SEF phase as $\Delta_- = 0$ throughout this region. Spin-splitting of the spectrum appears comparatively unimportant. For $\Delta_{s0}/2n > 2$, the solution 7.44 is characterized by the presence of both a spin-up and spin-down insulating gap.

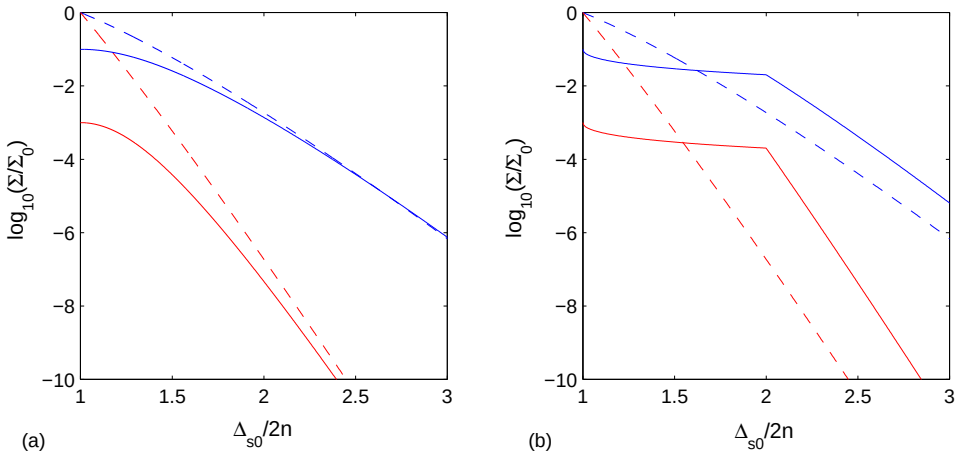

Figure 7.4: The variation of Σ in the SEF (solid lines) and sSEI phases (dashed lines) along (a) the boundary between the weak and strong ferromagnet regimes and (b) the diagonal $\Delta_{t0}/2n = \Delta_{s0}/2n$. The blue lines correspond to $\Sigma_0/2n = 0.1$, the red lines to $\Sigma_0/2n = 0.001$.

The opening of the spin-down gap clearly has a negative impact upon Σ, which now decreases at approximately the same rate as in the sSEI phase. This provides further evidence of the dominant effect that the insulating gap has upon the ability of the system to support Cooper-pairing.

The interpretation of the SEF curve for $\Delta_{s0}/2n - 1 \ll 1$ is subject to the same reservations attached to the $\phi \to 0$ limit of equation 7.40, *viz* the SEI phase may be more stable than the SEF in this region. We therefore consider the free energy per unit volume of the two phases around $\Delta_{s0}/2n = 1$. Expanding to first order, we have

$$\begin{aligned} \delta F_{\text{SEF}} &= -\frac{1}{2}\eta_{\text{N}}(0)\left[\frac{\Sigma_0^4}{4n^2} + \frac{\Sigma_0^4}{4n^2}\sqrt{2\pi}\left(\frac{\Delta_{s0}}{2n} - 1\right)^{1/2}\right. \\ &\qquad \left. + \left(\frac{\Sigma_0^4}{4n^2}(2+\pi^2) + 8n^2\right)\left(\frac{\Delta_{s0}}{2n} - 1\right) + \ldots\right] \qquad (7.46) \\ \delta F_{\text{sSEI}} &= -\frac{1}{2}\eta_{\text{N}}(0)\left[\Sigma_0^2 + 4\Sigma_0^2 \ln\left(\frac{\Sigma_0}{2n}\right)\left(\frac{\Delta_{s0}}{2n} - 1\right) + \ldots\right] \qquad (7.47) \end{aligned}$$

Solving the equation $\delta F_{\text{SEF}} = \delta F_{\text{sSEI}}$, we find that equality holds at

$$\frac{\Delta_{s0}}{2n} = 1 + \frac{(\Sigma_0/2n)^2}{2 - (\Sigma_0/2n)^2 \ln(\Sigma_0/2n)} + \ldots \approx 1 + \frac{1}{2}\left(\frac{\Sigma_0}{2n}\right)^2 \qquad (7.48)$$

This result indicates that the region along the diagonal where the SEF phase is less stable than the sSEI is extremely small. The result 7.48 complements 7.43, together indicating the presence of a narrow region on the SEF phase boundary where the SEF phase occurs as a metastable state.

For $\Delta_{s0}/2n = \Delta_{t0}/2n$, the boundary between the SEF and S phases may be determined in the general case. From equation 7.15 and 7.16 we obtain after some manipulation

$$\begin{aligned} 2\ln\left(\frac{\Delta_{s0}}{\Sigma_0}\right) &= -\frac{\Delta_t}{\Delta_s}\left(\mathcal{I}_{1+} - \mathcal{I}_{1-}\right) + \frac{\Delta_t}{\Delta_s}\frac{\Sigma^2}{\delta\mu}\left(\mathcal{I}_{2+} - \mathcal{I}_{2-}\right) \\ &\quad + \frac{\delta\mu^2 + \Sigma^2}{\delta\mu}\left(\mathcal{I}_{2+} + \mathcal{I}_{2-}\right) + \frac{1}{\delta\mu}\left(\Delta_+^2\mathcal{I}_{2+} + \Delta_-^2\mathcal{I}_{2-}\right) \qquad (7.49) \end{aligned}$$

where we have introduced the simplifying notation $\mathcal{I}_{j\sigma} = \mathcal{I}_j(\Delta_\sigma, \Sigma, \delta\mu)$. Approaching the boundary with the S phase, the two exciton order parameters vanish continuously; $\delta\mu$ and Σ converge to their values in the S phase, n and Σ_0 respectively. Taking the limit $\Delta_s,\ \Delta_t \to 0$ in 7.49 and noting

the asymptotic relations (see subsection A.4.2 of the mathematical appendix)

$$\mathcal{I}_{1+} - \mathcal{I}_{1-} \sim \mathcal{O}(\Delta_s \Delta_t), \qquad \mathcal{I}_{2+} - \mathcal{I}_{2-} \sim \mathcal{O}(\Delta_s \Delta_t) \tag{7.50}$$

we obtain the relation

$$\ln\left(\frac{\Delta_{t0}/2n}{\Sigma_0/2n}\right) = \ln\left(\frac{\Delta_{s0}/2n}{\Sigma_0/2n}\right) = \sqrt{1+4\left(\frac{\Sigma_0}{2n}\right)^2}\ln\left(\frac{1+\sqrt{1+4(\Sigma_0/2n)^2}}{2(\Sigma_0/2n)}\right) \tag{7.51}$$

We immediately recognize that the projection of the line 7.51 onto the $(\Delta_{s0}/2n, \Sigma_0/2n)$-plane ($(\Delta_{t0}/2n, \Sigma_0/2n)$-plane) defines the boundary between the sSEI (tSEI) phase and the S phase. This is the only line in $(\Delta_{s0}/2n, \Delta_{t0}/2n, \Sigma_0/2n)$-space upon which the SEF phase borders with the S. Thus, except upon this line, the SEF phase is separated from the S phase by a region in which an SEI phase is realized.

7.4 The Symmetric Solution

The solution to equation 7.6 for the symmetric coexistence gives the results

$$\mathcal{G}^{11}_{\alpha\beta}(\mathbf{k},\omega_n) = \delta_{\alpha\beta}\frac{((i\omega_n)^2 - \zeta_{2\mathbf{k}}^2)(i\omega_n+\zeta_{1\mathbf{k}}) + 2\Sigma\Sigma_2\Delta_\sigma - \Sigma^2(i\omega_n+\zeta_{1\mathbf{k}}) - \Sigma_2^2(i\omega_n+\zeta_{2\mathbf{k}}) - \Delta_\sigma^2(i\omega_n-\zeta_{2\mathbf{k}})}{\left((i\omega_n)^2-\omega^{+\,2}_{\mathbf{k}\sigma}\right)\left((i\omega_n)^2-\omega^{-\,2}_{\mathbf{k}\sigma}\right)} \tag{7.52}$$

$$\mathcal{G}^{21}_{\alpha\beta}(\mathbf{k},\omega_n) = \delta_{\alpha\beta}\frac{\Delta_\sigma\left((i\omega_n-\delta\mu)^2 - \xi_{\mathbf{k}}^2 - \Delta_\sigma^2 - \Sigma^2 - \Sigma_2^2\right) - 2\Sigma\Sigma_2(i\omega_n-\delta\mu)}{\left((i\omega_n)^2-\omega^{+\,2}_{\mathbf{k}\sigma}\right)\left((i\omega_n)^2-\omega^{-\,2}_{\mathbf{k}\sigma}\right)} \tag{7.53}$$

$$\mathcal{F}^{\dagger 11}_{\alpha\beta}(\mathbf{k},\omega_n) = -i\sigma^y_{\alpha\beta}\frac{\Sigma\left(\Sigma^2+\Delta_\sigma^2-\Sigma_2^2-(i\omega_n)^2-\zeta_{2\mathbf{k}}^2\right) - 2\Sigma_2\Delta_\sigma\zeta_{2\mathbf{k}}}{\left((i\omega_n)^2-\omega^{+\,2}_{\mathbf{k}\sigma}\right)\left((i\omega_n)^2-\omega^{-\,2}_{\mathbf{k}\sigma}\right)} \tag{7.54}$$

$$\mathcal{F}^{\dagger 21}_{\alpha\beta}(\mathbf{k},\omega_n) = -i\sigma^y_{\alpha\beta}\frac{\Sigma_2\left(\Sigma_2^2-\Sigma^2+\Delta_\sigma^2-(i\omega_n+\zeta_{1\mathbf{k}})(i\omega_n-\zeta_{2\mathbf{k}})\right) - 2\Delta_\sigma\Sigma\delta\mu}{\left((i\omega_n)^2-\omega^{+\,2}_{\mathbf{k}\sigma}\right)\left((i\omega_n)^2-\omega^{-\,2}_{\mathbf{k}\sigma}\right)} \tag{7.55}$$

The subscript σ takes the value $+(-)$ for $\alpha\beta = \uparrow\uparrow$ ($\downarrow\downarrow$) in 7.52, 7.53 and $\alpha\beta = \downarrow\uparrow$ ($\uparrow\downarrow$) in 7.54, 7.55. The Green's functions $\mathcal{G}^{22}$, $\mathcal{G}^{12}$, $\mathcal{F}^{\dagger 22}$ and $\mathcal{F}^{\dagger 12}$ are obtained by making the replacement $\zeta_{1\mathbf{k}} \leftrightarrow \zeta_{2\mathbf{k}}$ in the above expressions.

In the general case, the poles of the Green's functions 7.52, 7.53, 7.54 and 7.55 are spin-dependent:

$$\omega^{\pm\,2}_{\mathbf{k}\sigma} = (E_{\mathbf{k}\sigma} \pm \delta\widetilde{\mu})^2 + \widetilde{\Sigma}_\sigma^2, \qquad E^2_{\mathbf{k}\sigma} = \xi^2_{\mathbf{k}} + \widetilde{\Delta}^2_\sigma \tag{7.56}$$

where the effective gaps $\widetilde{\Sigma}$ and $\widetilde{\Delta}_\sigma$ and chemical potential $\delta\widetilde{\mu}$ are defined

$$\widetilde{\Delta}_\sigma = \frac{\delta\mu\Delta_\sigma + \Sigma\Sigma_2}{\delta\widetilde{\mu}}, \quad \widetilde{\Sigma} = \frac{\delta\mu\Sigma - \Delta_\sigma\Sigma_2}{\delta\widetilde{\mu}}, \quad \delta\widetilde{\mu}^2 = \delta\mu^2 + \Sigma_2^2 \tag{7.57}$$

It is simple to verify that these Green's functions are consistent with those for the symmetric sSEI and tSEI phases.

7.4.1 The Self-Consistency Equations

Using the derived expressions for the Green's functions, we obtain, after lengthy calculation, the following self-consistency equations for the symmetric system

$$\Sigma = -\frac{\lambda\eta_{\rm N}(0)}{2}\sum_{\sigma=-,+}\left[\Sigma\mathcal{I}_1\left(\widetilde{\Delta}_\sigma,\widetilde{\Sigma}_\sigma,\delta\mu\right) + \delta\mu\widetilde{\Sigma}_\sigma\mathcal{I}_2\left(\widetilde{\Delta}_\sigma,\widetilde{\Sigma}_\sigma,\delta\mu\right)\right] \tag{7.58}$$

$$\Sigma_2 = -\frac{\lambda_{12}\eta_{\rm N}(0)}{2}\sum_{\sigma=-,+}\left[\frac{\Sigma_2}{\delta\widetilde{\mu}}\mathcal{I}_3\left(\widetilde{\Delta}_\sigma,\widetilde{\Sigma}_\sigma,\delta\mu\right) - \frac{\delta\mu}{\delta\widetilde{\mu}}\widetilde{\Sigma}_\sigma\widetilde{\Delta}_\sigma\mathcal{I}_2\left(\widetilde{\Delta}_\sigma,\widetilde{\Sigma}_\sigma,\delta\mu\right)\right] \quad (7.59)$$

$$\Delta_s = -\frac{g_s\eta_{\rm N}(0)}{2}\sum_{\sigma=-,+}\left[\Delta_\sigma\mathcal{I}_1\left(\widetilde{\Delta}_\sigma,\widetilde{\Sigma}_\sigma,\delta\mu\right) - \Sigma_2\widetilde{\Sigma}_\sigma\mathcal{I}_2\left(\widetilde{\Delta}_\sigma,\widetilde{\Sigma}_\sigma,\delta\mu\right)\right] \quad (7.60)$$

$$\Delta_t = -\frac{g_t\eta_{\rm N}(0)}{2}\sum_{\sigma=-,+}\sigma\left[\Delta_\sigma\mathcal{I}_1\left(\widetilde{\Delta}_\sigma,\widetilde{\Sigma}_\sigma,\delta\mu\right) - \Sigma_2\widetilde{\Sigma}_\sigma\mathcal{I}_2\left(\widetilde{\Delta}_\sigma,\widetilde{\Sigma}_\sigma,\delta\mu\right)\right] \quad (7.61)$$

$$n = \frac{\delta\mu}{2\delta\widetilde{\mu}}\sum_{\sigma=-,+}\left[\mathcal{I}_3\left(\widetilde{\Delta}_\sigma,\widetilde{\Sigma}_\sigma,\delta\mu\right) + \left(\Sigma^2-\widetilde{\Sigma}_\sigma^2\right)\mathcal{I}_2\left(\widetilde{\Delta}_\sigma,\widetilde{\Sigma}_\sigma,\delta\mu\right)\right] \quad (7.62)$$

where the integrals $\mathcal{I}_j$ where $j = 1,2,3$ are as defined for the symmetric SEI analysis.

As in the antisymmetric case, it is clear that the expressions 7.58, 7.59, 7.60, 7.61 and 7.62 are consistent with the gap equations for the symmetric sSEI (tSEI) solution when $\Delta_t = 0$ ($\Delta_s = 0$). In particular, the inference drawn in section 6.4 as to the dependence of the order parameters upon $\delta\mu$ still holds. Thus, when $\Sigma \neq 0$, the condition $\delta\widetilde{\mu} = 0$ ensures that the concentrations of electrons and holes in the system is equal.

Finally, we present an expression for the magnetization of the system

$$M = 2\mu_B\eta_{\rm N}(0)\frac{\delta\mu}{\delta\widetilde{\mu}}\sum_{\sigma=-,+}\sigma\left[\mathcal{I}_3\left(\widetilde{\Delta}_\sigma,\widetilde{\Sigma}_\sigma,\delta\mu\right) + \left(\Sigma^2-\widetilde{\Sigma}_\sigma^2\right)\mathcal{I}_2\left(\widetilde{\Delta}_\sigma,\widetilde{\Sigma}_\sigma,\delta\mu\right)\right] \quad (7.63)$$

In the case of perfect nesting, equation 7.63 exhibits the characteristic disappearance of the magnetic moment.

7.4.2 The $n = 0$ System

Letting $\delta\widetilde{\mu} = 0$, we obtain the simplified expressions for the Green's functions

$$\mathcal{G}^{jj}_{\alpha\beta}(\mathbf{k},\omega_n) = \delta_{\alpha\beta}\frac{i\omega_n - \xi_{j\mathbf{k}}}{(i\omega_n)^2 - \omega^2_{\mathbf{k}\sigma}} \quad (7.64)$$

$$\mathcal{G}^{12}_{\alpha\beta}(\mathbf{k},\omega_n) = \mathcal{G}^{21}_{\alpha\beta}(\mathbf{k},\omega_n) = \delta_{\alpha\beta}\frac{\Delta_\sigma}{(i\omega_n)^2 - \omega^2_{\mathbf{k}\sigma}} \quad (7.65)$$

$$\mathcal{F}^{\dagger 11}_{\alpha\beta}(\mathbf{k},\omega_n) = \mathcal{F}^{\dagger 22}_{\alpha\beta}(\mathbf{k},\omega_n) = -i\sigma^y_{\alpha\beta}\frac{\Sigma}{(i\omega_n)^2 - \omega^2_{\mathbf{k}\sigma}} \quad (7.66)$$

where $j = 1,2$ in equation 7.64. At perfect nesting, the eight distinct poles of the general case reduce to only four at $\pm\omega_{\mathbf{k}\sigma}$:

$$\omega_{\mathbf{k}\sigma} = \sqrt{{\xi_{\mathbf{k}}}^2 + \Delta_\sigma^2 + \Sigma^2} \quad (7.67)$$

These poles define only the electron excitation spectrum in the 'rebuilt' system.

Evaluating the integrals in equations 7.58, 7.60 and 7.61 in the $\delta\widetilde{\mu} = 0$ limit, we have the self-consistency equations

$$\Sigma = -\frac{\lambda\eta_{\rm N}(0)}{2}\left[\Sigma\ln\left(\frac{2\varpi}{\sqrt{\Delta_+^2+\Sigma^2}}\right) + \Sigma\ln\left(\frac{2\varpi}{\sqrt{\Delta_-^2+\Sigma^2}}\right)\right] \quad (7.68)$$

$$\Delta_s = -\frac{g_s\eta_{\rm N}(0)}{2}\left[\Delta_+\ln\left(\frac{2\varpi}{\sqrt{\Delta_+^2+\Sigma^2}}\right) + \Delta_-\ln\left(\frac{2\varpi}{\sqrt{\Delta_-^2+\Sigma^2}}\right)\right] \quad (7.69)$$

$$\Delta_t = -\frac{g_t\eta_{\rm N}(0)}{2}\left[\Delta_+\ln\left(\frac{2\varpi}{\sqrt{\Delta_+^2+\Sigma^2}}\right) - \Delta_-\ln\left(\frac{2\varpi}{\sqrt{\Delta_-^2+\Sigma^2}}\right)\right] \quad (7.70)$$

After some rearrangement, we have in the general case when all three order parameters are non-zero

the simple expressions

$$4\ln(z_1^0) = \frac{z_2}{z_1}\ln\left[\frac{(z_1+z_2)^2+1}{(z_1-z_2)^2+1}\right], \qquad 4\ln(z_2^0) = \frac{z_1}{z_2}\ln\left[\frac{(z_1+z_2)^2+1}{(z_1-z_2)^2+1}\right] \tag{7.71}$$

where the dimensionless parameters z_1, z_1^0, z_2, z_2^0 are as defined in equation 7.25. Using the equations 7.71, we determine the boundary of the SEF phase in the (z_1^0, z_2^0)-plane.

We first investigate the boundary with the sSEI phase. Approaching this boundary, z_2 vanishes whilst z_1 remains finite. Taking this limit in equations 7.71, we obtain the parametric expressions for the boundary

$$z_1^0 = 1, \qquad z_2^0 = \exp\left(\frac{t^2}{t^2+1}\right) \tag{7.72}$$

where the parameter $0 \leq t = \Delta_s/\Sigma < \infty$. This defines the segment of the straight line $z_1^0 = 1$ lying between $z_2^0 = 1$ and $z_2^0 = e$. We similarly have for the boundary between the SEF and tSEI phases the parametric equations

$$z_1^0 = \exp\left(\frac{t^2}{t^2+1}\right), \qquad z_2^0 = 1 \tag{7.73}$$

where $0 \leq t = \Delta_t/\Sigma < \infty$. The boundary between the SEF and EF phases is obtained by letting both z_1 and z_2 diverge in 7.71 such that their ratio z_1/z_2 remains finite. We easily obtain the following relations

$$z_1^0 = \exp\left(-\frac{1}{2t}\ln\left|\frac{1-t}{1+t}\right|\right), \qquad z_2^0 = \exp\left(-\frac{t}{2}\ln\left|\frac{1-t}{1+t}\right|\right) \tag{7.74}$$

where $0 \leq t = \Delta_s/\Delta_t < \infty$. We complete the description of the phase diagram by including the double coexistence phases: the sSEI and tSEI phases are realized upon the straight lines $z_1^0 = 1$

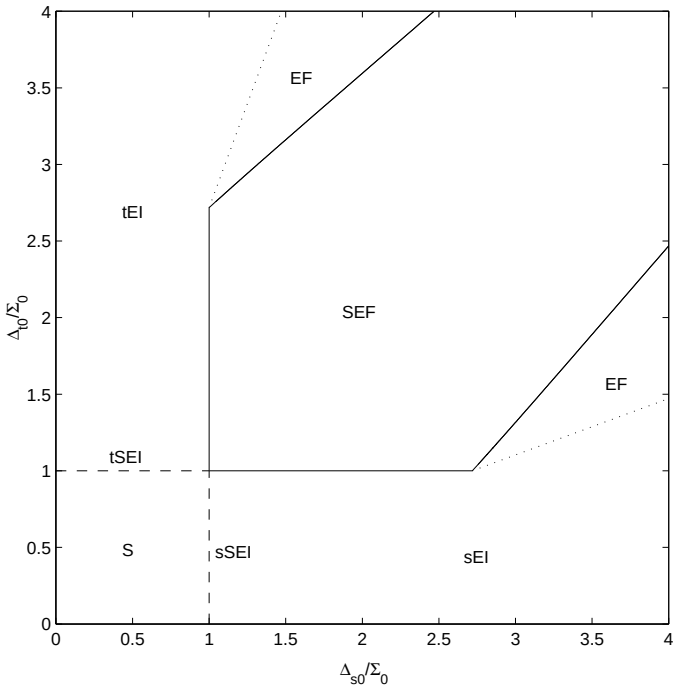

Figure 7.5: The phase diagram of the symmetric solution at equal electron and hole concentrations. The different phases are denoted using the standard abbreviations.

and $z_2^0 = 1$ respectively; a metastable EF phase is bounded by the lines $z_1^0 = ez_2^0$ and $z_1^0 = e^{-1}z_2^0$. Adopting the simplifying scheme used for the antisymmetric solution, we obtain the phase diagram for the symmetric solution as presented in figure 7.5.

We consider the stability of the SEF phase. Arguing as in the antisymmetric case, we find the free energy per unit volume of the symmetric SEF phase relative to the normal phase to be given by

$$\delta F_{\text{SEF}} = f\left(\frac{z_2}{z_1}, \frac{1}{z_1}\right)\delta F_{\text{sEI}} = f\left(\frac{z_1}{z_2}, \frac{1}{z_2}\right)\delta F_{\text{tEI}} \tag{7.75}$$

where the function $f(x,y)$ is defined

$$\begin{aligned}\ln\left(f(x,y)\right) &= \ln(1+x^2+y^2) + \frac{x}{2}\ln\left[\frac{(1-x)^2+y^2}{(1+x)^2+y^2}\right] \\ &\quad -\frac{1}{2}\ln\left[((1-x)^2+y^2)((1+x)^2+y^2)\right]\end{aligned} \tag{7.76}$$

where $x,\ y \geq 0$ real. It is easy to verify that the equation $f(x,y) > 1$ is never satisfied for any non-zero values of x or y: in the region where it is predicted by the gap equations, the SEF phase is always less stable than the sEI and tEI phases. Thus, for perfect nesting, the SEF phase is never realized except perhaps as a metastable state.

7.4.3 The $n \neq 0$ System

Despite our best efforts, the self-consistency equations for the symmetric solution at unequal electron and hole concentrations proved stubbornly resistant to analytic investigation. A purely numerical approach, which we did not have time enough to implement, appears to be required for the study of this system. This is particularly frustrating as the symmetric SEI phases display a region of co-operative coexistence between the S and EI phases; a similar situation might be realized in the symmetric SEF phase. As such, the numerical study of the symmetric system should be regarded as a priority of any future work.

7.5 Experimental Evidence?

As there is currently no unambiguous experimental realization of the EF phase, we are of course unable to point to any examples of the SEF phase. Nevertheless, it is interesting to speculate on the significance of certain anomalies in the low-temperature transport properties of the most promising EF candidates, the alkaline earth hexaborides. At very low temperatures ($T < 0.4$K), a large reduction in the resistivity ($\sim 50\%$) has been observed in both CaB_6 and SrB_6. This is accompanied by anomalies in the specific heat and the NMR spectra [91–93]. The former effect is somewhat reminiscent of the lambda transition in BCS superconductors. Application of magnetic fields is observed to suppress these effects, which disappear completely above a field of 7.5kOe. Similar phenomena have been observed in samples of $Ca_{1-x}La_xB_6$ as well [93]. All these effects bear at least a superficial resemblance to the situation in a so-called "dirty" superconductor [94]. We emphasize, however, that this is the speculation of a non-specialist; more work needs to be done before the precise nature of the low-temperature transport properties of these materials is comprehended.

Conclusions

This thesis presents an original investigation of the possibility of superconductivity in an excitonic ferromagnet (SEF phase) in the limit of zero temperature. We have demonstrated that the usual classification scheme for the solutions to the SEI phase equations of motion is valid also for the SEF phase equations of motion. The derived self-consistency equations in both the antisymmetric and symmetric cases were accordingly shown to be consistent with those for the SEI and EF phases. We were able to completely characterize the system in the $n = 0$ case, showing that the SEF phase could only occur as a metastable state. Phase diagrams for both the antisymmetric and symmetric cases were obtained. In the $n \neq 0$ antisymmetric case, we were able to present a detailed study of the behaviour of the superconducting order parameter Σ in the weak Cooper-pairing regime. The results were compared to those for the SEI phase: the spin-splitting of the excitation spectrum in the SEF phase had the predicted effect, generally suppressing superconductivity. Unexpectedly, the value of Σ in the SEF phase was found to significantly exceed that in the SEI phase in certain circumstances. The $n \neq 0$ symmetric case did not admit analytic study: we believe that a computational approach may be required. We have also discussed possible experimental evidence for the SEF phase.

In addition to this work, we have also presented a detailed development of the BCS superconductor, excitonic insulator, excitonic ferromagnet and superconducting excitonic insulator. In these chapters, we have adopted the approach most consistent with the quantum field theory of many-body systems outlined in chapter 2. Throughout the thesis, the relation of the examined models to experimental reality has been considered.

8.1 Future Directions

The study of the SEF phase has by no means been exhausted by our efforts this past year. There is wide scope for future work within the framework of the model presented here, as well as many possible improvements and alterations that can be made upon it.

As mentioned at the end of section 7.4, we were unable to make any headway in the analytical study of the symmetric solution in the $n \neq 0$ case. This failure presents the most obvious opportunity for future workers. The computational study of the self-consistency equations 7.58-7.62 might potentially yield rich dividends, in light of the co-operative coexistence found for the symmetric case in the sSEI phase (section 6.4). A computational analysis of both the antisymmetric and symmetric self-consistency equations also appears to us the only possible way to determine the general phase diagram in $(\Sigma_0/2n, \Delta_{s0}/2n, \Delta_{t0}/2n)$-space. The study of the system at finite temperature is also of interest; this may be possible to address analytically.

There are several directions in which one could move beyond the simple model adopted here. We list below what we consider to be the clearest points of departure from our analysis:

- the inclusion of interband transition terms has been demonstrated to change the form of the $n = 0$ symmetric sSEI phase diagram, allowing a region of coexistence of non-zero measure. [9]. It would be of interest to include such a term in the general case.
- the relaxation of the assumption of equal electron and hole effective masses in the overlapping bands in the model semimetal spectrum should be a simple but interesting improvement.

This would allow a more detailed comparison of the systems considered here with available experimental data.

- the effects of non-nested portions of the Fermi surface should be addressed. This presents a much more challenging problem, as the behaviour of these portions of the Fermi surface as particle reservoirs [60] must be reconciled with the appearance of Cooper-pairing in these regions [11]. It is not at all obvious how this would be achieved.

In considering which to pursue, we wish to draw the attention of future workers to the difficulty in obtaining analytic results in any but the simplest cases considered in this thesis. It might therefore be most profitable to (first) apply these suggestions to the EF or SEI phases. Even here, recourse to computational methods might eventually prove necessary.

Mathematical Appendix

A.1 The Homogeneous Electron Gas and the Infinite-Volume Limit

The normal phase is always regarded as a spatially infinite and homogeneous non-interacting electron gas. Mathematically, such a system may be profitably regarded as the limiting case of N non-interacting Fermions confined within a volume V. In the thermodynamic limit, we allow N and V to diverge such that their ratio, the particle concentration N/V, is constant. This limit is always taken at the end of the calculation.

For simplicity, we consider the confining volume to be a cube of side L. Under the assumption of periodic boundary conditions, the single-particle wave-functions are plane waves with wave-vector $\mathbf{k}$. The components of these wave-vectors are

$$k_i \;=\; \frac{2\pi n_i}{L} \qquad i \;=\; x,y,z \qquad n_i \;=\; 0,\pm 1,\pm 2,\ldots \tag{A.1}$$

Regarded as points in momentum space, the 'distance' between two nearest-neighbour wave-vectors is π/L: in the infinite volume limit ($L \to \infty$), therefore, the allowed wave-vectors form a dense set.

We consider some macroscopic extensive property of the system, H say. To calculate H, we must evaluate the sum

$$\mathcal{H} \;=\; \frac{H}{L^3} \;=\; \frac{1}{L^3}\sum_{\mathbf{k}} h(\mathbf{k}) \tag{A.2}$$

where $h(\mathbf{k})$ is some continuous function in momentum space and the summation extends over all occupied states as indexed by the allowed wave-vectors $\mathbf{k}$, and $\mathcal{H}$ is the value of H per unit volume: in the $V \to \infty$ limit, it is only sensible to speak of the value of extensive properties per unit volume.

We consider the expression A.2 in the limit $L \to \infty$. We may regard each allowed wave-vector as being a centre of a cube in momentum-space of 'volume' $(2\pi/L)^3$: these boxes partition the space. In the infinite-volume limit, therefore, the RHS of A.2 converges to $(2\pi)^{-3}$ times the integral of h over the region $\mathcal{R}$ of momentum-space in which the set of occupied wave-vectors is dense:

$$\lim_{L\to\infty} \mathcal{H} \;=\; \lim_{L\to\infty} \frac{1}{L^3}\sum_{\mathbf{k}} h(\mathbf{k}) \;=\; \frac{1}{(2\pi)^3}\int_{\mathcal{R}} h d^3k \tag{A.3}$$

As is well known, the region $\mathcal{R}$ is a sphere with radius k_{F} (the Fermi wave-vector) centred at the origin.

In this work, we assume that we may ignore the contribution to $\mathcal{H}$ from states with energies lying outside some narrow range about the Fermi energy μ. In order to evaluate the integral in A.3, therefore, it is most convenient to convert to an integral over the excitation spectrum ϵ_k. We assume that the range of integration is so narrow that the DOS may be regarded as constant, with value as defined at the Fermi surface ($\epsilon_k = \mu$):

$$\eta_{\mathrm{N}}(0) \;=\; \frac{1}{2\pi^2}\left[k^2\frac{dk}{d\epsilon_k}\right]_{\epsilon_k=\mu} \tag{A.4}$$

We therefore have

$$(2\pi)^{-3}d^3k \;=\; 4\pi k^2(2\pi)^{-3}dk \;\approx\; \eta_{\rm N}(0)d\epsilon \tag{A.5}$$

Hence, A.3 becomes

$$\lim_{L\to\infty}\mathcal{H} \;\approx\; \eta_{\rm N}(0)\int_{\mu-\varpi}^{\mu+\varpi} h d\epsilon \tag{A.6}$$

where ϖ is the 'cut-off' energy. We regard the expression A.6 as exact.

A.2 Matsubara Sums

When performing the inverse Fourier transform between the ω- and τ-spaces in the Matsubara finite-temperature formalism, we frequently encounter sums of the form

$$\lim_{\kappa\to 0^{\pm}}\sum_{n\ \rm odd}\frac{1}{i\omega_n - x}e^{i\omega_n\kappa} \tag{A.7}$$

where the $\omega_n = n\pi/\beta$ are the Fourier frequencies of the Green's functions and x is a real constant. Note that without the convergence factor κ, the sum would diverge logarithmically: $\kappa < \beta$ must therefore remain nonzero until after the sum is evaluated. We outline a procedure for evaluating this summation below. The approach utilized is based upon that presented in [25, 26].

For the case $\kappa > 0$, we consider the integral of the meromorphic function

$$F(z) \;=\; \frac{-\beta e^{\kappa z}}{(e^{\beta z}+1)(z-x)} \tag{A.8}$$

along the contour $\mathcal{C}_m$, the circle of radius $2m\pi/\beta > x$ centred at the origin, where m is a natural number. The analytic structure of $F(z)$ and the contour $\mathcal{C}_m$ are illustrated in figure A.1. By

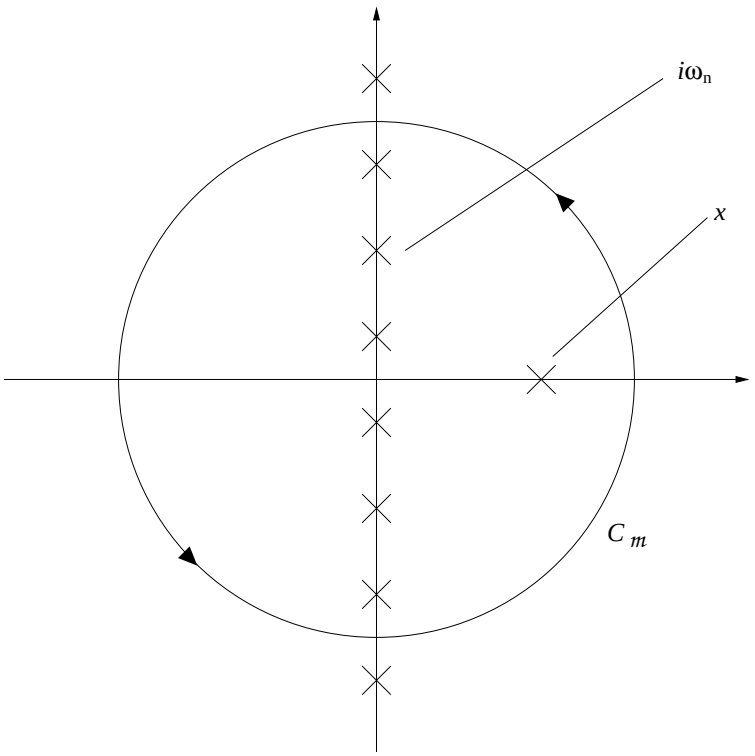

Figure A.1: The contour for the evaluation of the Matsubara sums. The (simple) poles of the function $F(z)$ are indicated by crosses.

Cauchy's theorem, we have

$$\frac{1}{2\pi i}\int_{\mathcal{C}_m} F(z)dz \;=\; \sum_{2m>n\ \text{odd}} \frac{1}{i\omega_n - x} e^{i\omega_n \kappa} - \frac{\beta e^{\kappa x}}{e^{\beta x}+1} \tag{A.9}$$

We consider the contour integral on the LHS in the limit $m \to \infty$. The asymptotic behaviour of the integrand as $|z| \to \infty$ whilst $\arg(z)$ remains constant is given by

$$\frac{1}{e^{\beta z}+1}\frac{e^{\kappa z}}{z-x} \;\sim\; \begin{cases} |z|^{-1}\exp[-(\beta-\kappa)\Re(z)] & \Re(z) > 0 \\ \\ |z|^{-1}\exp[\kappa\Re(z)] & \Re(z) < 0 \end{cases} \tag{A.10}$$

Thus, by Jordan's lemma, the integral along $\mathcal{C}$ vanishes in the considered limit. It immediately follows from A.9 that

$$\sum_{n\ \text{odd}} \frac{1}{i\omega_n - x} e^{i\omega_n \kappa} \;=\; \frac{\beta e^{\kappa x}}{e^{\beta x}+1} \tag{A.11}$$

Taking the limit $\kappa \to 0^+$ and using the identities we hence find the analytic expression for A.7

$$\lim_{\kappa\to 0^+} \sum_{n\ \text{odd}} \frac{1}{i\omega_n - x} e^{i\omega_n \kappa} \;=\; \frac{\beta}{2}\left[1 - \tanh\left(\frac{\beta x}{2}\right)\right] \tag{A.12}$$

In the case that $\kappa < 0$ in A.7, the analysis and final result A.12 are identical, with the exception that $F(z)$ is to be defined

$$F(z) \;=\; \frac{-\beta e^{(\beta+\kappa)z}}{(e^{\beta z}+1)(z-x)}$$

A.3 Evaluating the Free Energy at $n = 0$

A.3.1 EF and SEI Phases

We consider only the evaluation of the free energy of the EF phase at $n = 0$; the calculation for the antisymmetric case follows immediately.

We evaluate the integral

$$\delta F_{\text{EF}} \;=\; \int_{\mathcal{C}} \frac{{\Delta_s}^2}{{g_s}^2} dg_s + \frac{{\Delta_t}^2}{{g_t}^2} dg_t \tag{A.13}$$

where the contour $\mathcal{C}$ is the contour joining the point $(\Delta'_{s0}, \Delta'_{t0})$ with the origin, lying entirely within the region of coexistence. We choose the contour such that $z = \Delta_t/\Delta_s = k$ is constant. Referring to the self-consistency equations 5.52, we see that this contour is equivalent to the straight line on the phase diagram $z_0 = \Delta_{t0}/\Delta_{s0} = \text{constant} = k_0$. We therefore have

$$\frac{\Delta_t}{\Delta_s} \;=\; \frac{k}{k_0}\frac{\Delta_{t0}}{\Delta_{s0}}$$

Hence, we have for A.13

$$\begin{aligned} \int_{\mathcal{C}} \frac{{\Delta_s}^2}{{g_s}^2} dg_s + \frac{{\Delta_t}^2}{{g_t}^2} dg_t \;&=\; \int_{\mathcal{C}} \frac{{\Delta_s}^2}{{g_s}^2} dg_s + \frac{z^2{\Delta_s}^2}{{g_t}^2} dg_t \\ &=\; \int_{\mathcal{C}} \left(\frac{\Delta_s}{\Delta_{s0}}\right)^2 \frac{{\Delta_{s0}}^2}{{g_s}^2} dg_s + \left(\frac{k}{k_0}\frac{\Delta_{t0}}{\Delta_{s0}}\right)^2 \frac{{\Delta_s}^2}{{g_t}^2} dg_t \\ &=\; \int_{\mathcal{C}} \left(\frac{\Delta_s}{\Delta_{s0}}\right)^2 \frac{{\Delta_{s0}}^2}{{g_s}^2} dg_s + \left(\frac{k}{k_0}\frac{\Delta_s}{\Delta_{s0}}\right)^2 \frac{{\Delta_{t0}}^2}{{g_t}^2} dg_t \end{aligned} \tag{A.14}$$

From the self-consistency equations, we see also that the ratio Δ_{s0}/Δ_s is constant along the contour of integration. The coefficients of dg_s and dg_t are therefore functions only of g_s and g_t respectively;

we therefore split the integral and easily evaluate

$$\begin{aligned}\int_C \left(\frac{\Delta_s}{\Delta_{s0}}\right)^2 \frac{{\Delta_{s0}}^2}{{g_s}^2} dg_s + \left(\frac{k}{k_0}\frac{\Delta_s}{\Delta_{s0}}\right)^2 \frac{{\Delta_{t0}}^2}{{g_t}^2} dg_t &= -\frac{\eta_N(0)}{2}\left[\left(\frac{\Delta_s}{\Delta_{s0}}\right)^2 {\Delta'_{s0}}^2 + \left(\frac{k}{k_0}\frac{\Delta_s}{\Delta_{s0}}\right)^2 {\Delta'_{t0}}^2\right] \\ &= -\frac{\eta_N(0)}{2}{\Delta'_{s0}}^2 \left(\frac{\Delta_s}{\Delta_{s0}}\right)^2 \left[1 + \left(\frac{k}{k_0}\frac{\Delta'_{t0}}{\Delta'_{s0}}\right)^2\right] \\ &= \delta F_{\text{sEI}} \left(\frac{\Delta_s}{\Delta_{s0}}\right)^2 \left[1 + \left(\frac{\Delta_t}{\Delta_s}\right)^2\right] \qquad \text{(A.15)}\end{aligned}$$

The coefficient of δF_{sEI} in equation A.15 is the function $f(z)$; its logarithm is

$$\begin{aligned}\ln\left(f(z)\right) &= \ln\left(\left(\frac{\Delta_s}{\Delta_{s0}}\right)^2 \left[1 + \left(\frac{\Delta_t}{\Delta_s}\right)^2\right]\right) \\ &= 2\ln\left(\frac{\Delta_s}{\Delta_{s0}}\right) + \ln\left(1 + \left(\frac{\Delta_t}{\Delta_s}\right)^2\right) \qquad \text{(A.16)} \\ &= -\ln\left|1 - z^2\right| - z\ln\left|\frac{1+z}{1-z}\right| + \ln\left(1 + z^2\right) \qquad \text{(A.17)} \\ &= \ln\left|\frac{1+z^2}{1-z^2}\right| - z\ln\left|\frac{1+z}{1-z}\right| \qquad \text{(A.18)}\end{aligned}$$

where we have used definition of z and the self-consistency equations 5.52 in going from A.16 to A.17. We plot $\ln\left(f(z)\right)$ in figure A.2 for $0 \leq z \leq 5$. We see that $\ln\left(f(z)\right) < 0$ for all z in this range. The $z \to \infty$ limit of $\ln\left(f(z)\right)$ is -2, as suggested by figure A.2. A more rigorous analysis, which we do not present here, also demonstrates that $\ln\left(f(z)\right) < 0$ for all $z > 0$. Thus, $\delta F_{\text{EF}} < \delta F_{\text{sEI}}$ throughout the region in which the EF phase is predicted.

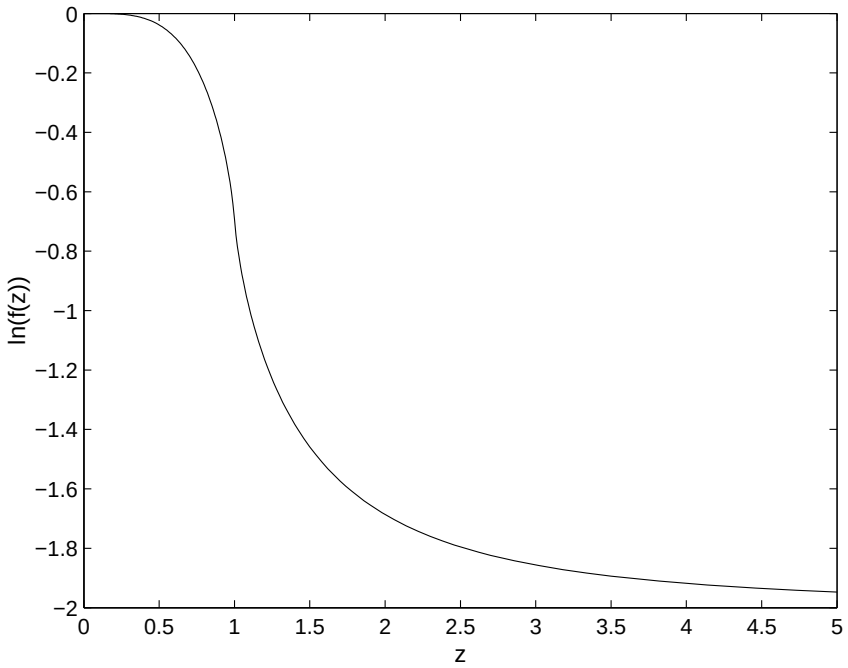

Figure A.2: The logarithm of $f(z)$. Note the behaviour in the limits $z \to 0$ and $z \to \infty$.

A.3.2 SEF Phase

We present only the calculation for the antisymmetric SEF phase; the calculation for the symmetric SEF phase does not significantly differ. The method of calculation is largely based upon that presented above.

For the SEF phase, we must evaluate the integral

$$\delta F_{\text{SEF}} = \int_{\mathcal{C}} \frac{\Delta_s^2}{{g_s}^2} dg_s + \frac{\Delta_t^2}{{g_t}^2} dg_t + \frac{\Sigma^2}{\lambda^2} d\lambda \tag{A.19}$$

where $\mathcal{C}$ in the contour joining the point $(\Delta'_{s0}, \Delta'_{t0}, \Sigma'_0)$ to the coordinate origin in $(\Delta_{s0}, \Delta_{t0}, \Sigma_0)$-space such that the ratios $z_1 = \Delta_s/\Sigma = k_1$ and $z_2 = \Delta_t/\Sigma = k_2$ are constant along it. It is easy to see from equations 7.23 and 7.24 that this corresponds to $z_1^0 = \Delta_{s0}/\Sigma_0 = \text{constant} = k_1^0$ and $z_2^0 = \Delta_{t0}/\Sigma_0 = \text{constant} = k_2^0$. We therefore have the relations

$$\frac{\Delta_s}{\Sigma} = \frac{k_1}{k_1^0}\frac{\Delta_{s0}}{\Sigma_0}, \qquad \frac{\Delta_t}{\Sigma} = \frac{k_2}{k_2^0}\frac{\Delta_{t0}}{\Sigma_0}$$

We hence have for the integral A.19

$$\begin{aligned}
&\int_{\mathcal{C}} \frac{\Delta_s^2}{{g_s}^2} dg_s + \frac{\Delta_t^2}{{g_t}^2} dg_t + \frac{\Sigma^2}{\lambda^2} d\lambda \\
&\quad = \int_{\mathcal{C}} \frac{z_1^2\Sigma^2}{{g_s}^2} dg_s + \frac{z_2^2\Sigma^2}{{g_t}^2} dg_t + \frac{\Sigma^2}{\lambda^2} d\lambda \\
&\quad = \int_{\mathcal{C}} \left(\frac{k_1}{k_1^0}\frac{\Delta_{s0}}{\Sigma_0}\right)^2 \frac{\Sigma^2}{{g_s}^2} dg_s + \left(\frac{k_2}{k_2^0}\frac{\Delta_{t0}}{\Sigma_0}\right)^2 \frac{\Sigma^2}{{g_t}^2} dg_t + \left(\frac{\Sigma}{\Sigma_0}\right)^2 \frac{\Sigma_0^2}{\lambda^2} d\lambda \\
&\quad = \int_{\mathcal{C}} \left(\frac{k_1}{k_1^0}\frac{\Sigma}{\Sigma_0}\right)^2 \frac{\Delta_{s0}^2}{{g_s}^2} dg_s + \left(\frac{k_2}{k_2^0}\frac{\Sigma}{\Sigma_0}\right)^2 \frac{\Delta_{t0}^2}{{g_t}^2} dg_t + \left(\frac{\Sigma}{\Sigma_0}\right)^2 \frac{\Sigma_0^2}{\lambda^2} d\lambda
\end{aligned} \tag{A.20}$$

From equation 7.22, we may without difficulty obtain the expression

$$4\ln\left(\frac{\Sigma}{\Sigma_0}\right) = z_1 \ln\left|\frac{(z_1-1)^2 - z_2^2}{(z_1+1)^2 - z_2^2}\right| + z_2 \ln\left|\frac{(z_2-1)^2 - z_1^2}{(z_2+1)^2 - z_1^2}\right| - \ln\left|((z_1-z_2)^2-1)((z_1+z_2)^2-1)\right| \tag{A.21}$$

Thus, the ratio Σ/Σ_0 is constant along the contour of integration. As before, the coefficients of the dg_s, dg_t and $d\lambda$ in equation A.20 are functions only of g_s, g_t and λ respectively. Arguing as in the EF case, we hence obtain

$$\delta F_{\text{SEI}} = \delta F_{\text{S}} \left(\frac{\Sigma}{\Sigma_0}\right)^2 \left[1 + \left(\frac{\Delta_s}{\Sigma}\right)^2 + \left(\frac{\Delta_t}{\Sigma}\right)^2\right] \tag{A.22}$$

where the coefficient of δF_{S} in A.22 is the function $f(x,y)$. Using the relation A.21 it is a simple matter to obtain the expression 7.34 for $\ln(f(x,y))$.

In figure A.3, we plot the line $f(z_1,z_2) = 1$ in the (z_1,z_2)-plane. We note that there is a region where the inequality $f(z_1,z_2) > 1$ is satisfied. Mapping this line into the (z_1^0, z_2^0)-plane using equations 7.23 and 7.24, we obtain the boundary between the SEF1 and SEF2 regions in the phase diagram figure 7.3.

A.4 Important Integrals

In chapters 6 and 7, we frequently utilize the integrals $\mathcal{I}_j$ where $j = 1, 2, 3$. For the sSEI phase, these are defined

$$\mathcal{I}_1(\widetilde{\Delta}_s, \widetilde{\Sigma}, \delta\widetilde{\mu}) = \lim_{\beta\to\infty} \int_0^{\varpi} \frac{d\xi}{2E} \left[\frac{E+\delta\widetilde{\mu}}{\omega^+} \tanh\left(\frac{\beta\omega^+}{2}\right) + \frac{E-\delta\widetilde{\mu}}{\omega^-} \tanh\left(\frac{\beta\omega^-}{2}\right)\right] \tag{A.23}$$

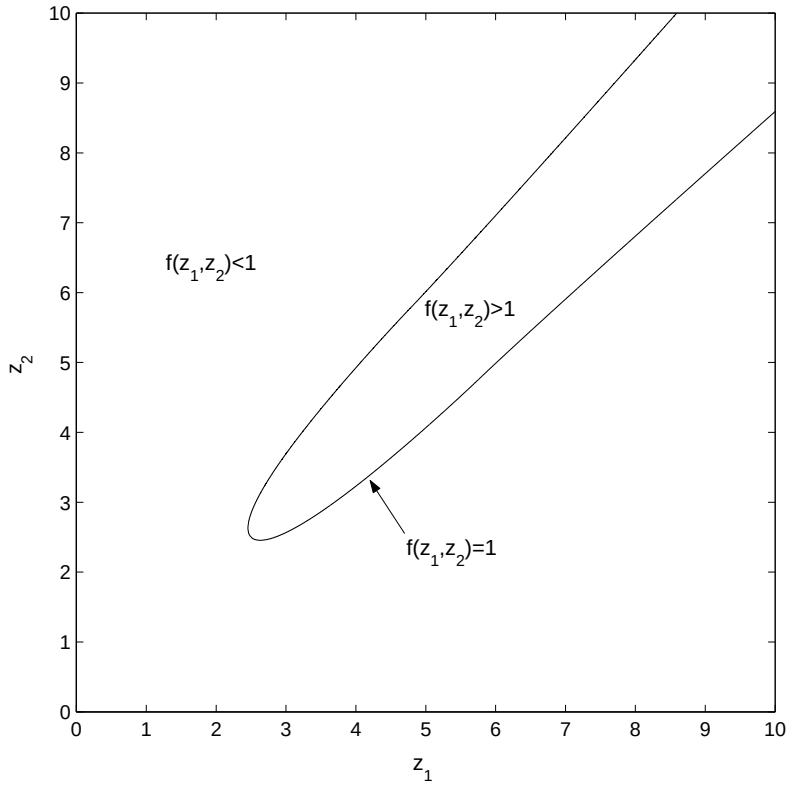

Figure A.3: The line $f(z_1, z_2) = 1$ in the (z_1, z_2)-plane. Note the region where the inequality $f(z_1, z_2) > 1$ is satisfied.

$$\mathcal{I}_2(\widetilde{\Delta}_s, \widetilde{\Sigma}, \delta\widetilde{\mu}) = \lim_{\beta\to\infty} \int_0^{\varpi} \frac{d\xi}{2E} \left[\frac{1}{\omega^-} \tanh\left(\frac{\beta\omega^-}{2}\right) - \frac{1}{\omega^+} \tanh\left(\frac{\beta\omega^+}{2}\right) \right] \tag{A.24}$$

$$\mathcal{I}_3(\widetilde{\Delta}_s, \widetilde{\Sigma}, \delta\widetilde{\mu}) = \lim_{\beta\to\infty} \int_0^{\varpi} \frac{d\xi}{2E} \left[\frac{E + \delta\widetilde{\mu}}{\omega^+} \tanh\left(\frac{\beta\omega^+}{2}\right) - \frac{E - \delta\widetilde{\mu}}{\omega^-} \tanh\left(\frac{\beta\omega^-}{2}\right) \right] \tag{A.25}$$

where E and $\omega_\pm$ are as defined in chapter 6. We let $\delta\widetilde{\mu} = \delta\mu$ in the antisymmetric case. In this section we present several important properties of these integrals that we have made reference to in the body of the thesis.

We list the values of these integrals in some special cases. For $\mathcal{I}_1$ we have the following useful identities

$$\begin{aligned}
\mathcal{I}_1(\widetilde{\Delta}_s = \Delta_s, 0, 0) &= \ln\left(\frac{2\varpi}{\Delta_s}\right) \\
\mathcal{I}_1(\widetilde{\Delta_s} = \Delta_s, 0, \delta\widetilde{\mu} = \delta\mu) &= \ln\left(\frac{2\varpi}{\delta\mu + \sqrt{\delta\mu^2 - \Delta_s^2}}\right) \\
\mathcal{I}_1(0, \widetilde{\Sigma} = \Sigma, 0) &= \ln\left(\frac{2\varpi}{\Sigma}\right) \\
\mathcal{I}_1(0, \widetilde{\Sigma} = \Sigma, \delta\widetilde{\mu} = \delta\mu) &= \ln\left(\frac{2\varpi}{\Sigma}\right) - \frac{\delta\mu}{\sqrt{\Sigma^2 + \delta\mu^2}} \ln\left(\frac{\delta\mu + \sqrt{\delta\mu^2 + \Sigma^2}}{\delta\mu}\right)
\end{aligned} \tag{A.26}$$

for $\mathcal{I}_2$ we have

$$\begin{aligned} \mathcal{I}_2(\widetilde{\Delta}_s = \Delta_s, 0, 0) &= \mathcal{I}_2(0, \widetilde{\Sigma} = \Sigma, 0) = 0 \\ \mathcal{I}_2(0, \widetilde{\Sigma} = \Sigma, \delta\widetilde{\mu} = \delta\mu) &= \frac{\delta\mu}{\sqrt{\Sigma^2 + \delta\mu^2}} \ln\left(\frac{\delta\mu + \sqrt{\delta\mu^2 + \Sigma^2}}{\delta\mu}\right) \end{aligned} \tag{A.27}$$

and finally for $\mathcal{I}_3$

$$\begin{aligned} \mathcal{I}_2(\widetilde{\Delta}_s = \Delta_s, 0, 0) &= \mathcal{I}_2(0, \widetilde{\Sigma} = \Sigma, 0) = 0 \\ \mathcal{I}_1(\widetilde{\Delta_s} = \Delta_s, 0, \delta\widetilde{\mu} = \delta\mu) &= \sqrt{\delta\mu^2 - \Delta_s^2} \\ \mathcal{I}_2(0, \widetilde{\Sigma} = \Sigma, \delta\widetilde{\mu} = \delta\mu) &= \delta\mu \end{aligned} \tag{A.28}$$

When $\delta\mu \neq 0$, the integral $\mathcal{I}_2(\Delta_s, 0, \delta\mu)$ does not exist: we are able, however, to obtain an asymptotic expression in the limit $\Sigma \to 0$ (see subsection A.4.1).

Before considering special properties of these integrals, we first examine the behaviour of their integrands in the $\xi \to \infty$ limit. Expanding as a Taylor series in ξ^{-1}, we obtain

$$\begin{aligned} \text{integrand of } \mathcal{I}_1 : &\quad 2\xi^{-1} - (\widetilde{\Sigma} + \widetilde{\Delta}_s)\xi^{-3} + \mathcal{O}(\xi^{-5}) \\ \text{integrand of } \mathcal{I}_2 : &\quad 2\delta\widetilde{\mu}\xi^{-3} + \mathcal{O}(\xi^{-5}) \\ \text{integrand of } \mathcal{I}_2 : &\quad 2\delta\widetilde{\mu}\widetilde{\Sigma}^2\xi^{-3} + \mathcal{O}(\xi^{-5}) \end{aligned} \tag{A.29}$$

Because of the ξ^{-1} behaviour of the integrand of $\mathcal{I}_1$ as $\xi \to \infty$, it is necessary to keep the cut-off ϖ finite in this integral; for the integrals $\mathcal{I}_2$ and $\mathcal{I}_3$ we may let $\varpi \to \infty$.

A.4.1 The $\Sigma \to 0$ form of $\mathcal{I}_2$

In the general case when all three of its arguments are non-zero, we may express $\mathcal{I}_2$ as follows

$$\mathcal{I}_2(\widetilde{\Delta}_s, \widetilde{\Sigma}, \delta\widetilde{\mu}) = \int_0^\infty \frac{d\xi}{2E}\left[\frac{1}{\sqrt{(E - \delta\widetilde{\mu})^2 + \widetilde{\Sigma}^2}} - \frac{1}{\sqrt{(E + \delta\widetilde{\mu})^2 + \widetilde{\Sigma}^2}}\right]$$

We change the variable of integration to E:

$$\begin{aligned} &\mathcal{I}_2(\widetilde{\Delta}_s, \widetilde{\Sigma}, \delta\widetilde{\mu}) \\ &= \int_{\widetilde{\Delta}_s}^\infty dE \left[\frac{1}{\sqrt{\left(E^2 - \widetilde{\Delta}_s^2\right)\left((E - \delta\widetilde{\mu})^2 + \widetilde{\Sigma}^2\right)}} - \frac{1}{\sqrt{\left(E^2 - \widetilde{\Delta}_s^2\right)\left((E + \delta\widetilde{\mu})^2 + \widetilde{\Sigma}^2\right)}}\right] \end{aligned} \tag{A.30}$$

Examining the first term in the square brackets, we see that in the limit $\Sigma \to 0$ it has a simple pole the point $E = \delta\widetilde{\mu}$. As this point lies within the limits of integration, the integral $\mathcal{I}_2$ has a logarithmic divergence in the limit $\Sigma \to 0$. We therefore seek an asymptotic expression for $\mathcal{I}_2$ in this limit. The second term in the integrand clearly does not have this problem; it may be analytically evaluated in the limit $\Sigma \to 0$.

We consider the first term in equation A.30 as an integral in its own right. Because of the square-root divergence at $E = \widetilde{\Delta}_s$, we may discard the integration in the range $E > \delta\widetilde{\mu}$. Integrating therefore over the range $\widetilde{\Delta}_s < E < \delta\widetilde{\mu}$, we may write the result as an elliptic integral of the first

kind [95]:

$$\int_{\widetilde{\Delta}_s}^{\delta\widetilde{\mu}} \frac{dE}{\sqrt{\left(E^2-\widetilde{\Delta}_s^2\right)\left((E-\delta\widetilde{\mu})^2+\widetilde{\Sigma}^2\right)}} = \frac{1}{\sqrt{pq}} F\left(2\arctan\sqrt{\frac{q(\delta\widetilde{\mu}-\widetilde{\Delta}_s)}{p(\delta\widetilde{\mu}-\widetilde{\Delta}_s)}}, \frac{1}{2}\sqrt{\frac{(p+q)^2-4\widetilde{\Delta}_s^2}{pq}}\right) \tag{A.31}$$

where the terms p and q are defined

$$p^2 = (\delta\widetilde{\mu}-\widetilde{\Delta}_s)^2+\widetilde{\Sigma}^2, \qquad q^2 = (\delta\widetilde{\mu}+\widetilde{\Delta}_s)^2+\widetilde{\Sigma}^2, \tag{A.32}$$

In the limit $\Sigma \to 0$, the modulus of the elliptic integral in equation A.31,

$$k = \frac{1}{2}\sqrt{\frac{(p+q)^2-4\widetilde{\Delta}_s^2}{pq}},$$

converges to unity. For k close to one, we have the asymptotic expansion (8.118.1 in [96]) of the elliptic integral of the first kind:

$$F(\varphi,k) \;=\; \frac{2}{\pi}K' \ln\left|\tan\left(\frac{\varphi}{2}+\frac{\pi}{4}\right)\right| + \mathcal{O}(1-k^2) \tag{A.33}$$

where $K' = K\left(\sqrt{1-k^2}\right)$ is the complementary complete elliptic integral of the first kind. For $k \to 1$, we therefore have for K' the Taylor expansion 8.113.1 in [96]:

$$K' = \frac{\pi}{2}\left[1+\frac{1}{4}(1-k^2)+\frac{9}{64}(1-k^2)^2+\ldots\right] \tag{A.34}$$

Keeping the first term in this expansion and discarding higher order terms in equation A.33, we have therefore

$$\begin{aligned}\lim_{\Sigma\to 0}\int_{\widetilde{\Delta}_s}^{\delta\widetilde{\mu}} &\frac{dE}{\sqrt{\left(E^2-\widetilde{\Delta}_s^2\right)\left((E-\delta\widetilde{\mu})^2+\widetilde{\Sigma}^2\right)}} \\ &\approx \frac{1}{\sqrt{\delta\mu^2-\Delta_s^2}} \ln\left|\lim_{\Sigma\to 0}\tan\left(\arctan\sqrt{\frac{q(\delta\widetilde{\mu}-\widetilde{\Delta}_s)}{p(\delta\widetilde{\mu}-\widetilde{\Delta}_s)}}+\frac{\pi}{4}\right)\right|\end{aligned} \tag{A.35}$$

using the elementary relation

$$\tan\left(\theta+\frac{\pi}{4}\right) \;=\; \frac{1+\tan(\theta)}{1-\tan(\theta)}$$

and letting $\widetilde{\Sigma} \ll \delta\widetilde{\mu}$, $\widetilde{\Delta}_s$, we have for the tangent in equation A.35

$$\begin{aligned}\tan\left(\arctan\sqrt{\frac{q(\delta\widetilde{\mu}-\widetilde{\Delta}_s)}{p(\delta\widetilde{\mu}-\widetilde{\Delta}_s)}}+\frac{\pi}{4}\right) &\approx \frac{\sqrt{(\delta\mu+\Delta_s)\sqrt{\widetilde{\Sigma}^2+(\delta\mu-\Delta_s)^2}}+\sqrt{\delta\mu^2-\Delta_s^2}}{\sqrt{(\delta\mu+\Delta_s)\sqrt{\widetilde{\Sigma}^2+(\delta\mu-\Delta_s)^2}}-\sqrt{\delta\mu^2-\Delta_s^2}} \\ &\sim \frac{8(\delta\mu^2-\Delta_s^2)}{\widetilde{\Sigma}^2(\delta\mu+\Delta_s)^2}\end{aligned} \tag{A.36}$$

where we have also assumed that $\delta\widetilde{\mu} \approx \delta\mu$ and $\widetilde{\Delta}_s \approx \Delta_s$ in deriving A.36. We thus obtain

$$\lim_{\Sigma\to 0}\int_{\widetilde{\Delta}_s}^{\delta\widetilde{\mu}} \frac{dE}{\sqrt{\left(E^2-\widetilde{\Delta}_s^2\right)\left((E-\delta\widetilde{\mu})^2+\widetilde{\Sigma}^2\right)}} \sim \frac{1}{\sqrt{\delta\mu^2-\Delta_s^2}} \ln\left|\frac{8(\delta\mu^2-\Delta_s^2)}{\widetilde{\Sigma}^2(\delta\mu+\Delta_s)^2}\right| \tag{A.37}$$

To obtain the full expression for $\mathcal{I}_2$ in the $\Sigma \to 0$ limit, we must include the integral of the other term in equation A.30. After some unenlightening manipulation, we hence obtain the result

$$\mathcal{I}_2(\Delta_s, \Sigma \to 0, \delta\mu) \sim \frac{1}{\sqrt{\delta\mu^2 - \Delta_s^2}} \ln \left| \frac{4(\delta\mu^2 - \Delta_s^2)}{\widetilde{\Sigma}\left(\delta\mu + \sqrt{\delta\mu^2 - \Delta_s^2}\right)} \right| \tag{A.38}$$

In the case of the strong SEF phase, the integral $\mathcal{I}_2(\Delta_+, 0, \delta\mu)$ may be evaluated exactly; there is no singularity of the integrand when we convert to an integral over E_+, as $E_+ > \delta\mu$ by definition. We therefore obtain the exact result

$$\mathcal{I}_2(\Delta_+, 0, \delta\mu) = \frac{1}{\sqrt{\Delta_+^2 - \delta\mu^2}} \left[\frac{\pi}{2} - \arctan\left(\frac{\sqrt{\Delta_+^2 - \delta\mu^2}}{\delta\mu} \right) \right] \tag{A.39}$$

We further note that $\mathcal{I}_1$ and $\mathcal{I}_3$ also may be written as elliptic integrals in the general case. Although they do not diverge in the limit $\Sigma \to 0$ as $\mathcal{I}_2$, determining the small-Σ corrections requires an analysis similar to that above, although much more complicated. As demonstrated in [82], the lowest-order corrections are $\sim \Sigma \ln \Sigma$.

A.4.2 Asymptotic Relations for the Antisymmetric Case

Laurent Series in $\delta\mu$ for $\mathcal{I}_2$ and $\mathcal{I}_3$

In the general case when $\Sigma \neq 0$, we may obtain Laurent series expansions for the integrals $\mathcal{I}_2$ and $\mathcal{I}_3$. Performing the expansions upon the integrands, and evaluating, we have

$$\mathcal{I}_2(\widetilde{\Delta}_s, \widetilde{\Sigma}, \delta\mu) = \frac{1}{\Delta_s \Sigma} \ln \left| \frac{\Delta_s + \Sigma}{\Delta_s - \Sigma} \right| \delta\mu + \mathcal{O}(\delta\mu^3) \tag{A.40}$$

$$\mathcal{I}_3(\widetilde{\Delta}_s, \widetilde{\Sigma}, \delta\mu) = \Delta_s \Sigma \ln \left| \frac{\Delta_s - \Sigma}{\Delta_s + \Sigma} \right| \delta\mu^{-1} + \mathcal{O}(\delta\mu) \tag{A.41}$$

Substituting these relationships in the equation for n (equation 6.31), it is simple to see that $n \sim \mathcal{O}(\delta\mu)$ in the $\delta\mu \to 0$ limit.

The Δ_s, $\Delta_t \to 0$ limit of $\mathcal{I}_{1+} - \mathcal{I}_{1-}$ and $\mathcal{I}_{2+} - \mathcal{I}_{2-}$

When Δ_s and Δ_t simultaneously approach zero, we may expand the integrands of $\mathcal{I}_{1+} - \mathcal{I}_{1-}$ and $\mathcal{I}_{2+} - \mathcal{I}_{2-}$:

$$\begin{aligned} \text{integrand of } \mathcal{I}_{1+} - \mathcal{I}_{1-} : \quad & 2\left\{ \frac{\Sigma^2}{\delta\mu^2} \left[\frac{\xi + \delta\mu}{((\xi+\delta\mu)^2 + \Sigma^2)^{3/2}} + \frac{\xi - \delta\mu}{((\xi-\delta\mu)^2 + \Sigma^2)^{3/2}} \right] \right. \\ & - \left(1 + \frac{\Sigma^2}{\delta\mu}^2\right) \left[\frac{(\xi+\delta\mu)^2}{\xi^2((\xi+\delta\mu)^2 + \Sigma^2)^{3/2}} + \frac{(\xi-\delta\mu)^2}{\xi^2((\xi-\delta\mu)^2 + \Sigma^2)^{3/2}} \right. \\ & \left. \left. + \frac{\delta\mu}{\xi^2\sqrt{(\xi+\delta\mu)^2 + \Sigma^2}} - \frac{\delta\mu}{\xi^2\sqrt{(\xi-\delta\mu)^2 + \Sigma^2}} \right] \right\} \Delta_s \Delta_t + \mathcal{O}(\Delta_s^2 \Delta_t^2) \end{aligned} \tag{A.42}$$

$$\begin{aligned} \text{integrand of } \mathcal{I}_{2+} - \mathcal{I}_{2-} : \quad & \left\{ \frac{\Sigma^2}{\delta\mu^2} \left[\frac{1}{\xi((\xi+\delta\mu)^2 + \Sigma^2)^{3/2}} - \frac{1}{\xi((\xi-\delta\mu)^2 + \Sigma^2)^{3/2}} \right] \right. \\ & + \left(1 + \frac{\Sigma^2}{\delta\mu}^2\right) \left[\frac{(\xi+\delta\mu)^2}{\xi^2((\xi+\delta\mu)^2 + \Sigma^2)^{3/2}} - \frac{(\xi-\delta\mu)^2}{\xi^2((\xi-\delta\mu)^2 + \Sigma^2)^{3/2}} \right. \end{aligned}$$

$$+\frac{1}{\xi^3\sqrt{(\xi+\delta\mu)^2+\Sigma^2}}-\frac{1}{\xi^3\sqrt{(\xi-\delta\mu)^2+\Sigma^2}}\Bigg]\Bigg\}\,\Delta_s\Delta_t+\mathcal{O}(\Delta_s^2\Delta_t^2) \tag{A.43}$$

These expansions demonstrate that the integrals $\mathcal{I}_{1+}-\mathcal{I}_{1-}$ and $\mathcal{I}_{2+}-\mathcal{I}_{2-}$ vanish as the boundary between the SEF and S phases is approached.

A.5 Important Limits

We state here some important limits utilized in the study of the phase diagram of the $n=0$ SEF phase.

$$\lim_{\substack{y\to 0\\ x\neq 0}}\ \frac{1}{y}\ln\left|\frac{(1-y)^2-x^2}{(1+y)^2-x^2}\right| \;=\; \frac{4}{x^2-1} \tag{A.44}$$

$$\lim_{\substack{y\to 0\\ x\neq 0}}\ \frac{1}{y}\ln\left|\frac{1-(x-y)^2}{1-(x+y)^2}\right| \;=\; \frac{4x}{1-x^2} \tag{A.45}$$

$$\lim_{\substack{y\to 0\\ x\neq 0}}\ \frac{1}{y}\ln\left|\frac{1+(x+y)^2}{1+(x+y)^2}\right| \;=\; \frac{4x}{1+x^2} \tag{A.46}$$

Bibliography

[1] N. W. Ashcroft and N. D. Mermin, *Solid State Physics*, Holt, Rinehardt and Winston, 1976.

[2] L. N. Cooper, Phys. Rev. **104**, 1189 (1956).

[3] J. Bardeen, L. N. Cooper, and J. R. Schrieffer, Phys. Rev. **106**, 162 (1957).

[4] J. Bardeen, L. N. Cooper, and J. R. Schrieffer, Phys. Rev. **108**, 1175 (1957).

[5] N. F. Mott, Phil. Mag. series 8 **6**, 287 (1961).

[6] N. F. Mott, *Metal-Insulator Transitions*, Taylor and Francis Ltd., 1974.

[7] L.-P. Lévy, *Magnetism and Superconductivity*, Springer-Verlag, 2000.

[8] L. V. Keldysh and Y. V. Kopaev, Sov. Phys. Solid State **6**, 2219 (1965).

[9] V. L. Ginzburg and D. A. Kirzhnits, editors, *High-Temperature Superconductivity*, Consultants Bureau, 1982.

[10] Y. A. Izyumov and E. Z. Kurmaev, Sov. Phys. Uspekhi **19**, 26 (1976).

[11] G. Bilbro and W. L. McMillan, Phys. Rev. B **14**, 1887 (1976).

[12] Y. V. Kopaev and R. K. Timerov, Sov. Phys. JETP **36**, 153 (1973).

[13] M. Gulácsi and Z. Gulácsi, Phys. Rev. B **39**, 714 (1989).

[14] V. L. Ginzburg, Sov. Phys. JETP **4**, 153 (1957).

[15] B. T. Mathias, H. Suhl, and E. Corenzwit, Phys. Rev. Lett. **1**, 92 (1958).

[16] V. L. Ginzburg, editor, *Superconductivity, Superdiamagnetism, Superfluidity*, Mir, 1987.

[17] S. S. Saxena et al., Nature **406**, 587 (2001).

[18] C. Pfleiderer et al., Nature **412**, 58 (2001).

[19] N. I. Karchev et al., Phys. Rev. Lett. **86**, 846 (2001).

[20] D. P. Young et al., Nature **397**, 412 (1999).

[21] T. Terashima et al., J. Phys. Soc. Japan **69**, 2423 (2000).

[22] M. E. Zhitomirsky, T. M. Rice, and V. I. Ansimov, cond-mat/9904330.

[23] L. Balents and C. M. Varma, Phys. Rev. Lett. **84**, 1264 (2000).

[24] Z. Fisk et al., Physica B **312-313**, 808 (2002).

[25] W. E. Parry, *The Many-Body Problem*, Oxford University Press, 1973.

[26] A. L. Fetter and J. D. Walecka, *Quantum Theory of Many-Particle Systems*, McGraw Hill, 1971.

[27] A. A. Abrikosov, L. P. Gor'kov, and I. E. Dzyaloshinski, *Methods of Quantum Field Theory in Statistical Physics*, Dover, 1973.

[28] T. D. Schultz, *Quantum Field Theory and the Many-Body Problem*, Gordon and Breach, 1964.

[29] G. D. Mahan, *Many-Particle Physics*, Plenum Press, second edition, 1990.

[30] R. D. Mattuck, *A Guide to Feynman Diagrams in the Many-Body Problem*, Dover, second edition, 1992.

[31] J. R. Schrieffer, *Theory of Superconductivity*, Benjamin, 1964.

[32] L. D. Landau and E. M. Lifshitz, *Course of Theoretical Physics*, volume 5, Pergamon Press, 1958.

[33] L. P. Gor'kov, Sov. Phys. JETP **34**, 505 (1958).

[34] D. H. Martin, *Magnetism in Solids*, MIT Press, 1967.

[35] G. T. Rado and H. Suhl, editors, *Magnetism*, volume IV, Academic Press, 1966.

[36] F. H. Zong et al., cond-mat/0205339 v1.

[37] G. Ortiz et al., Phys. Rev. Lett. **82**, 5317 (1999).

[38] J. Kübler, *Theory of Itinerant Electron Magnetism*, Oxford University Press, 2000.

[39] J. C. Slater, Phys. Rev. **49**, 537 (1936).

[40] E. C. Stoner, Proc. Roy. Soc. **165A**, 372 (1938).

[41] K. Shimizu et al., Nature **412**, 316 (2001).

[42] N. F. Berk and J. R. Schrieffer, Phys. Rev. Lett. **17**, 433 (1966).

[43] G. T. Rado and H. Suhl, editors, *Magnetism*, volume V, Academic Press, 1973.

[44] A. M. Gabovich, A. I. Voitenko, and M. Ausloos, Physics Reports **367**, 583 (2002).

[45] Y. V. Kopaev, Sov. Phys. Solid State **8**, 175 (1966).

[46] Y. V. Kopaev, Sov. Phys. Solid State **12**, 1 (1970).

[47] J. des Cloizeaux, J. Phys. Chem. Solids **26**, 259 (1965).

[48] A. N. Kozlov and L. A. Maksimov, Sov. Phys. JETP **21**, 790 (1965).

[49] B. I. Halperin and T. M. Rice, Solid State Physics **21**, 115 (1968).

[50] B. A. Volkov and Y. V. Kopaev, Sov. Phys. JETP Lett. **27**, 7 (1978).

[51] D. Jérome, T. M. Rice, and W. Kohn, Phys. Rev. **158**, 462 (1967).

[52] J. Zittartz, Phys. Rev. **165**, 612 (1968).

[53] A. I. Rusinov, D. C. Kat, and Y. V. Kopaev, Sov. Phys. JETP **38**, 991 (1974).

[54] G. Grüner, *Density Waves in Solids*, Addison-Wesley, 1994.

[55] B. A. Volkov, Y. V. Kopaev, and A. I. Rusinov, Sov. Phys. JETP **41**, 952 (1975).

[56] B. A. Volkov and Y. V. Kopaev, Sov. Phys. JETP Lett. **19**, 104 (1973).

[57] B. A. Volkov, A. I. Rusinov, and R. K. Timerov, Sov. Phys. JETP **43**, 589 (1976).

[58] T. Soda and Y. Wada, Prog. Theor. Phys. **36**, 1111 (1966).

[59] Y. V. Kopaev and V. V. Tugushev, Sov. Phys. Solid State **19**, 632 (1977).

[60] T. M. Rice, Phys. Rev. B **2**, 3619 (1970).

[61] N. I. Kulikov and V. V. Tugushev, Sov. Phys. Uspekhi **27**, 954 (1984).

[62] E. Fawcett et al., Rev. Mod. Phys. **66**, 25 (1994).

[63] V. A. Volkov and Y. K. Kopaev, Sov. Phys. JETP **37**, 1103 (1973).

[64] P. Wachter et al., Phys. Rev. B **51**, 5542 (1995).

[65] B. Bucher et al., Phys. Rev. Lett. **67**, 2717 (1991).

[66] V. V. Glushkov et al., Physica B **284-288**, 1179 (2000).

[67] I. Hase and Y. Nishihara, Phys. Rev. B **62**, 13426 (2000).

[68] I. I. Lyapilin and I. M. Tsidil'kovskii, Sov. Phys. Uspekhi **28**, 349 (1985).

[69] V. G. Idlis et al., Sov. Phys. JETP **48**, 713 (1978).

[70] H. R. Ott et al., Physica B **281-282**, 423 (2000).

[71] S. Massidda et al., Z. Phys. B **102**, 83 (1997).

[72] H. Kino et al., J. Phys. Chem. Solids **63**, 1595 (2002).

[73] M. Y. Veillette and L. Balents, Phys. Rev. B **65**, 014428/1 (2002).

[74] K. Taniguchi et al., cond-mat/0206101 v1.

[75] H. Suhl, B. T. Matthias, and L. R. Walker, Phys. Rev. Lett. **3**, 552 (1959).

[76] J. Kondo, Prog. Theor. Phys. **29**, 1 (1963).

[77] Y. K. Kopaev, Sov. Phys. JETP **31**, 544 (1970).

[78] Y. V. Kopaev and R. K. Timerov, Sov. Phys. Solid State **14**, 69 (1972).

[79] M. Gulácsi and Z. Gulácsi, Phys. Rev. B **33**, 6147 (1986).

[80] S. N. Molotkov and R. K. Timerov, Sov. Phys. Solid State **21**, 2081 (1979).

[81] S. C. Lo and K. W. Wong, Il Nuovo Cimento B **10**, 361 (1972).

[82] J. G. Brankov and N. S. Tonchev, Physica **84A**, 371 (1976).

[83] A. I. Buzdin and L. N. Bulaevskii, Sov. Phys. Uspekhi **27**, 11 (1984).

[84] J. W. Lynn et al., Phys. Rev. B **55**, 6584 (1997).

[85] C. W. Chu et al., Phys. Rev. B **4**, 320 (1971).

[86] J. Nagamatsu et al., Nature **410**, 63 (2001).

[87] I. Hase and K. Yamaji, J. Phys. Soc. Jpn. **70**, 2376 (2001).

[88] K. Machida, J. Phys. Soc. Jpn. **30**, 2195 (1981).

[89] E. W. Fenton, Solid State Commun. **50**, 961 (1984).

[90] D. C. Kat, Sov. Phys. JETP **59**, 1241 (1984).

[91] H. R. Ott et al., Z. Phys. B **102**, 337 (1997).

[92] J. L. Gavilano et al., Physica B **281-282**, 428 (2000).

[93] P. Vonlanthen et al., Phys. Rev. B **62**, 10076 (2000).

[94] J. M. Blatt, *Theory of Superconductivity*, Academic Press, 1964.

[95] W. Gröbner and N. Hofreiter, *Integraltafel erster teil Unbestimmte Integrale*, Springer-Verlag, 1949.

[96] I. S. Gradshteyn and I. M. Ryzhik, *Table of Integrals, Series and Products*, Academic Press, 1980.